Aristotle University of Thessaloniki
Faculty of Sciences
School of Geology
Department of Geophysics

Laterally Constrained Inversion of Electrical Resistivity Tomography Data

Patsia Ourania
Master Thesis

2021

PATSIA OURANIA

GEOLOGIST

Laterally Constrained Inversion of Electrical Resistivity Tomography Data

Submitted to the Department of Geophysics of School of Geology, Aristotle University of Thessaloniki within the postgraduate program “Applied and Environmental Geology” with specialization in “Applied Geophysics”

Date of Oral Examination: 13 / 01 / 2021

Advisory Committee

Professor Panagiotis Tsourlos (Supervisor)

Associate Professor George Vargemezis (Advisory Committee member)

Professor Constantinos Papazachos (Advisory Committee member)

Laterally Constrained Inversion of Electrical Resistivity Tomography Data, Master Thesis

To my family,
for their constant support.

ACKNOWLEDGMENTS

I would like to express my gratitude towards my supervisor Professor Panagiotis Tsourlos for his constant support and guidance through my undergraduate and postgraduate studies. I could not thank him enough for the knowledge that he imparted to me and the opportunities that he gave me. He is a true mentor to me and his encouragement through the years was invaluable.

I also want to thank Associate Professor George Vargemezis for his guidance, his advices and the opportunities he gave me to participate in several geophysical projects that helped me gain insight into the application of geophysics in real life problems.

I would also like to thank Professor Constantinos Papazachos for his help and the knowledge I gained from his courses throughout the postgraduate studies, which where vital for this project.

I want to sincerely thank the staff of the Department of Geophysics of the Aristotle University of Thessaloniki and especially Dr. Ilias Fikos for their help and advices during my Master studies. Moreover, I would like to thank my fellow postgraduate students for their partnership through the years and the times that we had working together.

Last but not least, I would like to thank my family for their moral support and unconditional love. They were always there for me during these difficult years. Completing this work would have been difficult without them.

ABSTRACT

In the present thesis a laterally-constrained (LCI) scheme is presented for the inversion of the electrical resistivity tomography (ERT) data. Initially, a detailed review of the basic theory of the resistivity method, the surveying methods, the resistivity arrays and the instrumentation is given. The forward problem and techniques for its solution are addressed. In addition, the inversion theory and the inversion methods are presented, with emphasis given on the LCI technique.

The LCI algorithm which was developed uses the smoothness-constrained inversion to find the correction of the model. The ERT data are divided into soundings and the forward problem is calculated using the filter method as 1-D forward solver for each sounding. The data are inverted as one system by introducing lateral constraints between adjacent soundings in order to produce a 2-D geoelectrical image of the subsurface. The lateral constraints were implemented using a 2-D smoothness matrix with the modification that it changes throughout the inversion procedure as the final solution converges. The perturbation technique was used to calculate the Jacobian matrix for the total system. The software was developed in a graphical user interface (GUI) using Matlab.

The performance and efficiency of the algorithm is tested using both synthetic and real data acquired from different applications. Numerical modeling is used to provide the synthetic data for realistic models. The evaluation shows that the laterally-constrained approach is efficient and can be successfully used to locate layer boundaries. On the contrary, the results clearly show that this method cannot resolve small targets that are within greater structures due to the 1-D formulation of the problem.

In addition, these data are used to make comparisons between the finite element and the laterally-constrained method and to address the benefits and drawbacks of the latter. By comparing the two schemes, it is obvious that both the laterally-constrained and the 2-D smooth-structure methods are able to provide an accurate approximation of the subsurface, while their combination yields a model even closer to the real one.

ΠΕΡΙΛΗΨΗ

Η παρούσα διατριβή επικεντρώνεται στην αναπτυξη τεχνικών αντιστροφής των δεδομένων ηλεκτρικής τομογραφίας (ERT) με τη χρήση της μεθόδου των πλευρικών περιορισμών (LCI). Αρχικά, παρουσιάζονται οι βασικές αρχές της ηλεκτρικής μεθόδου, οι τεχνικές διασκόπησης, οι διατάξεις των ηλεκτροδίων και ο εξοπλισμός που χρησιμοποιείται. Γίνεται αναφορά στο ευθύ πρόβλημα και στις τεχνικές επίλυσης του. Ακόμη, παρουσιάζεται αναλυτικά η θεωρία της αντιστροφής και οι μέθοδοι αντιστροφής δίνοντας έμφαση στην μέθοδο των πλευρικών περιορισμών.

Ο αλγόριθμος που αναπτύχθηκε χρησιμοποιεί τη μέθοδο της εξομαλυμένης αντιστροφής για την εύρεση της διόρθωσης του μοντέλου. Τα δεδομένα της τομογραφίας χωρίζονται σε βυθοσκοπήσεις και η λύση του 1-D ευθέος προβλήματος υπολογίζεται για κάθε μία από αυτές χρησιμοποιώντας τη μέθοδο των φίλτρων. Τα δεδομένα ενώνονται σε ένα σύστημα για την αντιστροφή, χρησιμοποιώντας πλευρικούς περιορισμούς μεταξύ γειτονικών βυθοσκοπήσεων, ώστε να κατασκευαστεί μία 2-D εικόνα της γεωηλεκτρικής δομής του υπεδάφους. Οι πλευρικοί περιορισμοί ενσωματώθηκαν με τη χρήση ενός 2-D πίνακα εξομάλυνσης με την τροποποίηση ότι ο πίνακας αυτός μεταβάλλεται κατά τη διάρκεια της αντιστροφής. Για τον υπολογισμό του Ιακωβιανού πίνακα χρησιμοποιήθηκε η τεχνική διαταραχών. Το λογισμικό αναπτύχθηκε σε γραφικό περιβάλλον χρησιμοποιώντας την Matlab.

Η επίδοση και η αποτελεσματικότητα του αλγορίθμου ελέγχεται χρησιμοποιώντας συνθετικά αλλά και πραγματικά δεδομένα που συλλέχθηκαν από διάφορες εφαρμογές. Με κατάλληλη αριθμητική προσομοίωση παράχθηκαν τα συνθετικά δεδομένα για ρεαλιστικά μοντέλα. Η αξιολόγηση δείχνει ότι η μέθοδος με πλευρικούς περιορισμούς είναι αποτελεσματική και μπορεί να εντοπίσει επιτυχώς τις απότομες επαφές των στρωμάτων. Αντίθετα, τα αποτελέσματα έδειξαν ότι η μέθοδος δεν μπορεί να εντοπίσει μικρούς στόχους μέσα σε μεγαλύτερα στρώματα λόγω της 1-D μορφοποίησης του προβλήματος.

Επιπλέον, αυτά τα δεδομένα χρησιμοποιήθηκαν για την σύγκριση των μεθόδων των πεπερασμένων στοιχείων και των πλευρικών περιορισμών και για την μελέτη των πλεονεκτημάτων και των μειονεκτημάτων της τελευταίας.

Συγκρίνοντας τις 2 μεθόδους είναι φανερό ότι και η μέθοδος των πλευρικών περιορισμών και της 2-D εξομαλυμένης δομής μπορούν να δώσουν μία αξιόπιστη προσέγγιση της πραγματικής εικόνας του υπεδάφους, ενώ με τον συνδυασμό τους επιτυγχάνεται μεγαλύτερη ακρίβεια.

Contents

List of Figures

List of Tables

1. INTRODUCTION

1.1 Motivations and aims of this thesis

Electrical Resistivity Tomography (ERT) is a popular geophysical technique with a wide range of applications. Geophysics, engineering, hydrology and archaeology are some of the fields in which the ERT method has been successfully used. The ERT method uses the geoelectrical characteristics of the subsurface in order to find its structure. This is achieved by acquiring measurements of the electrical resistivity of the subsurface and generating a 2-D image of its distribution.

As with any geophysical method, due to the fact that the earth is non-homogeneous, the measurements do not represent the true resistivity distribution of the subsurface and therefore, the interpretation cannot be performed directly. In contrast, they require complex processing in order to provide a 2-D image of the subsurface's true resistivity. The technological advances gave rise to many different processing methods. In most methods, the processing is handled using the inversion theory. For decades, the 2-D smooth-structure inversion schemes are used to interpret the data. These schemes provide a smooth geoelectrical model of the survey area. Despite the impressive results of the smooth-structure method, it cannot resolve accurately sharp layer boundaries. Thus, different schemes were in need, in order to overcome this limitation.

Recently, the laterally-constrained technique (LCI) has been proposed by Auken et al. (2002). This technique makes the assumption that the earth is consisted of horizontal layers and uses an 1-D scheme to locate sharp interfaces. Although, this method can resolve the sharp layer boundaries, it should not be consider as a substitute of the smooth-structure but as a supplement, which can provide significant information to the interpretation by combining the results and therefore, a better resolved geological model.

The LCI technique has been successfully used in sedimentary environments and other areas with a layered appearance (Auken et al., 2005; Wisén et al., 2005). Although, the LCI is mostly used for layered cases, it has been effectively used even in cases with significant 2-D structures (Auken and Christiansen, 2004). As this is a relative new technique, improvements and developments of the existing schemes can be made.

This thesis deals with inversion schemes of ERT data using the 1-D laterally-constrained method. The goal of this work is to provide an approach that will increase the accuracy of the inversion results.

The key objectives of the present thesis are:

- Present the inversion theory and review the existing techniques with focus given on the laterally-constrained scheme.
- Create a scheme for the LCI method which will increase the accuracy of the inversion results.
- Develop software for the proposed scheme.
- Use this software to evaluate the efficiency of the LCI scheme by processing real and synthetic data.

The methodology that was followed throughout this work is presented as follows:

- A detailed review of the basic principles of the electrical resistivity method and the surveying techniques with emphasis given on the electrical tomography.
- Study of the numerical modelling of ERT data, which is one of the most important tools for this project. Numerical modeling is essential not only for solving the inverse problem, but also to assess the performance of the ERT method and furthermore to evaluate the efficiency of the interpretation schemes. The algorithms can be tested using a wide range of different models and in different conditions. Also it is a means to explore the link between subsurface properties and the ERT data.
- In-depth examination of the inversion theory and techniques. Emphasis was given to the laterally-constrained inversion and the schemes that were proposed so far.
- Development of the software based on the existing LCI schemes.

- Formulation of a different approach for the LCI scheme and implementation into the previous algorithm. In particular, modifications were made in the way the constraints are imposed in the problem and also in the calculation of the lagrange multiplier.
- Testing of this new scheme with both synthetic and real data to find possible limitations and evaluate its efficiency.
- Comparison of the results from the LCI software with the DC2DPRO software, which uses a 2-D smooth structure scheme.
- Interpretation of the results and final assessment of the accuracy of the algorithm.

1.2 Structure of this thesis

The structure of this thesis is comprised of the following chapters:

Chapter 2: This chapter introduces the fundamental concepts that are necessary in order to understand the work behind the present thesis. The basic principles of the electrical resistivity method are presented. The equations that govern the flow of the electrical current into the earth are discussed and the concept of the apparent resistivity is introduced. Furthermore, the resistivity arrays and data acquisition techniques are explained. Finally, the instrumentation used to gather the resistivity measurements is descripted.

Chapter 3: The aim of this chapter is to provide the basic background of the inversion theory. The forward problem is addressed and ways of solving it are presented. A detailed description of the inversion procedure is given, as well as its key elements and problems. In addition, the inversion methods are discussed with emphasis given on the smoothness constrained scheme. First, the basic theory and the equations that lead to the correction of the model are presented. Then, the smoothness matrix and its formulation are described. Moreover, the lagrange multiplier and its role in constrained problems are introduced and the active constrained balancing method for finding its value is explained. Furthermore, the laterally-constrained inversion method, which is the main subject of this thesis, is descripted in detail.

Chapter 4: The modifications that were made to the LCI scheme are described and examples are used for justification. Also, the algorithm behind the software that was constructed is analytically descripted and every step of the procedure is explained. The algorithm is tested using both synthetic and real data in order to evaluate its efficiency. Numerical modeling is used to provide the synthetic data. The results are presented as images and discussed. Also, they are compared with the results acquired using a 2-D smooth-structure inversion scheme.

Chapter 5: This chapter summarizes the conclusions of this thesis and suggests future work.

2. BASIC PRINCIPLES OF THE ELECTRICAL RESISTIVITY METHOD

This chapter is a brief introduction of the basic theory of electrical resistivity method. The principles regarding the flow of the electric current into the earth are presented and the concepts of geometrical factor and apparent resistivity are introduced. In addition, the resistivity measuring techniques and the resistivity arrays are demonstrated. Finally, the instrumentation used for the acquisition of electrical resistivity data is described.

2.1 Introduction

Electrical Resistivity Method is one of the most widely used techniques belonging to a group called applied geophysics. Applied geophysics is a term used to describe a number of geophysical methods (Electrical Resistivity Method, GPR, Seismic Refraction-Reflection, Potential Field Methods and so on.) that are used to acquire information about the distribution of the subsurface's physical properties (electrical resistivity, dielectric properties etc.). Electrical Resistivity Method has a wide range of applications as it is extensively used for geophysical, geological, hydrological, environmental and engineering problems, as well as for archaeological investigations. For instance, it has been used in order to map mineral deposits and groundwater distribution, to locate fault zones etc.

The resistivity technique is used to map the distribution of the electrical resistivity (or conductivity) of the subsurface. This method belongs to a category called "active" methods, since the field, that is used, is created artificially, in contrast with "passive" methods, which use an existing field. An electric current is introduced into the ground and the potential difference due to this current is measured giving an indication of the resistivity of the subsurface. The interpretation of these measurements can reveal the subsurface's structure and the nature of the targets found.

When compared to other methods, the resistivity method has many advantages. The rapid data acquisition and the lower cost of the instruments than other methods are two of its benefits. Furthermore, the modern algorithms can provide an image of the resistivity distribution really fast, even in the field directly after gathering the measurements, while the interpretation of these results is relatively easy.

2.2 Ohm's law

In 1827, Georg Simon Ohm defined the relationship between the potential difference ΔV and the electric current I by using a parameter characteristic of a conductor called resistance R. This relationship describes the flow of electricity through a single conductor with two ends and is given by the mathematical equation:

$$I = \frac{\Delta V}{R} \tag{2.1}$$

Ohm's law states that the current passing through a conductor is directly proportional to the voltage across the two ends. The parameter R is defined as the ratio of the voltage to the current and its SI unit is Ohm (Ω).

The resistance of a material depends not only on its nature but also on its shape and size. It is convenient to introduce a quantity that depends only on the nature of the material. This quantity is called electrical resistivity ρ. The electrical resistivity of a cylinder with cross section A, length L and resistance R is given by the equation:

$$\rho = \frac{RA}{L} \tag{2.2}$$

where L is in meters, A is in square meters and R is in Ohms. The SI unit of resistivity is Ohm·meter (Ω·m).

As mentioned above, the aim of the resistivity method is to find the distribution of the geoelectrical resistivity of the subsurface by measuring the potential difference due to flow of electric current into the ground. The measured voltage reflects the difficulty with which the current flows through the subsurface and thus gives an indication of the ground's electrical resistivity ρ. The reciprocal of resistivity (1/ρ) is called conductivity and represents the ease with which the current flows through the earth and is measured in Siemens per meter (S/m).

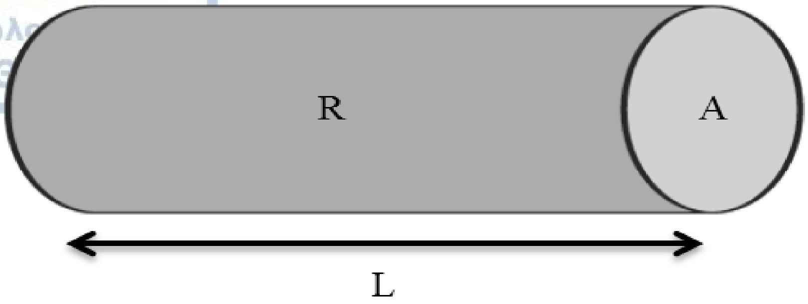

Figure 2.1: Electrical resistivity of a cylinder with resistance R, length L and cross section A.

The potential difference is given by the equation:

$$\Delta V = EL \tag{2.3}$$

where E is the intensity of the electric field. By substituting this equation to equation (2.1), Ohm's law becomes:

$$I = \frac{EL}{R} \tag{2.4}$$

The current density J is defined as the electric current per unit area of cross section:

$$J = \frac{I}{A} \tag{2.5}$$

The substitution of equation (2.4) to this equation yields:

$$J = \frac{EL}{AR} \tag{2.6}$$

From this equation and the equation for electrical resistivity the generalized Ohm's law is derived:

$$J = \sigma E \tag{2.7}$$

The intensity of the electric field E is the gradient of the electric potential V and thus can be written as:

$$E = -\nabla V \tag{2.8}$$

The minus sign denotes that the potential rise occurs when moving against the electric field. Ohm's law is now written as:

$$J = -\sigma \nabla V \tag{2.9}$$

By taking the divergence on both sides of this equation:

$$\nabla \cdot J = \nabla \cdot (-\sigma \nabla V) \tag{2.10}$$

Assuming that there are no sources or sinks into the medium, which is generally true for the earth's case, the divergence of the current density is zero:

$$\nabla \cdot J = 0 \tag{2.11}$$

And thus:

$$\nabla \cdot (-\sigma \nabla V) = 0 \tag{2.12}$$

From vector analysis, equation (2.12) can be written as:

$$\nabla \cdot (-\sigma \nabla V) = -\frac{\partial(\sigma \nabla V)}{\partial x} - \frac{\partial(\sigma \nabla V)}{\partial y} - \frac{\partial(\sigma \nabla V)}{\partial z}$$

$$= -(\nabla V \cdot \nabla \sigma + \sigma \nabla^2 V) = 0 \tag{2.13}$$

This equation is one form of the so called Poisson's equation and governs the flow of electric current in an inhomogeneous ground. In case of an electrically homogeneous ground, where $\nabla\sigma = 0$, the equation becomes:

$$\nabla^2 V = 0 \tag{2.14}$$

This is called Laplace's equation and it applies only to homogeneous earth.

2.3 Poisson's equation for homogeneous earth

As mentioned above Poisson's equation yields Laplace's equation for homogeneous earth. This equation can be used to find the potential at every point of the space while having a current point source on the surface of a homogeneous ground. Because of the spherical symmetry of the current flow, it is convenient to write the equation in spherical coordinates (r,θ,φ):

$$\frac{1}{r^2}\frac{\partial}{\partial r}\left(r^2\frac{\partial V}{\partial r}\right)+\frac{1}{r^2 sin\theta}\frac{\partial}{\partial \theta}\left(sin\theta\frac{\partial V}{\partial \theta}\right)+\frac{1}{r^2 sin^2\theta}\frac{\partial^2 V}{\partial \varphi^2}=0 \qquad (2.15)$$

where r is the distance from the source point. Also due to the spherical symmetry the derivatives with respect to the angles θ and ψ can be eliminated and thus the equation is reduced to:

$$\frac{1}{r^2}\frac{\partial}{\partial r}\left(r^2\frac{\partial V}{\partial r}\right)=0 \implies$$

$$\frac{\partial}{\partial r}\left(r^2\frac{\partial V}{\partial r}\right)=0 \qquad (2.16)$$

By integrating:

$$\int \frac{\partial}{\partial r}\left(r^2\frac{\partial V}{\partial r}\right)dr=\int 0dr \implies$$

$$r^2\frac{\partial V}{\partial r}=C \implies \frac{\partial V}{\partial r}=\frac{C}{r^2} \qquad (2.17)$$

With further integration:

$$\int \frac{\partial V}{\partial r}dr=\int \frac{C}{r^2}dr \implies$$

$$V=-\frac{C}{r}+D \qquad (2.18)$$

where C,D are constants.

Constant D equals zero because V should be zero when r reaches infinity. Since the medium is homogeneous, the current flows radially away from the point source. The equipotential lines form a hemisphere surface and the current flow is perpendicular to the equipotential surface. The current density J crossing the hemisphere surface of radius r is given by:

$$J = \frac{I}{2\pi r^2} = \sigma E \tag{2.19}$$

$$E = -\frac{\partial V}{\partial r} = -\frac{C}{r^2} \Longrightarrow$$

$$\frac{J}{\sigma} = -\frac{C}{r^2} \Longrightarrow J\rho = -\frac{C}{r^2} \Longrightarrow$$

$$\frac{I\rho}{2\pi r^2} = -\frac{C}{r^2} \Longrightarrow$$

$$C = -\frac{I\rho}{2\pi} \tag{2.20}$$

The substitution of C to equation (2.18) yields the equation of the potential at every point of a homogeneous space with a point source on surface:

$$V = \frac{I\rho}{2\pi r} \tag{2.21}$$

Thus, the potential varies inversely with the distance from the source. The equipotential lines and the direction of the electrical current for a point source in a homogeneous ground are shown in figure (2.2).

When the point source is within the homogeneous ground and not on the surface, the equation becomes:

$$V = \frac{I\rho}{4\pi r} \tag{2.22}$$

For more than one source the potential is given as the sum of the individual potentials due to all the current sources:

$$V = \sum_{i=1}^{n} \frac{I_i \rho}{2\pi r_i} \tag{2.23}$$

In practice, at least two current electrodes are required, a positive and a negative current source, as a single electrode cannot introduce current into the ground. The positive electrode A sends current I into the earth and the negative B receives the returning current. The potential measured at a point P is thus the algebraic sum of the individual potentials due to each one of the two current sources:

$$V_p = \frac{I\rho}{2\pi r_A} + \frac{-I\rho}{2\pi r_B} = \frac{I\rho}{2\pi}\left(\frac{1}{r_A} - \frac{1}{r_B}\right) \tag{2.24}$$

where r_A, r_B are the distances from point P to electrodes A and B, respectively.

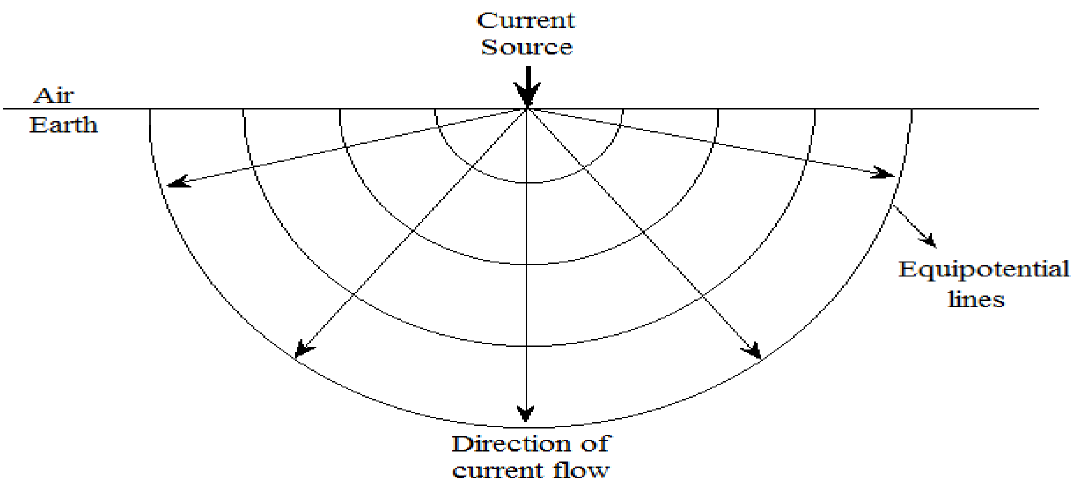

Figure 2.2: The equipotential surfaces and the direction of the electrical current in case of a point source.

In order to measure the potential difference due to current flow two electrodes are needed as well. The two current electrodes could be used also to measure the potential but due to high contact resistances between current electrodes and the ground, two different electrodes are used. The contact resistance is the resistance that current faces in order to be inserted into the ground due to small air gaps and is different from the resistivity, which is a physical property of the ground.

Therefore, in a resistivity survey four electrodes are used, two current (A and B) and two potential electrodes (M and N). The potential difference between M and N due to A and B will be:

$$\Delta V = V_M - V_N = \frac{I\rho}{2\pi}\left(\frac{1}{AM} - \frac{1}{BM} - \frac{1}{AN} + \frac{1}{BN}\right) = \frac{I\rho}{2\pi} G \qquad (2.25)$$

Solving the equation (2.25) for ρ:

$$\rho = 2\pi \frac{\Delta V}{I} \frac{1}{G} = 2\pi \frac{R}{G} \qquad (2.26)$$

where:

ΔV = the potential difference

R = the resistance

I = the intensity of the current

ρ = the resistivity

AM, BM, AN, BN = the distances between the electrodes

G = the geometrical factor

The first term (R=ΔV/I) shows the resistivity's dependence on the geoelectrical structure of the subsurface, while the second term, called geometrical factor, shows its dependence on the way the electrodes are arranged. In case of a homogeneous ground, the equation (2.26) yields the true resistivity of the subsurface.

2.4 Apparent Resistivity

Equation (2.26) is valid only when the ground is homogeneous. However, in reality the earth is non-homogeneous and thus, this equation does not yield the true electrical resistivity of the subsurface but an "apparent" value of the resistivity, which would be equal to the true resistivity if the ground was geoelectrically homogeneous. This value is called apparent resistivity and is denoted by ρ_α. Robinson (1988) describes the apparent resistivity as a weighted average of the true resistivities of the formations that constitute the subsurface. Although, this definition is by no means mathematically true, it is accepted when it comes to the interpretation of simple problems.

Therefore, this quantity does not represent the real but a distorted image of the geoelectrical structure of the subsurface and thus, the interpretation should not be made using the measurements of apparent resistivity, directly. Instead, the apparent resistivity measurements are used to retrieve the true resistivity distribution. This is achieved by a complex process called inversion, which is described in a later chapter. After inversion, the results can then be interpreted and information about the subsurface's structure can be acquired.

2.5 Electrical properties of materials

The electric current can be conducted into the earth via three ways:

- **Electronic conduction:** In this conduction the electric current is flowing via the crystalline structure (free electrons) of some materials, such as metals. This conduction is important when conductive minerals are present.
- **Electrolytic conduction:** The electric current is propagating through the ions of the groundwater which fills the pores of the rocks or soil. It is the most common mechanism of conduction of the electric current in the ground.
- **Dielectric conduction:** An alternating electric current can cause a cyclic movement in the ions of the crystalline structure of an electrical insulator. This movement produces secondary alternating current. This conduction is considered to be negligible.

The electrical resistivity is one of the most variable geophysical quantities due to the fact that it is dependent on a large number of factors. The most important factors are:

a) The porosity of the rocks and the possible fractures

b) The amount of water

c) The chemical composition and salinity of water

d) Temperature and pressure

Since these parameters are very variable, a certain rock type can have a wide range of resistivity values, from a few Ohm·m to millions. Thus, similar formations can appear with completely different resistivities and different formations with similar resistivities, making it difficult to distinguish different rock types. Therefore, resistivity values cannot be correlated with certain lithological types and only relative conclusions should be made when interpreting the data. Prior information, such as geological data or data from other geophysical methods, should be used in order to achieve better interpretations.

Material	Resistivity (Ohm•m)	Conductivity (S/m)
Clay	1-100	0.01-1
Alluvium	$10\text{-}10^{3}$	$10^{-3}\text{-}10^{-1}$
Sandstone	$10\text{-}10^{3}$	$10^{-3}\text{-}10^{-1}$
Limestone	$10^{2}\text{-}10^{4}$	$10^{-4}\text{-}10^{-2}$
Granite	$5\cdot10^{3}\text{-}10^{6}$	$10^{-6}\text{-}10^{-3}$
Basalt	$10^{3}\text{-}10^{7}$	$10^{-7}\text{-}10^{-3}$

Table 2.1: Typical resistivity values of different rock types.

Typically, igneous and metamorphic rocks have high resistivities, whilst sedimentary rocks have lower values due to the fact that they are more porous and have larger quantities of water. Unconsolidated sediments have even lower resistivities because the porosity is higher. Typical resistivity values of different rock types are shown in Table (2.1).

The resistivity of water ranges from about 0.1 to 200 Ohm·m depending on its salt content. Generally, low resistivities (<10 Ohm·m) are indicative of salted water, while 20-100 Ohm·m are typical values of potable water. Metallic minerals have extremely low resistivity values, usually lower than 1 Ohm·m.

2.6 Resistivity Arrays

There are many different ways to arrange the electrodes in a resistivity survey. The main feature of each array is its geometrical factor, which is uniquely related to the distances between the electrodes. In practice, only a few of them are being used as they have both theoretical and practical benefits, in contrast to others that have practical drawbacks despite their theoretical advantages. Most of the arrays offer an internal symmetry and the electrodes are placed across a line.

In each case, the choice of a specific array depends on the survey requirements, the targeted depth of investigation and resolution and the environmental setting of the area that the survey is taking place. The most widely used arrays are presented below:

a) Wenner: In this array the potential electrodes M, N are placed between the current electrodes A,B. The distances between adjacent probes are equal (α). Thus, the geometrical factor equals:

$$G = \left(\frac{1}{a} - \frac{1}{2a} - \frac{1}{2a} + \frac{1}{a}\right) = \frac{1}{a} \tag{2.27}$$

By substituting this in equation (2.26) we get the apparent resistivity for the Wenner array:

$$\rho_\alpha = 2\pi\alpha\frac{\Delta V}{I} \tag{2.28}$$

b) Schlumberger: The Schlumberger configuration is similar to Wenner. The potential probes are again placed between the current electrodes, but the distance between the current probes is much greater than the separation between the potential probes. If the distance between the current probes is 2L, then the distance between potential electrodes is 2l with L>>l and the apparent resistivity equals:

$$\rho_\alpha = \frac{\pi L^2}{2l}\frac{\Delta V}{I} \tag{2.29}$$

c) Dipole-Dipole: In this configuration the dipole with the current electrodes is placed at a large distance from the dipole with the potential electrodes. The separation of each dipole equals α, whereas the distance between them equals nα. This yields the following apparent resistivity:

$$\rho_\alpha = -\pi n(n+1)(n+2)\alpha \frac{\Delta V}{I} \tag{2.30}$$

d) Pole-Dipole: In Pole-Dipole the potential electrodes are between the current electrodes, but one of the current electrodes is placed at a great distance from the other three. For instance, if the remote current electrode is B, then the distances BM, BN are considered to be infinite and as a result the terms 1/BM and 1/BN in the geometrical factor are considered to be negligible and are set to zero. If the distance between the potential probes MN is α and the distance AM between current probe A and potential probe M is nα, then the apparent resistivity equals:

$$\rho_\alpha = 2\pi n(n+1)\alpha \frac{\Delta V}{I} \tag{2.31}$$

e) Pole-Pole: This array is similar to Pole-Dipole and is achieved by placing not only a current electrode but also a potential electrode, for example N, at a sufficient far distance from the remaining two electrodes. Therefore, the distances BM, BN and AN are considered to be infinite and if AM=a, the geometrical factor becomes the 1/α. Thus, this array has the same geometrical factor as the Wenner array and so, apparent resistivity is the same:

$$\rho_\alpha = 2\pi\alpha \frac{\Delta V}{I} \tag{2.32}$$

f) Twin-probe: This is a variation of the Pole-Pole array and it is achieved by placing the two remote electrodes B and N closely together. The distance between these two electrodes is not considered infinite now and the apparent resistivity value becomes:

$$\rho_\alpha = 2\pi \frac{\alpha b}{\alpha + b} \frac{\Delta V}{I} \qquad (2.33)$$

Where b = distance BN.

g) Multiple Gradient: This is a relatively new array (Dahlin and Zhou, 2006). The potential electrodes are placed between the current electrodes. The current is injected by two electrodes with spacing (s+2)α and the potential differences between all the possible dipoles of potential electrodes with spacing α are measured sequentially. As seen in Figure (2.3), the terms in geometrical factor for this array are:

$$\begin{aligned} &AM=n\alpha \\ &AN=(n+1)\alpha \\ &BM=(s+2-n)\alpha \\ &BN=(s+1-n)\alpha \end{aligned} \qquad (2.34)$$

where s is the maximum number of potential measurements for a specific current injection.

Each array has some benefits and some drawbacks when compared to the others. Due to the fact that they have different internal geometry, they are sensitive to different types of variation of the resistivity. For instance, Wenner and Schlumberger arrays are more sensitive to variations with depth, while the dipole arrays are more sensitive to lateral changes. Ward (1990) evaluated a number of resistivity arrays based on 14 criteria. The most important of them are shown in Table (2.2).

Array	S/N ratio	Lateral Resolution	Resolution with depth
Wenner	1	4	1
Schlumberger	2	3	1
Dipole-Dipole	4	1	2
Pole-Dipole	3	2	2
Code: 1 = Best, 4 = Worst			

Table 2.2: Evaluation of the most widely used arrays using three criteria (after Ward, 1990).

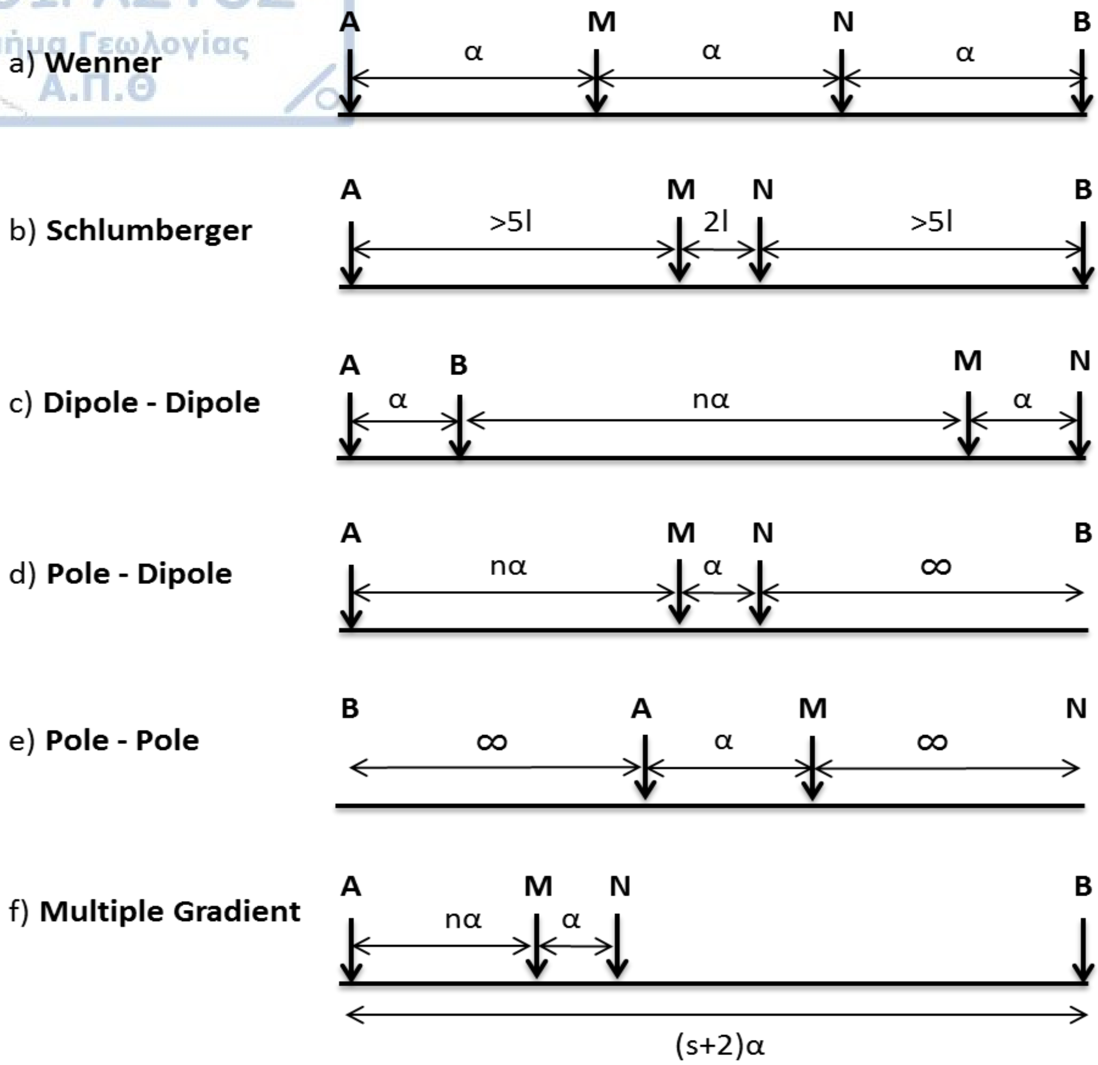

Figure 2.3: Widely used resistivity arrays: a) Wenner, b) Schlumberger, c) Dipole-Dipole, d) Pole-Dipole, e) Pole-Pole, f) Multiple Gradient

2.7 Measuring Modes

There are three measuring modes used to acquire the resistivity data, depending on the desired type of resistivity variations (with depth, lateral or both). These are: Vertical Electrical Sounding (VES), Lateral Profiling and Electrical Resistivity Tomography (ERT).

a) Vertical Electrical Sounding (VES): With the VES technique the variations of resistivity with depth are located, considering the ground to be consisted of horizontal layers (1D survey). In this case the resistivity is assumed to change vertically but not in the horizontal direction. This method is achieved by taking a series of measurements while keeping the distance between the potential electrodes, as well as the center of the array, fixed and increasing gradually the spacing between the current electrodes. While the spacing between the current electrodes is increased, the penetration depth is also increased and therefore, information about how resistivity changes in deeper parts of the subsurface, below the center point, is obtained. It is really difficult to define an absolute value for the penetration depth. In practice, it is assumed to be the 1/3-1/4 of the spacing AB between the current probes. For this method arrays with internal symmetry are used, with the Schlumberger array being the most common.

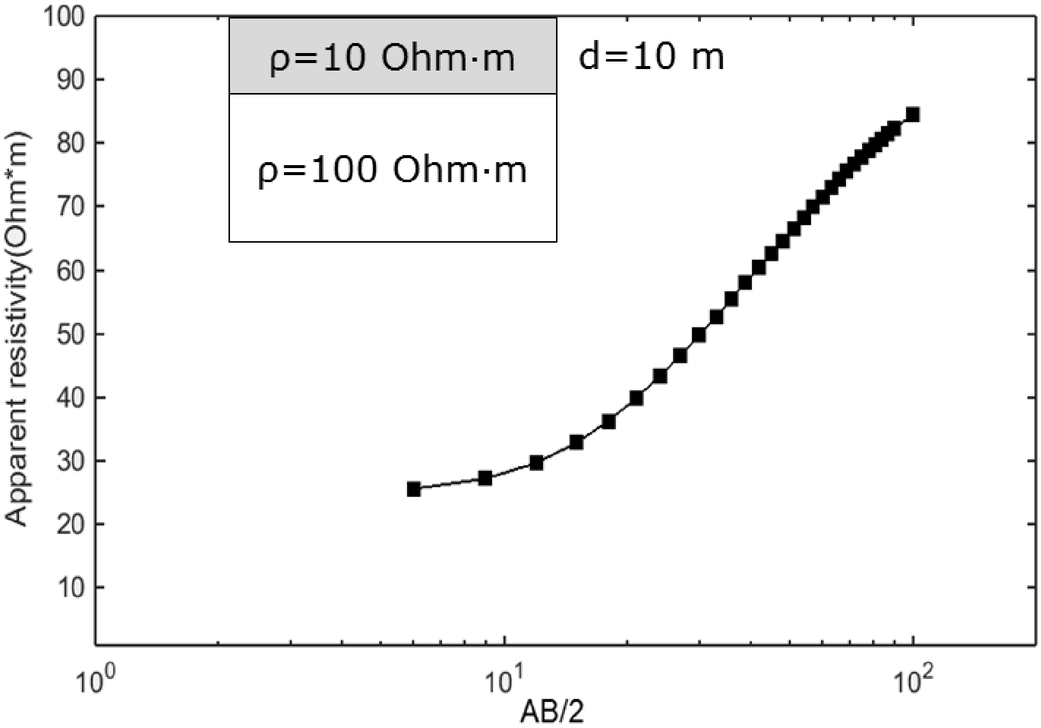

Figure 2.4: Example of an apparent resistivity curve constructed from VES data for a two-layer model with resistivity ρ=10 Ohm·m and thickness d=10m for the first layer and ρ=100 Ohm·m for the half-space.

While conducting a VES, the distance AB is constantly increasing, starting from a few meters to hundreds of meters or even reaching above one kilometer. The spacing between the potential electrodes remains fixed until the value of the potential becomes very small due to sufficiently great distance between the current probes.

Subsequently, the measured apparent resistivities are plotted versus the AB/2 distances and thus, the apparent resistivity curve is constructed.

An example of an apparent resistivity curve using the VES data is presented in figure (2.4). This curve corresponds to a two-layer model or one layer and half-space model. The resistivity and the thickness of the first layer are ρ=10 Ohm•m and d=10m, respectively and the resistivity of the half-space is ρ=100 Ohm•m. The penetration depth is approximately 60m, as shown from the graph. It is noted that this curve might correspond to other models as well.

b) Lateral Profiling: In this method, a series of measurements are taken while keeping the distance between all electrodes fixed and moving the entire array in a lateral direction. Therefore, with profiling, only lateral changes in resistivity are located, at a fixed depth, as the spacing between the current probes remains steady. In this procedure the most frequently used arrays are Wenner, Dipole-Dipole and Pole-Dipole.

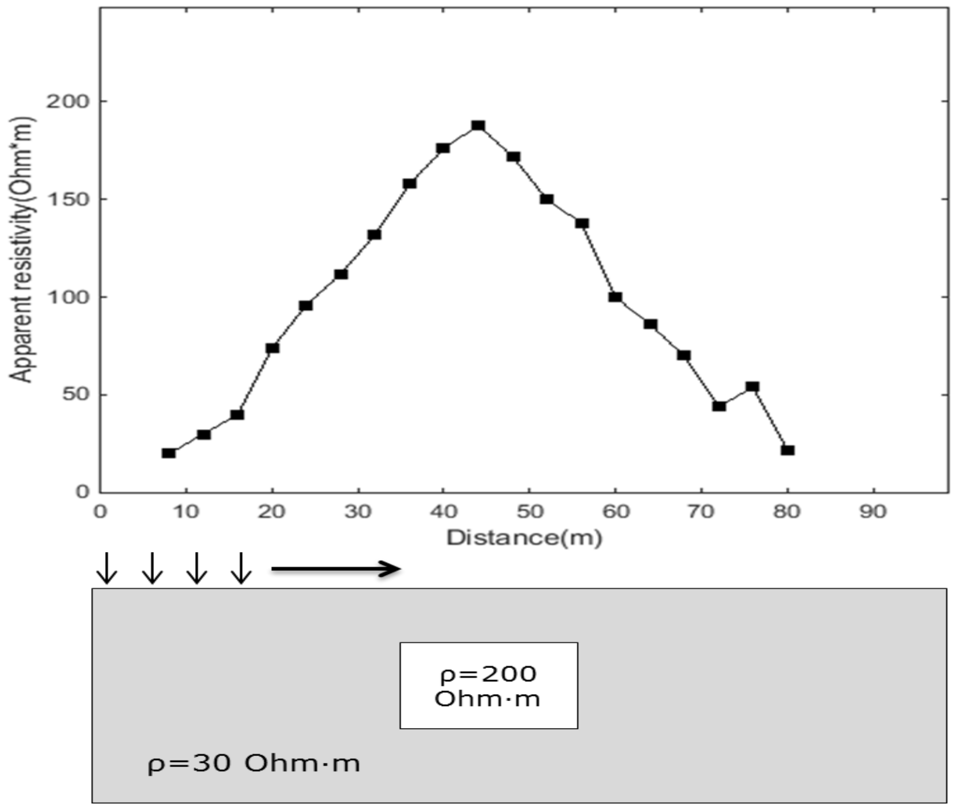

Figure 2.5: Example of an apparent resistivity curve constructed from lateral profiling data for a medium with resistivity ρ=30 Ohm·m with a smaller buried body with ρ=200 Ohm·m.

An example of an apparent resistivity curve constructed from lateral profiling data for a medium with resistivity ρ=30 Ohm•m with a smaller buried body with ρ=200 Ohm•m is shown in figure (2.5). The curve starts with low resistivities depicting the effect of the conductive medium. While moving towards the resistive body, which is close to the center of the profile line, the resistivity values are increasing, showing that the measurements are taking into account the effect of the resistive body, too. When moving away from this body, the resistivity is decreasing. The penetration depth is equal to the depth of the bottom surface of the resistive block and remains constant.

c) Electrical Resistivity Tomography (ERT): The electrical resistivity tomography is actually a combination of VES and profiling methods. With this mode information about changes in resistivity with depth, as well as about lateral changes is acquired and thus, the limitations of the previous measuring modes are overcome. The geoelectrical model of the subsurface is now considered to be two-dimensional (2-D), which is more accurate.

Figure (2.6) shows an example of a sequence of measurements using 20 electrodes and the Wenner array. First, all the possible measurements with a probe spacing of “1a” are made. The first measurement (data 1 in Figure 2.6) is collected using the electrodes with number 1, 2, 3 and 4, as shown in the figure. Electrodes 1 and 4 are used as current electrodes, while electrodes 2 and 3 are used as potential electrodes. For the second measurement, electrodes 2, 3, 4 and 5 are used as A, M, N, and B, correspondingly. After collecting all the measurements with spacing “1a”, the next sequence with spacing “2a” is made. The electrodes 1, 3, 5 and 7 are used for the first measurement (data 18 in Figure 2.6) with spacing 2a. This process is repeated until all the possible measurements for all the possible spacings are obtained. It is obvious that as the spacing between the electrodes increases, the number of data decreases. In practice it is really important not to use an electrode that has been used as a current electrode as a potential electrode in a short time frame, in order to avoid electrode polarization effects. Thus, the sequence of measurements should be chosen carefully.

ERT is the most widely used technique today. One of the main features of this method is that a large number of data is obtained. The recent advances in the instrumentation allowed the rapid collection of this large amount of measurements, which can be processed with the efficient interpretation algorithms that have also been developed the last decades.

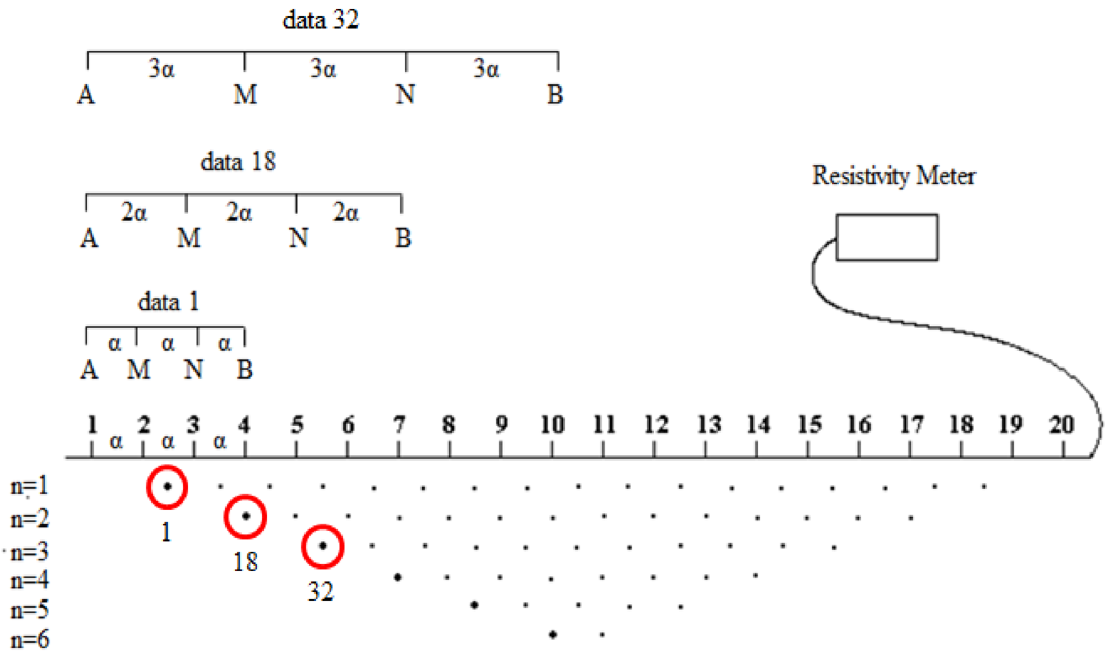

Figure 2.6: Electrical Resistivity Tomography survey.

The interpretation of the ERT data is commonly carried out by advanced algorithms called inversion schemes, which reconstruct reliably the image of the true resistivity distribution. These schemes will be presented analytically in the following chapters.

2.8 Resistivity Instrumentation

Electrical Resistivity Tomography surveys are usually carried out using a large number of probes, 20 and more, which are connected to a multi-core cable. The instruments used to measure the resistivity are called resistivity meters. These instruments measure the resistance R, which is the ratio of the voltage to the intensity of the inserted current. Subsequently, the apparent resistivity is found.

The resistivity meters contain an internal microprocessor, which along with a switching unit is used to select the four (or more for modern instruments) electrodes for each measurement. The type of the array, the sequence of measurements and other parameters of the survey are transferred within the resistivity meter from a computer.

The design of the measuring system is different on each instrument, depending on the purpose of the survey. For instance, archaeological problems require a system with different specifications from geological applications (e.g. small output voltage is required for shallow surveys in archaeology, whereas large output voltage is required to reach greater depths in geological applications).

3. RESISTIVITY INVERSION PROBLEM

In this chapter the resistivity inversion problem is addressed. Inversion schemes are used in order to find the true distribution of the subsurface's resistivity and provide an accurate interpretation of the data. The theoretical background and the basic elements of the inversion are discussed. In addition, the limitations of this method are presented.

Before addressing the inverse problem, the forward problem is introduced, as the solution to the forward problem is essential for finding a solution to the inverse problem.

3.1 Forward Problem

Generally, the forward problem (forward modelling) is the procedure of obtaining the measurements, while the model is known. In case of resistivity, it is the process of finding the potential differences, due to current injection, of a known resistivity distribution. In other words, it is the solution of the equations that govern the flow of the electrical current into the subsurface for a particular resistivity distribution and current source in order to find the potential distribution and thus, the apparent resistivities that respond to this specific model. The model is an idealized mathematical representation of a part of the earth. It has a set of parameters, which are physical quantities. For the resistivity method, these parameters are the resistivity and thickness of each layer.

Many different methods of solving the forward model have been developed. These are divided into two categories, the analytical and the numeric approach:

a) Analytical approach: In the analytical approach, the field equations are directly solved. The formulation of these equations is difficult due to their complexity and thus they are not used in practice. Fully analytical methods have been used only for simple cases, such as a sphere in a homogeneous medium.

b) Numerical approach: For an arbitrary resistivity distribution, which exists in reality, numerical approaches are used. The numerical techniques are subdivided into two categories. The first one is based on differential methods and the other on integration methods.

In case of 1-D survey, the filter method (Koefoed, 1979) is used to solve the forward problem, whereas for the 2-D and 3-D cases, the finite element method and the finite difference method are used.

The forward problem can be denoted as:

$$d = T(x) \tag{3.1}$$

where: $d=\{d_1,d_2,\ldots,d_M\}$ is a vector with M elements, which contains the observed apparent resistivities

$x=\{x_1,x_2,\ldots,x_N\}$ is a vector with N elements, which contains the model parameters, that is resistivity and thickness for the resistivity case and

T is the transformation equation used to find the response to the model x.

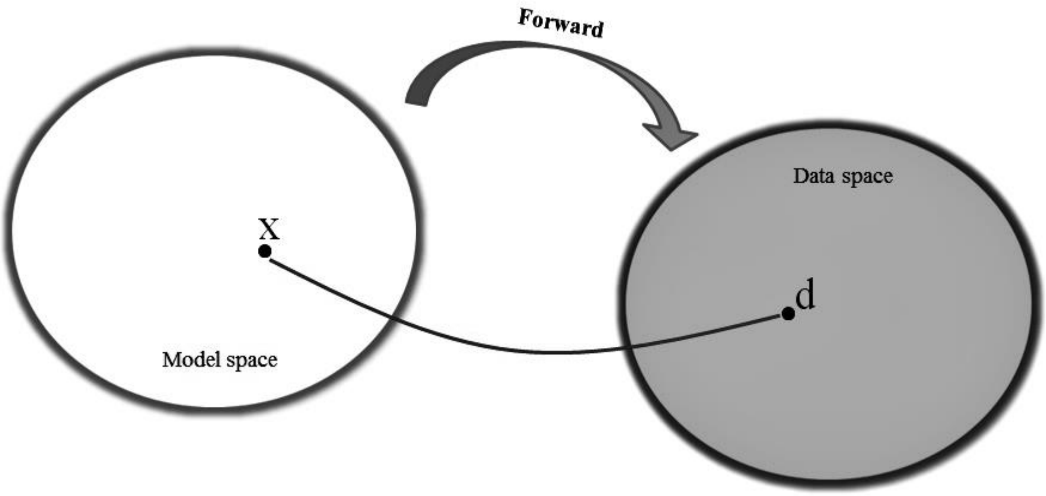

Figure 3.1: Forward Problem.

3.1.1. 1-D Resistivity Forward Modeling

For the 1-D case, where the subsurface is assumed to be consisted of horizontal layers, Stefanesco (1930) expressed the potential due to a point source of current in the form of a Hankel integral, which is a product of a Bessel function and a function dependent on the layer parameters called the kernel function. Koefoed (1968) modified his solution by introducing a new function called the resistivity transform, which is related to the kernel function. Using the Schlumberger array in Koefoed's method, as it is the most commonly used in soundings, the apparent resistivity ρ_α is given by the equation:

$$\rho_\alpha = \left(\frac{AB}{2}\right)^2 \int_0^\infty T_1(\lambda) J_1\left(\frac{AB}{2}\lambda\right) \lambda d\lambda \tag{3.2}$$

where AB is half the electrode spacing

J_1 is the first-order Bessel's function of the first kind

λ is a Hankel transform variable and

T_1 is the resistivity transform

The resistivity transform, which is a function of the layer parameters only, can be calculated recursively as:

$$T_{i-1} = \frac{T_i + \rho_{i-1} \tanh(\lambda t_{i-1})}{1 + T_i \tanh(\lambda t_{i-1}) / \rho_{i-1}} \tag{3.3}$$

where ρ_i and t_i are the resistivity and the thickness of the i layer, respectively. For the half-space $T_N=\rho_N$, where N is the number of layers.

It is common to use the linear filter method (Ghosh, 1971; Koefoed, 1979) in order to evaluate the equation for the apparent resistivity and thus equation (3.2) can be rewritten as:

$$\rho_\alpha = \sum_K T_1(\lambda_K) f_K \tag{3.4}$$

where f_K are the coefficients of the filter and K is the number of coefficients.

3.1.2 2-D Resistivity Forward Modeling

In the 2-D case, the forward problem needs to be discretized and solved at certain points. The most popular methods, which achieve this, are the Finite Element

Method (Pridmore et al, 1981; Sasaki, 1994; LaBrecque et al, 1996; Tsourlos and Ogilvy, 1999; Pain et al, 2002; Yi et al, 2001) and the Finite Difference Method (Ellis and Oldenburg, 1994; Park and Van, 1991). Both methods subdivide the subsurface into different regions.

In the Finite Difference Method (FDM) the subsurface is subdivided into rectangular cells. Each cell is related to a point to which a resistivity value is attributed. Therefore, a grid of distinct points is formed at which the potential must be calculated.

In the Finite Element Method (FEM) the area is subdivided into elements, in which the unknown potential is approximated by simple interpolation functions linked to specific points of the element called nodes.

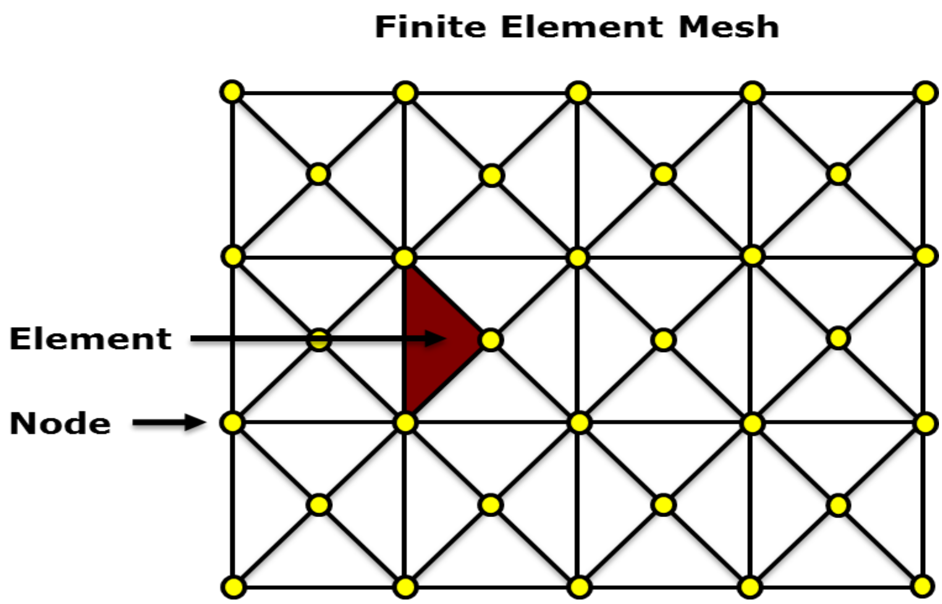

Figure 3.2: Example of a finite element mesh.

One advantage of this method compared to FD is that FEM can handle structures with irregular shape, which is of great importance as the resistivity is sensitive to topography. The elements share common nodes and thus, the element equations can be combined into a single set of linear equations, which will have the form:

$$\boldsymbol{K} \cdot \boldsymbol{V} = \boldsymbol{F} \tag{3.5}$$

where **K** is the stiffness matrix (which contains the nodal coordinates)

V is matrix containing the nodal potential, and

F contains the current sources and boundary terms.

By solving this system of equations, the vector **V** with the potential at each node, can be obtained.

3.2 Inversion Procedure

Now that the forward problem has been introduced, the inverse problem can be defined. Inversion is exactly the inverse process of the forward problem: to find a model that responds to given measurements. In case of resistivity, that is to find the true resistivity distribution of the subsurface given the data-set with the apparent resistivity measurements that are collected through a geophysical survey. The inverse problem can be defined as:

$$x = T^{-1}(d) \tag{3.6}$$

where T^{-1} is the inverse transformation function.

The purpose of inversion is to find a geoelectrical model that gives a response that best fits the observed apparent resistivities. The model generates synthetic measurements by solving the forward problem and thus having a robust way of solving it, is needed.

Equation (3.6) cannot be solved with inversion directly due to its non-linearity. In order to handle this problem, the inversion schemes use an iterative process. A typical algorithm starts by defining an initial resistivity model x_o, which is consecutively corrected through the iterative process until the synthetic data that correspond to this model f(x) fit the observed data d. Assuming a really small change in resistivity, dx, we can expand f(x) in Taylor series:

$$f(x_i + dx_i) = f(x_i) + \frac{\partial f(x_i)}{\partial x_i} dx_i + O((dx_i)^2) \qquad i = 1,2,\dots,N \tag{3.7}$$

where $O((dx_i)^2)$ represents the higher order terms and N is the number of the model parameters. Because dx is considered to be a very small change, the higher order terms can be neglected. The term $\partial f(x_i)/\partial x_i$ expresses the Jacobian matrix with dimensions MxN, which will be discussed in a following section. Hence, equation (3.7) can be rewritten as:

$$f(x + dx) = f(x) + Jdx \tag{3.8}$$

Thus, an iterative scheme can be defined as: At first an initial model x_o is chosen and its forward response is calculated. Afterwards, the degree of fit between the observed and the calculated data is found. If this degree is satisfying or any of the other stopping criteria is met, the iteration procedure terminates. Otherwise, the correction of the model dx_k is calculated, where k is the iteration number, and this correction is added to the previous model, that is $x_{k+1}=x_k+dx_k$. Then, the forward is calculated for the new model and the iterations continue until one of the stopping criteria is satisfied.

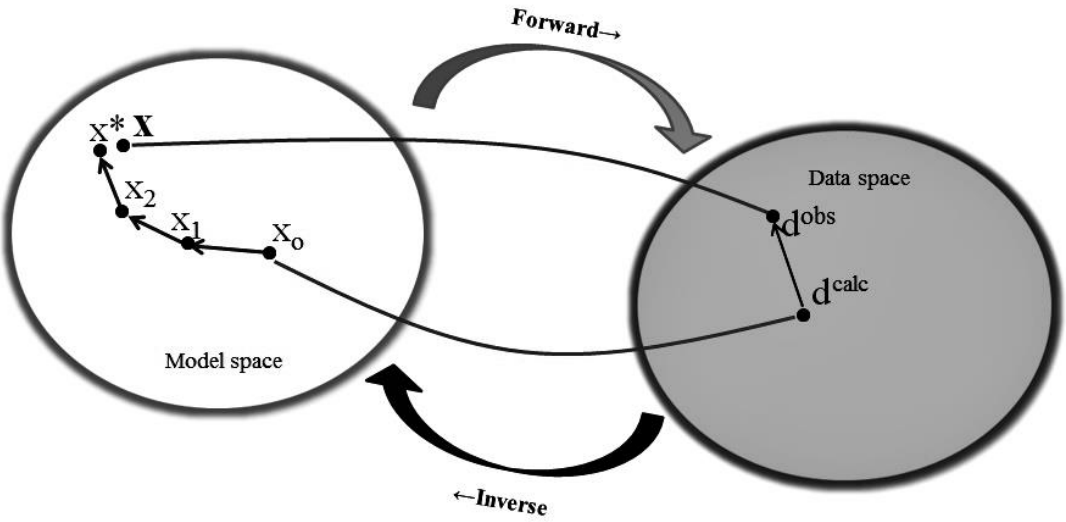

Figure 3.3: Graphical representation of the inverse problem. An initial model, x_o, is corrected through iterations until an optimal model, x*, is reached, which produces synthetic data, d^{calc}, that best fit the observed data, d^{obs}. The observed data is the response of the unknown true model x.

3.3 Problems in inversion

Most inverse problems in geophysics belong to the category of ill-posed problems. According to Hadamard (1902) a problem is well-posed if:

- It has a solution
- The solution is unique
- The solution changes proportionally to the initial conditions

Based on these three conditions, the inversion schemes have to handle the following three problems:

a) Existence of a solution: It is possible there is no model that can fit the data, that is that the forward calculation cannot result to similar apparent resistivities with the observed data. This might be due to noise in the data and the error of the model or due to the method used to find the model.

b) Uniqueness of the solution: If a solution exists, this might not be the only one. Many models could fit the same data-set.

c) Instability of the solution: Inversion is an ill-posed procedure, meaning that small changes in the data could lead to great changes in the model obtained by the solution. As a result, the acquisition of accurate data is of great importance.

3.4 Stopping criteria

As mentioned above, in the inversion procedure the degree of fit between the observed and the synthetic apparent resistivities needs to be found. This is done by calculating the relative Root Mean Square (RMS) error, which is given by the following equation:

$$RMS = \sqrt{\frac{1}{M}\sum_{i=1}^{M}\frac{(d_i^{obs}-d_i^{calc})^2}{(d_i^{obs})^2}} \tag{3.9}$$

where d_i^{obs} are the real measurements, d_i^{calc} are the synthetic measurements and M is the number of data. In an iterative process, like inversion, the RMS error can be used as a stopping criterion. Specifically, the inversion terminates if one of the following criteria is met:

a) Divergence: The iteration algorithm terminates if the relative RMS error between the synthetic data resulting from the inversion and the real data increases in the next iteration. Divergence is observed rarely, mostly in cases where the noise in the data is great or due to very wrong choice of lagrange multiplier, which is used to control the constraints in the inverse problem and will be discussed in a later chapter.

b) Small improvement: The procedure stops if there is no significant improvement in the error between calculated and observed data in the next iteration, meaning that the RMS decreases at a small rate. It is true that the iteration procedure could be continued, but it is possible for the synthetic data to fit the noise and not the actual useful information.

c) Maximum number of iterations: Inversion terminates if the predefined maximum number of iterations is reached.

3.5 Jacobian Matrix

From equation (3.8), it is obvious that the use of a matrix with first-order derivatives is necessary. This matrix is called Jacobian matrix J and it is necessary for most inversion schemes. Jacobian matrix relates the changes in the model parameters with the changes of the observed data. It is also called sensitivity matrix, as it depicts the sensitivity of the apparent resistivity measurements to small variations in the model parameters.

If M is the number of measurements, d, and N is the number of the model parameters, x, then the Jacobian matrix J has M×N dimensions and its i,j elements are given by:

$$J_{ij} = \frac{\partial d_i}{\partial x_j} \tag{3.10}$$

If the observed data are apparent resistivities, equation (3.10) can be rewritten as:

$$J_{ij} = \frac{\partial \rho_{\alpha i}}{\partial \rho_j} = -\frac{\partial \rho_{\alpha i}}{\partial \sigma_j} = \frac{2\pi}{GI}\frac{\partial \Delta V_i}{\partial \sigma_j} \tag{3.11}$$

where ρ_α is the apparent resistivity

ρ is the model parameter

G the geometrical factor

I the current intensity

ΔV the potential difference and

σ the conductivity.

In matrix form, equation (3.11) can be written as:

$$J = \begin{bmatrix} \frac{\partial\rho_{\alpha1}}{\partial\rho_1} & \frac{\partial\rho_{\alpha1}}{\partial\rho_2} & \cdots & \frac{\partial\rho_{\alpha1}}{\partial\rho_{jN}} \\ \frac{\partial\rho_{\alpha2}}{\partial\rho_1} & \ddots & \cdots & \frac{\partial\rho_{\alpha2}}{\partial\rho_N} \\ \vdots & \cdots & \ddots & \vdots \\ \frac{\partial\rho_{\alpha M}}{\partial\rho_1} & \frac{\partial\rho_{\alpha M}}{\partial\rho_2} & \cdots & \frac{\partial\rho_{\alpha M}}{\partial\rho_N} \end{bmatrix} \tag{3.12}$$

Generally, there are three methods that can be used to calculate the Jacobian matrix (McGillivray and Oldenburg, 1990): a) The sensitivity method, b) The adjoint equation method and, c) The perturbation technique. In this thesis the perturbation method, which is presented in the following section, was used.

3.5.1 The Perturbation Technique

The perturbation approach gives an approximation of the sensitivities using a finite-difference formula. The computation of this approximation of the Jacobian is simple and gives an indication of how the model parameters affect the measurements.

At first, in order to calculate the Jacobian, a resistivity model ρ is assumed and the forward response for this model is calculated $\rho_{\alpha i}$. Then, one of the model parameters is changed by a very small amount Δρ, while the others are kept as it is, and the forward response $\rho_{\alpha i}(\rho+\Delta\rho)$ for this model is calculated. This shows the degree to which the synthetic measurements will change due to changes in the model parameter. This procedure is repeated for every parameter, changing only one parameter each time, until all the elements of the matrix have been calculated.

Afterwards, the Jacobian matrix can be used for the correction of the previous model. The ij element of J is given by the equation:

$$J_{ij} = \frac{\partial \rho_{\alpha i}}{\partial \rho_j} \approx \frac{\rho_{\alpha i}(\rho + \Delta\rho_j) - \rho_{\alpha i}(\rho)}{\Delta \rho_j} \qquad (3.13)$$

The amount of change Δρ is chosen arbitrary but it should be chosen carefully in order to avoid errors and to meet the conditions of the first derivative. Geometrically, the derivative can be viewed as the slope of the tangent of a function at a point. The slope of the tangent is very close to the slope of the line passing through this point and a nearby point at a distance Δρ from the former point. The closer the point, the better the approximation to the derivative and thus a small Δρ is required for an accurate approximation.

Figure (3.4) illustrates an example of a Jacobian matrix for the 1D resistivity case. The 1-D model consists of 2 layers and the half-space and therefore, the model parameters are 5; 3 resistivities and 2 thicknesses, as the half-space is considered to have infinite thickness and thus, is not accounted for as a model parameter.

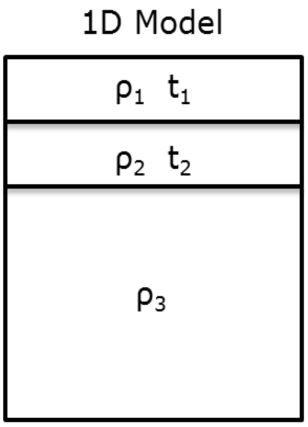

	ρ_1	ρ_2	ρ_3	t_1	t_2
ρ_{a1}	0.880	0.025	0.004	-0.080	-0.001
ρ_{a2}	0.817	0.077	0.003	-0.214	-0.004
ρ_{a3}	0.745	0.135	0.008	-0.329	-0.008
ρ_{a4}	0.678	0.188	0.016	-0.397	-0.015
ρ_{a5}	0.621	0.230	0.025	-0.425	-0.022

Figure 3.4: Example of the Jacobian matrix for a 1-D model with 3 layers (2 layers and half-space) and five parameters.

3.6. Inversion Methods

Several schemes have been suggested for solving the resistivity inversion. These are divided into two categories, the approximate and the accurate inversion techniques:

a) Approximate inversion methods: These methods simplify the inverse problem by assuming that it is linear. Some of them are the pseudosection technique, the Zhody method (1975) and back-projection techniques. As these algorithms have been overcome by more accurate techniques and also due to their weaknesses since they are approximate methods, they are no longer used.

b) Accurate inversion methods: These schemes treat the inversion as a nonlinear problem, which is actually the case. The most widely used are: the non-linear least-squares method (Lines και Treitel, 1984), the SVD technique (Lanczos, 1960; Lawson and Hanson, 1974), the weighted least-squares method, Marquadt's method (Levenberg, 1944, Marquadt, 1969) and the smoothness constrained (Occam) method. These techniques use the least-squares method to solve the inverse problem but there are other schemes, such as the L1-norm minimization, that do not use the least-squares method.

In this thesis, the smoothness constrained (Occam) inversion, which is the most popular, was used. This method is presented in detail in the following section.

3.7 Smoothness Constrained (Occam) Inversion

3.7.1 Basic Principles

The smoothness constrained inversion (also called Occam) was proposed by Constable et al. (1987), who applied it to 1D VES and magnetotelluric (MT) data. This method imposes the smoothness of the solution as a constraint to the inverse problem. The use of that kind of constraint belongs to a category of techniques known as regularization techniques of the ill-posed problems, and more specifically it belongs to the Tikhonov regularization (Tikhonov, 1963).

This method generates the solution with the smallest possible roughness. Meaning that the smoothest model is sought, which would depart from the simplest case only as much as it needs in order to fit the data. The major advantage of this technique, when compared to other methods, is that it does not depend on the choice of the initial model. The smoothness inversion might not yield the best solution, but its solution will have a physical meaning and thus, it will be a reasonable representation of the earth. In addition, smoothness guarantees the stability of the solution and the solution is dependent on the predefined characteristics that were chosen.

The non-linear problem of the resistivity can be defined as:

$$f(x) = y \tag{3.14}$$

where y are the observed data, that is the apparent resistivities, x is the unknown resistivity distribution and f(x) is the forward problem, which is a known function of the model. As mentioned in a previous section, the function f(x) can be expanded in Taylor series and ignoring the higher-order terms, the following equation is derived:

$$f(x + dx) = f(x) + Jdx \tag{3.15}$$

where dx is the model correction and J is the Jacobian matrix.

The regularization procedure aims to minimize the error between the observed and the synthetic data. The least-squares method seeks to find the resistivity correction dx for which the sum of squared errors, e, becomes minimum. The e is given by the relationship:

$$e = \left(y - f(x)\right)^T \left(y - f(x)\right) \tag{3.16}$$

In order to achieve the minimization of e, its derivative with respect to dx is set equal to zero:

$$\frac{\partial e}{\partial dx} = 0 \tag{3.17}$$

The differentiation with respect to dx yields the equation:

$$J^T J dx = J^T dy \tag{3.18}$$

Assuming that the matrix J^TJ is non-singular, that is it has an inverse matrix, the correction of the model is given by the equation:

$$dx = (J^T J)^{-1} J^T dy \tag{3.19}$$

This correction is given by the method known as least-squares method or Gauss-Newton method. In the smoothness constrained method, where the model roughness must be also minimized, a constraint is imposed to the problem and thus, the following quantity is minimized:

$$e = \|y - Jdx\|^2 + \lambda^2 \|Cx\|^2 \tag{3.20}$$

where C is the smoothness matrix, λ is the lagrange multiplier and x is the matrix with the resistivity model parameters. The second term accounts for the smoothness sought, while the degree of smoothness is controlled by λ which will be described in a later section.

Including the smoothness term, the correction of the model is given by the relationship:

$$dx = (J^T J + \lambda C^T C)^{-1} J^T dy \tag{3.21}$$

where dy is the difference between the observed and the calculated data (d^{obs}-d^{calc}).

Therefore, the new model is obtained by adding the correction of each iteration to the previous model:

$$x_{k+1} = x_k + dx_k \tag{3.22}$$

where k is the iteration number.

Equation (3.21) yields the model correction with smoothness applied only to the model changes. This is the standard smoothness constrained inversion. Another type of inversion is applying smoothness, not only to the model changes, but also to the model itself. This is similar to the previous type, but includes an additional smoothness term. For this type, the new model is given by the equation:

$$x_{k+1} = x_k + dx_k = x_k + (J^T J + \lambda C^T C)^{-1} J^T dy_k - \lambda C^T C x_k \tag{3.23}$$

This type of model correction produces a smoother model than the first option but it converges to higher RMS error. It is suitable only in cases of extremely noisy data.

3.7.2 Smoothness matrix

The minimization of the roughness is achieved using the smoothness matrix C. This matrix defines the relationships between adjacent parameters in the model. If N is the number of the model parameters, then the smoothness matrix has NxN dimensions.

For the 1D case the model roughness can be expressed as:

$$R = \|Cx\|^2 \tag{3.24}$$

where the smoothness matrix C differences the model parameters vertically. This equation corresponds to a first derivative penalty. Every row in the smoothness matrix refers to one specific parameter and how that parameter is related to its adjacent parameters and is given by:

$$C = \begin{bmatrix} 0 & 0 & 0 & \cdots & 0 \\ -1 & 1 & 0 & \cdots & 0 \\ 0 & -1 & 1 & \cdots & 0 \\ \vdots & \vdots & \vdots & \ddots & \vdots \\ 0 & 0 & \cdots & -1 & 1 \end{bmatrix} \tag{3.25}$$

The elements of the matrix take value -1 for the parameter itself and 1 for the parameters on which it depends, whereas all the other elements are set to zero. For the 2D case where the resistivity is considered to change both laterally and with depth, the model roughness can be expressed as (deGroot and Constable, 1990):

$$R = \|C_x x\|^2 + \left\|C_y x\right\|^2 \tag{3.26}$$

where C_x and C_y are NxN smoothness matrices that difference the model parameters laterally and vertically, respectively. Again, this expression is for a first derivative

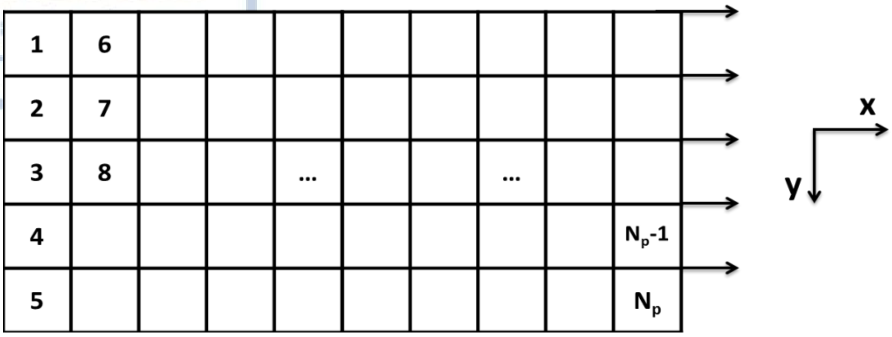

Figure 3.5: Example of a regularization mesh of the model parameters. N_p denotes the number of parameters.

penalty. An example of the C_x and C_y matrices, based on the regularization mesh of the model parameters shown in figure (3.5) and numbering the parameters from top to bottom as shown in the figure, is given by:

$$C_x = \begin{bmatrix} 0 & 0 & & \cdots & & & & 0 \\ & & & \vdots & & & & \\ -1 & 0 & \cdots & 0 & 1 & 0 & & \cdots \\ 0 & -1 & 0 & \cdots & 0 & 1 & 0 & \\ & & \ddots & & & \ddots & & \\ & & & & & & \vdots & \\ 0 & 0 & \cdots & -1 & & \cdots & 0 & 1 \end{bmatrix} \longrightarrow 6^{\text{th}} \text{ parameter}$$

$$C_y = \begin{bmatrix} C_{y1} & & 0 & \\ & C_{y2} & & \\ & & \ddots & \\ 0 & & & C_{yP} \end{bmatrix}, with\ \ C_{yi} = \begin{bmatrix} 0 & 0 & 0 & 0 & 0 \\ -1 & 1 & 0 & 0 & 0 \\ 0 & -1 & 1 & 0 & 0 \\ 0 & 0 & -1 & 1 & 0 \\ 0 & 0 & 0 & -1 & 1 \end{bmatrix} \quad (3.27)$$

where yP is the number of columns in the mesh. These two matrices can be combined to form the total smoothness matrix C. Using a second derivative penalty, the model roughness for the 2-D case is expressed as:

$$R = \left\| {C_x}^2 x \right\|^2 + \left\| {C_y}^2 x \right\|^2 \quad (3.28)$$

Figure (3.6) illustrates an example of the total smoothness matrix using a second derivative penalty and a model of 9 parameters. In each row, corresponding to a specific parameter, the element that refers to this parameter will have a value of -4, while its neighbors will have value of 1 and all other elements will be equal to zero. For instance line 5 corresponds to the 5th parameter and has value -4 for itself and 1 for its adjacent parameters.

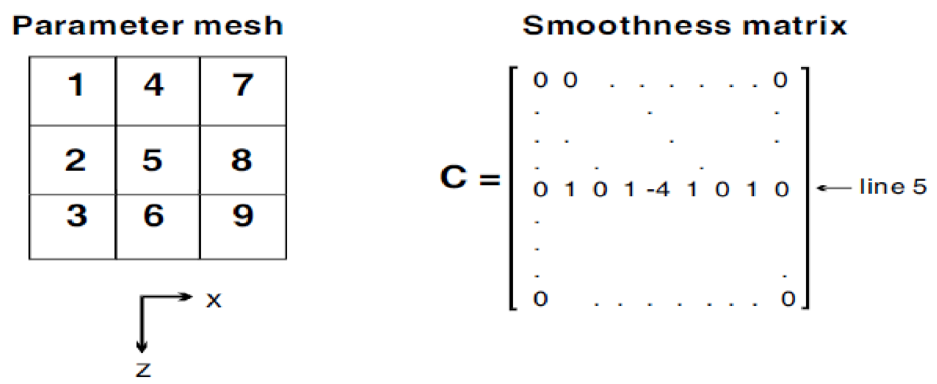

Figure 3.6: An example of a smoothness matrix using a second derivative penalty for the 2-D case and a model with 9 parameters (Tsourlos, 1995).

3.7.3 Lagrange Multiplier

When a constraint must be imposed to a problem, the lagrange multiplier λ is used. In this case it is used to controls the degree of smoothness in the solution. One of the problems in the smoothness inversion procedure is to decide the suitable value of λ in order to balance the minimization of the error and the amount of smoothing. Large values lead to very smooth models, whereas very small values make the effect of smoothness small and as a result the solution becomes unstable.

Many methods of finding the value of the lagrange multiplier have been suggested. One of these methods is to start the inversion with a relatively high value, in order to avoid instability, and to decrease it gradually at each iteration as the solution converges. Another approach is the L-curve method (Lawson και Hanson, 1974), which uses the angle of a curve to calculate λ. Specifically, the solution for many values of λ is calculated and then a plot of the $\|x\|^2$ versus $\|Jx-y\|^2$, in log scale, is made. The resultant curve has a shape similar to the letter L. The value corresponding to the angle of L is considered to be a suitable lagrange multiplier for the given problem. Here the symbol $\|\cdot\|$ denotes the Euclidean norm.

The Active Constrained Balancing method (ACB) by Yi et al. (2003) follows a different approach and treats the lagrange multiplier as a spatial variable. In order to achieve this, the resolution matrix and the Backus-Gilbert spread function are used.

The resolution matrix R shows how well resolved or not, the parameters of the model are and it defined as:

$$R = (J^T J + \lambda C^T C)^{-1} J^T J \tag{3.29}$$

Each row of R corresponds to a single model parameter. If this parameter is perfectly resolved, the matrix element for that parameter should have value of one and zero for all the other elements on the row corresponding to his parameter. In contrast, if a parameter is not well-resolved, there will be values different from zero in other elements in the corresponding row. In any case, the sum of all the matrix elements in one row should be equal to one. An example of the resolution matrix for a model with four parameters is shown below:

$$R = \begin{bmatrix} 1 & 0 & 0 & 0 \\ 0.1 & 0.7 & 0.1 & 0.1 \\ 0.1 & 0.2 & 0.6 & 0.1 \\ 0.1 & 0.1 & 0.3 & 0.5 \end{bmatrix}$$

where the first parameter is perfectly resolved as shown in the first row, whereas the others are not that well resolved.

In practice, the resolution of the model is satisfactory if the entries in the main diagonal take values close to one and the other elements close to zero. Figure (3.7) shows a graphical representation of the divergence of the synthetic model from the real model. Great divergence of the peaks from the main diagonal depicts a model with poor resolution.

The Backus-Gilbert spread function is used in order to evaluate the spatial distribution of each row, corresponding to one parameter, of the resolution matrix. The spread function SP for the ith parameter is given by:

$$SP_i = \sum_{j=1}^{N} \left\{ w_{ij} (1 - S_{ij}) R_{ij} \right\}^2 \tag{3.30}$$

where N is the number of parameters

w is a weighting factor depending on the spatial distance between two parameters i and j

S is a matrix used to incorporate the effect of smoothness

The element S_{ij} of the matrix S takes value of one if the corresponding element C_{ij} in the smoothness matrix C is nonzero, and zero otherwise. A large value of the SP function for a parameter means that it is poorly resolved and vice versa.

Using the lagrangian multiplier as spatial variable results from the fact that the model parameters are not equally resolvable and thus, different smoothness constraint needs to be applied to each parameter. In ACB, first the minimum and maximum values, that the multipliers can take, are chosen. Next, the spread function is calculated for a very small value of the lagrange multiplier. The spatially varying lagrangian multipliers λ (x_i, y_i, z_i) using the spread function are given by the equation:

$$\log(\lambda_i) = \log(\lambda_{min}) + \frac{\log(\lambda_{max}) - \log(\lambda_{min})}{\log(SP_{max}) - \log(SP_{min})} \times \{\log(SP_i) - \log(SP_{min})\} \quad (3.31)$$

where λ_i is the lagrange multiplier for the ith parameter, λ_{min} and λ_{max} are the min and max limits of the multiplier, correspondingly and SP_{min} and SP_{max} are the lower and upper limits of the SP function, respectively. If the SP function has a large value for a

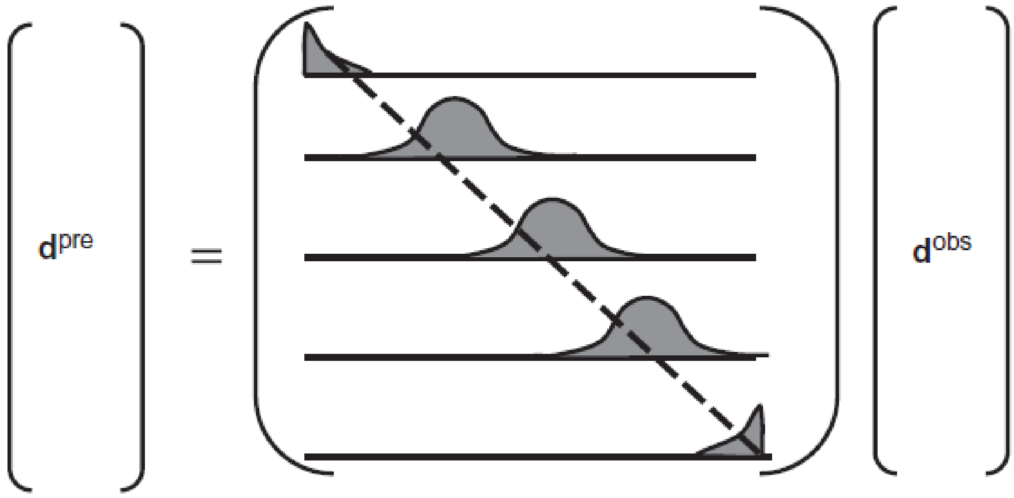

Figure 3.7: Graphical representation of selected rows of the resolution matrix. This plot indicates how well the data can be resolved. Peaks occurring near the main diagonal (dashed line) of the matrix show a good resolution (after Menke, 1989).

specific parameter, meaning that it is poorly resolved, the ACB method assigns a large value of λ to that parameter.

3.8 2D Inversion Schemes

Most 2D inversion techniques use the smoothness-constrained method, as mentioned above, and the FEM or FDM as forward solvers. The area is subdivided in a large number of regions. The positions of the regions remain fixed and only the resistivities are allowed to vary in the inversion and therefore, the resistivities are the parameters of the model. In this case a 2D smoothness matrix is used, defining relationships between a parameter and its north, south, west and east adjacent parameters. One of the limitations of the 2D smoothness inversion, which is an L2-norm method, is its inability to resolve sharp layer interfaces, as it produces models with smooth structure. Using a robust inversion technique (L1-norm), the model takes a blocky appearance but still the layer interfaces are not clearly resolved.

Recently, the laterally constrained inversion (LCI) method (Auken and Christiansen, 2004) has been suggested, in order to overcome the limitation of the previous methods to resolve sharp layer boundaries. The LCI method is the subject of this thesis and it is presented in the following section.

3.9 Laterally Constrained Inversion (LCI)

In the Laterally Constrained Inversion (LCI) the electrical resistivity tomography is subdivided into soundings based on the spatial sensitivity of each apparent resistivity measurement. The LCI inverts the series of soundings as one system and produces a series of 1-D models through the inversion. The neighboring models are connected together using lateral constraints between the parameters of the models, as shown in figure (3.8) for a system with 3 models. Due to these constraints, information from one model will spread to the adjacent ones. The parameters of the whole system are the resistivities and thicknesses of the layers of each model.

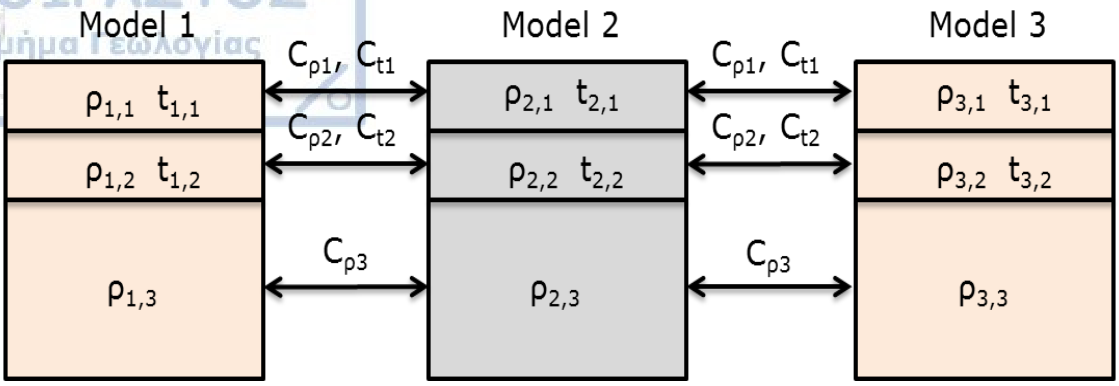

Figure 3.8: The LCI scheme for a system with three 1-D models. The data-sets are inverted as one system simultaneously by imposing lateral constraints ($C_{\rho 1}$, C_{t1}, …, $C_{\rho 3}$) between the models.

This method is robust to the choice of the initial model and results to a pseudo-2D section with sharp layer interfaces. Although the LCI technique has overcome the limitation of the 2D smooth-structure inversion to resolve sharp boundaries, it should not be considered as a substitute to this method, but as a supplement which can provide valuable information. Therefore, the combination of these two techniques will enhance the accuracy of the interpretation of the data and result to a better resolved model.

3.9.1 Methodology

Consider a set of ERT data divided into Ns soundings. Concatenating the data belonging to each sounding, the vector d_{obs} is formed:

$$d_{obs} = (\rho_{\alpha 1}, \rho_{\alpha 2}, \dots, \rho_{\alpha Ns}) \qquad (3.32)$$

where $\rho_{\alpha i}$ is the data-set of apparent resistivities corresponding to the ith sounding. Each sounding corresponds to a 1-D model with equal number of parameters. The full model is presented as:

$$m = \begin{pmatrix} m_1 \\ m_2 \\ m_3 \\ \vdots \\ m_{Ns} \end{pmatrix} \qquad (3.33)$$

The m_i corresponds to a specific ith model and is represented as:

$$m_i = (\rho_{i1}, \rho_{i2}, \dots, \rho_{iN}, t_{i1}, t_{i2}, \dots, t_{i(N-1)})^T \tag{3.34}$$

where ρ is the resistivity, t is the thickness, N is the number of layers and T denotes the transpose matrix.

The LCI scheme solves the forward problem for each one of the 1-D models separately with 1-D calculations using the filter method, as previously described. Using this 1-D formulation, this scheme can locate sharp layer boundaries by making the assumption of the layered earth. This solution is very effective in sedimentary environments. In cases where the subsurface is disturbed by geological phenomena or a layered appearance exists but with significant 2-D structures, the 1-D solution will not produce the optimum results. To reconstruct these complex structures a modification to this scheme must be made. This is achieved by using a 2-D forward solver such as FEM or FD.

Then, the jacobian matrix, for each one of the models, is calculated, and all the separate matrices are combined to a single matrix J for the total system. This matrix has the individual jacobian matrices on its main diagonal and zero in every other element. It is given by:

$$J = \begin{bmatrix} J_1 & & & \\ & J_2 & & \\ & & \ddots & \\ & & & J_{Ns} \end{bmatrix} \tag{3.35}$$

where J_i is the Jacobian matrix for the ith model.

Similar to the smoothness constrained method, the smoothness matrix is used to connect the adjacent 1-D models by imposing lateral constraints between the parameters of the separate 1-D models. Figure (3.9) demonstrates four cases of applying constraints. These cases are the vertical, the lateral, both vertical and lateral and the last case also includes diagonal constraints, which will have as a result for the center parameter to be dependent on its 8 adjacent parameters. Normally, only lateral constraints are used in the LCI scheme, but vertical can be used as well to connect parameters in the same model. When only lateral constraints in the x direction are implemented, a single smoothness matrix C_x is used, which can take the form:

$$C_x = \begin{bmatrix} 0 & 0 & & \cdots & & & & 0 \\ & & & \vdots & & & & \\ -1 & 0 & \cdots & 0 & 1 & 0 & & \cdots \\ 0 & -1 & 0 & \cdots & 0 & 1 & 0 & \\ & & \ddots & & & \ddots & & \\ & & & & & & \vdots & \\ 0 & 0 & \cdots & -1 & & \cdots & 0 & 1 \end{bmatrix} \tag{3.36}$$

If N_s is the number of models, N is the number of layers at each model and assuming the parameters of the model are both resistivities and thicknesses, then C_x has dimensions $N_s \cdot (2N-1)$ x $N_s \cdot (2N-1)$. Each row of this matrix corresponds to one model parameter and takes 1 for the parameter itself and -1 for the laterally adjacent parameter. If vertical constraints in the z direction are also applied, a second smoothness matrix C_z is required, which may be given by:

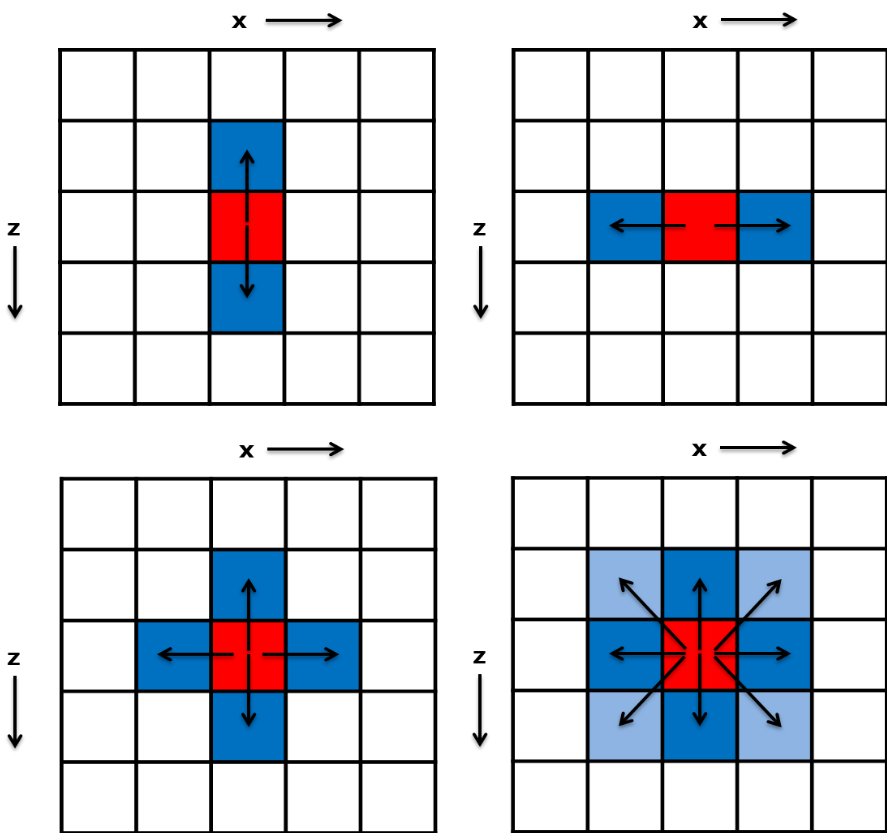

Figure 3.9: Cases of imposing constraints: a) Vertical, b) Lateral, c) Both vertical and lateral, d) Including diagonal constraints.

$$C_z = \begin{bmatrix} C_{z1} & & 0 & \\ & C_{z2} & & \\ & & \ddots & \\ & 0 & & C_{zNs} \end{bmatrix} \quad , with\ C_{zi} = \begin{bmatrix} 0 & & \cdots & & 0 \\ -1 & 1 & & & \\ 0 & -1 & 1 & \cdots & \\ & & \ddots & & \\ 0 & & \cdots & -1 & 1 \end{bmatrix} \tag{3.37}$$

where C_{zi} corresponds to the smoothness matrix with the vertical constraints for the ith model and has dimensions (2N-1)x(2N-1).

The models are inverted as one system and in this case, the correction dx of the full model for the system would be given by:

$$dx = [\,J^T J + \lambda\big({C_x}^T C_x + {C_z}^T C_z\big)\,]^{-1} J^T dy \tag{3.38}$$

Different weight can be applied for the horizontal and vertical constraints by introducing two constant factors α_x and α_z, resulting in the following model correction:

$$dx = [\,J^T J + \lambda\big(\alpha_x {C_x}^T C_x + \alpha_z {C_z}^T C_z\big)\,]^{-1} J^T dy \tag{3.39}$$

In this case, all horizontal constraints have equal weight α_x and all vertical constraints have equal weight α_z. Different weight on each horizontal and vertical constraint can be applied using the weighting matrices W_x and W_z, that contain the weights for each component of the lateral and the vertical smoothness matrix, respectively:

$$dx = [\,J^T J + \lambda\big({C_x}^T W_x C_x + {C_z}^T W_z C_z\big)\,]^{-1} J^T dy \tag{3.40}$$

For the LCI scheme a small or even zero weight should be given to the vertical components. Finally, the output of the LCI is a profile of multiple models, which are plotted to produce a pseudo-2D graph.

4. MODIFIED LATERALLY CONSTRAINED INVERSION SCHEME

In this chapter a description of a modified LCI scheme, which was developed through this thesis and implemented in code, is presented. Modifications were made to the LCI scheme compared to previous work, which resulted in a more accurate inversion solution. The changes, the algorithm that lies behind the LCI software and its capabilities, as well as, its limitations will be discussed and examples of testing the scheme with both real and synthetic data will be presented. The results of the LCI method will be compared with the results from a 2-D smooth-structure algorithm using the software DC2DPRO (Kim 2017). All synthetic data in this thesis were produced using DC2DPRO.

4.1 Discard low-information VES

Figure (4.1a) shows an example of a typical sequence of ERT measurements. At first, these data are divided into soundings based on the center of each measurement, as illustrated in figure (4.1b), resulting in 18 different soundings for this example.

As the spacing between the electrodes increases, the number of measurements decreases and thus, the soundings which are closer to the center of the profile will have a greater number of data, whereas those that are close to the boundaries of the profile will have limited data. It is obvious that at the boundaries of the tomography, the small number of measurements is not adequate to form a sounding. These data represent a small part of information which cannot be used to give accurate inversion results and therefore, they are discarded and only the remaining are used for the inversion as shown in figure (4.1c). Although this means that smaller part of information and therefore, smaller covered area, than the original will be used, this part will produce more accurate results through the inversion.

Before applying the scheme the algorithm was tested without removing any of the data and although the inversion produced correct results for most of the profile area, the final models acquired for the soundings near the boundaries were erroneous due to the lack of information at great depths in this area. An example is shown in figure (4.2). Synthetic data were produced for a model that consists of 2 layers and half-space with 50, 10 and 100 Ohm·m, respectively. Figure (4.2b) illustrates the results using all data in the inversion, while figure (4.2c) when discarding VES with small number of measurements. It is obvious that at the boundaries of the domain the solution is incorrect when using all data due to the lack of information, whereas after discarding the VES, the inversion resulted in a more accurate model showing clearly the layered structure.

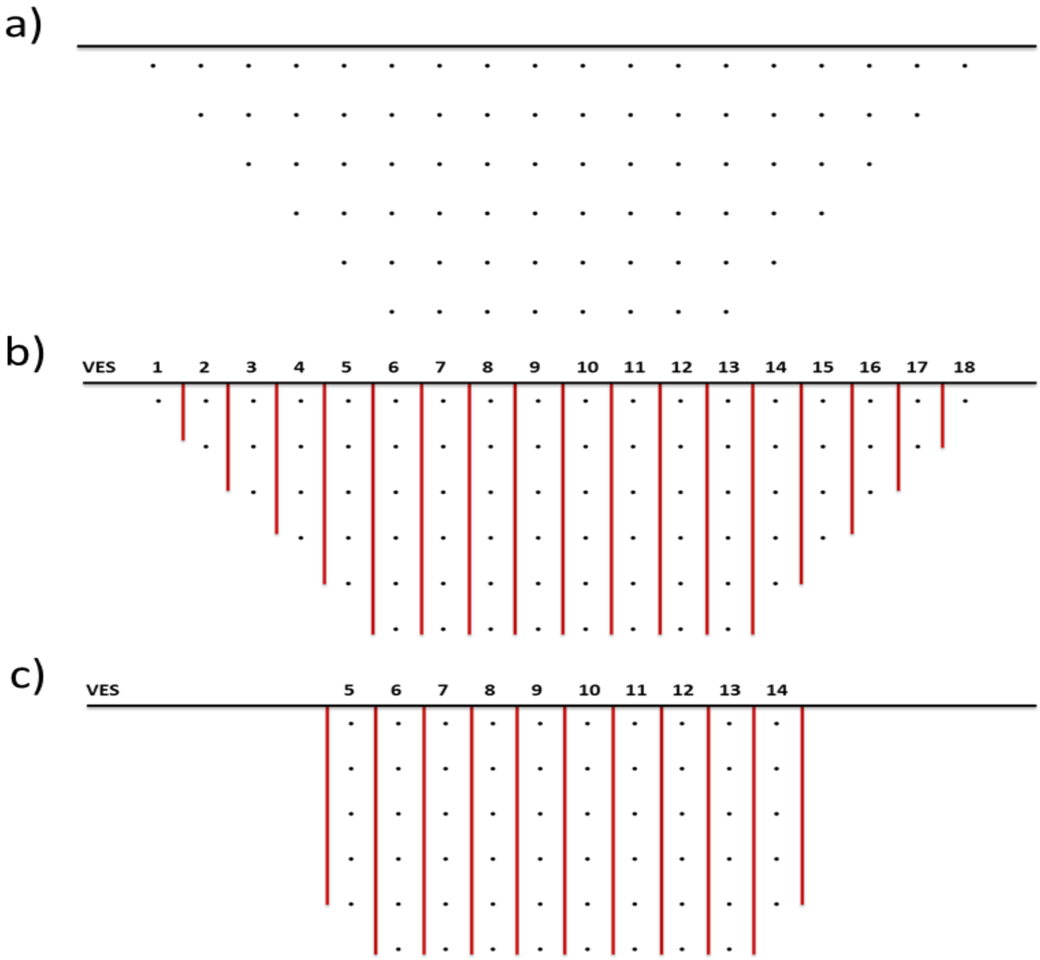

Figure 4.1: a) A typical sequence of ERT measurements b) ERT divided into soundings c) Discard VES with low-information.

After removing these data, the column vectors with the electrode spacings and the apparent resistivity measurements are reformed and sorted by sounding order such as:

$$\rho_\alpha = (\rho_{\alpha 1}, \rho_{\alpha 2}, \dots, \rho_{\alpha Ns})$$

$$AB2 = (AB2_1, AB2_2, \dots, AB2_{Ns}) \tag{4.1}$$

$$MN2 = (MN2_1, MN2_2, \dots, MN2_{Ns})$$

where $\rho_{\alpha 1}$ denotes the data-set for the 1st sounding, $\rho_{\alpha 2}$ for the 2nd and so on, and AB2 and MN2, are the distances between current and potential electrodes, respectively, which are formed in the same concept as the apparent resistivities. All datasets used in the following chapters have been processed to discard the VES with a small number of measurements before inversion.

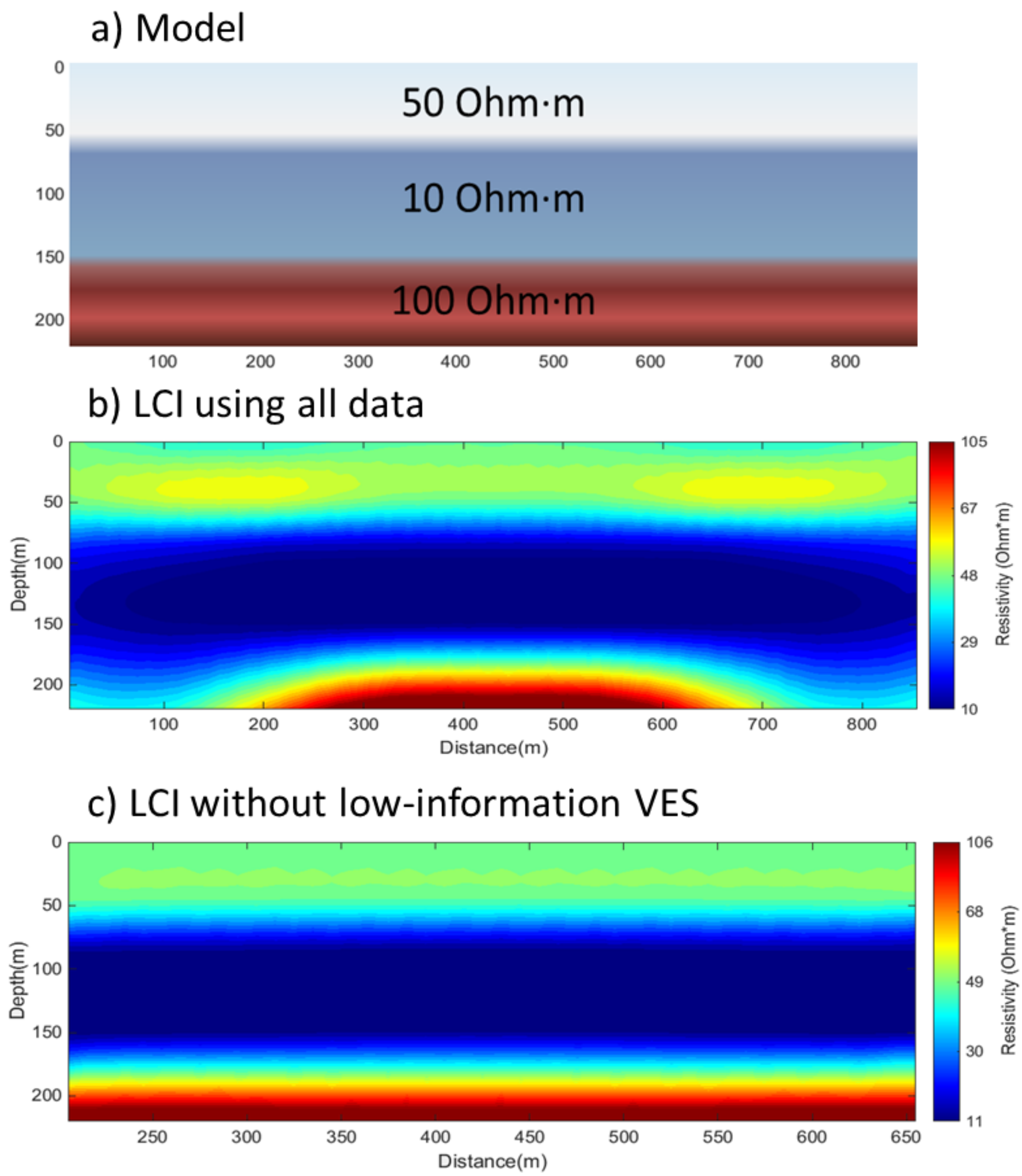

Figure 4.2: a) Model used to produce the synthetic data. b) LCI using all data. c) LCI without including soundings with low-information/small number of measurements.

4.2 Modification of smoothness matrix

The second change was a modification of the smoothness matrix. In the inversion method not only the resistivities but also the thicknesses of each layer change through the iterations. The thicknesses can also remain fixed and therefore, no changes will be required in the smoothness matrix and only the resistivities will vary through the inversion. But, in the case the thicknesses change, the constraints between the parameters, for both resistivities and thicknesses, can also change and therefore the smoothness matrix will be updated.

An example with two different cases of smoothness constraints, using five models with 6 layers each, is shown in figure (4.3). Case (a) shows that the parameter with number 15, which belongs to model 3, depends on its north, south, east and west adjacent parameter (number 9, 14, 15 and 21) since all the parameters have equal thickness. The constraints in this case are 4, one for each side. In case (b), parameter 15 has greater thickness than its lateral neighbors from models 2 and 4, and as a result it is dependent on more parameters. In this case, the constraints are 6; one for north and south parameters, whereas east and west are accounted for two, as shown in the figure.

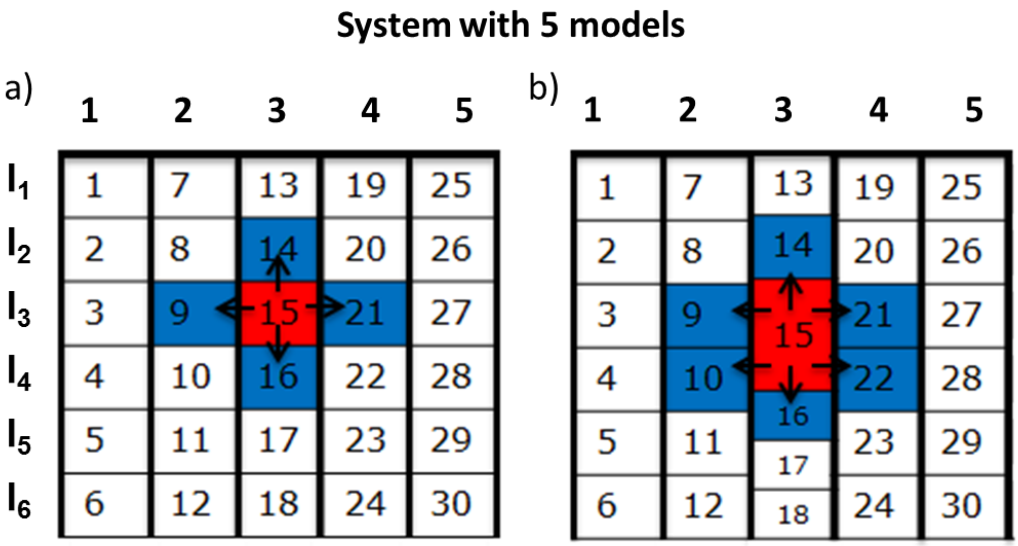

Figure 4.3: A five model system with 6 layers, where l_i represents the ith layer, is used to demonstrate two different cases of smoothness constraints and give a justification for the modification of the smoothness matrix: a) All parameters for all models have equal thicknesses, b) Parameters between models have varying thicknesses.

Since the lateral constraints are the ones that are changing, the smoothness matrix C_x will be updated at each iteration of the inversion loop, while the C_z matrix, with the vertical constraints, will remain fixed. An example of the smoothness matrices using second order derivatives is shown in figure (4.4) for a 3-model system and 4 layers for each model. It is clear that the 6^{th} parameter depends on four lateral parameters, two from the model that is on its left and two from the model on its right. Therefore, the smoothness matrix C_x has to account for these dependencies and takes the value of -4 for the 6^{th} parameter itself and 1 for the lateral parameters.

In order to update the smoothness matrix, the algorithm compares the layer thicknesses and depths of neighboring models at each iteration and then adjusts the constraints accordingly. This comparison can be demonstrated using figure (4.5) for 2 models with 4 layers each, where l_i represents the ith layer and A-E represent the layer interfaces. Consider the first case and the lateral constraints for the 2^{nd} layer of the first model. The depth of interface C is the same as of interface A, so the 2^{nd} layer of the first model does not depend on the 1^{st} layer of the 2^{nd} model. Next, interface D is examined. This interface is at a greater depth from A and at a smaller depth from B so, the 2^{nd} layer of the first model will depend on both the 2^{nd} and 3^{rd} layer of the second model and constraints will be applied for both. Finally, interface E is at a greater depth from both A and B and thus, no lateral constraint between the 4^{th} layer of the second model and the 2^{nd} layer of the first will be applied. Similarly for case b, where the 2^{nd} layer of the first model depends on the 3 top layers of the second.

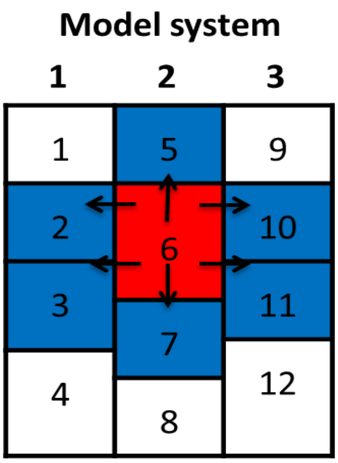

$$C_x = \begin{bmatrix} 0 & 0 & & & & \cdots & & & & & 0 & \\ & \ddots & & & & & & & & & 0 & \\ 0 & 1 & 1 & 0 & 0 & -4 & 0 & 0 & 0 & 1 & 1 & 0 \\ & & & & & \vdots & & & & & & \\ 0 & & & & & \cdots & & & & & & \end{bmatrix}$$

$$C_z = \begin{bmatrix} 0 & 0 & & & \cdots & & & 0 & \\ & \ddots & & & & & & & \\ 0 & & \cdots & 1 & -2 & 1 & \cdots & 0 & 0 \\ \vdots & & & & \vdots & & & \vdots & \\ 0 & & & & \cdots & & & & \end{bmatrix}$$

Figure 4.4: Example of smoothness matrices using second order derivatives for a 3-model system with 4 layers.

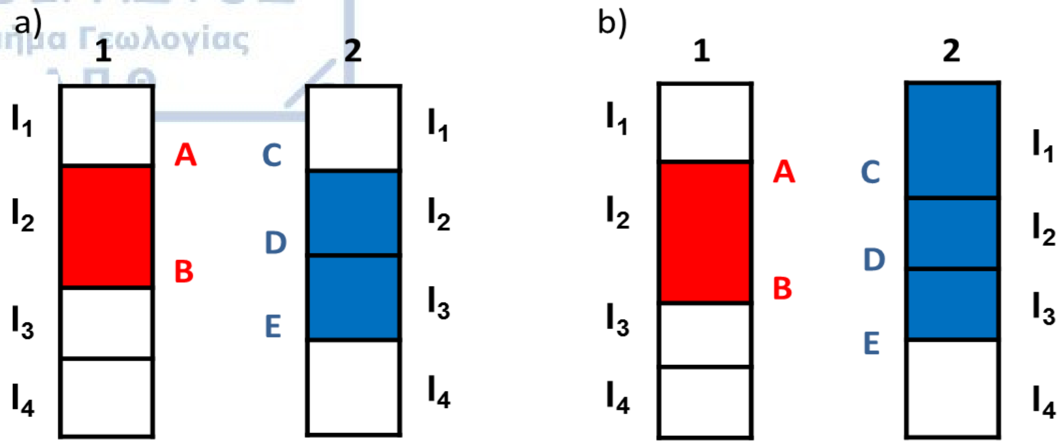

Figure 4.5: Layers with greater thickness affect more than one lateral adjacent parameters: Example using two models with 4 layers, where l_i represents the ith layer and A-E represent the layer interfaces. a) Layer l_2 (red color) of the first model depends on layers l_2, l_3 (blue color) of the second model. b) Layer l_2 of the first model depends on layers $l_1 – l_3$ of the second model.

As mentioned previously, usually in the LCI scheme only lateral constraints are imposed. In case both vertical and lateral are applied, it is of great importance to find the optimal ratio of the weight given to the vertical versus the weight given to the lateral. Small weight should be given to the vertical constraints, otherwise the resultant scheme will start to resemble the 1-D inversion of each VES separately with increasing weight to the vertical constraints. To demonstrate this, consider again the model in figure (4.2a). Figure (4.6) illustrates the resultant inversion pseudo-2D images for a) the 1-D inversion of each VES separately and combining to form the pseudo-2D graph, b) LCI with equal weights on vertical and lateral constraints and fixed smoothness matrix, c) LCI with 1:5 ratio of the vertical versus the lateral weight and fixed smoothness matrix and d) LCI with 1:5 ratio and varying smoothness matrix. It is obvious from figures a) and b) that large weight given to the vertical constraints leads to similar results as performing the 1-D inversion of each VES separately. In the latter, only vertical constraints are used between the parameters of each model and as the vertical weight is increasing in the LCI, it has a greater impact than the horizontal weight and therefore, the scheme tends to resemble the 1-D inversion more. When smaller vertical weight is used, the accuracy of the solution is increasing as shown in case (c). Finally, when using the LCI with varying smoothness

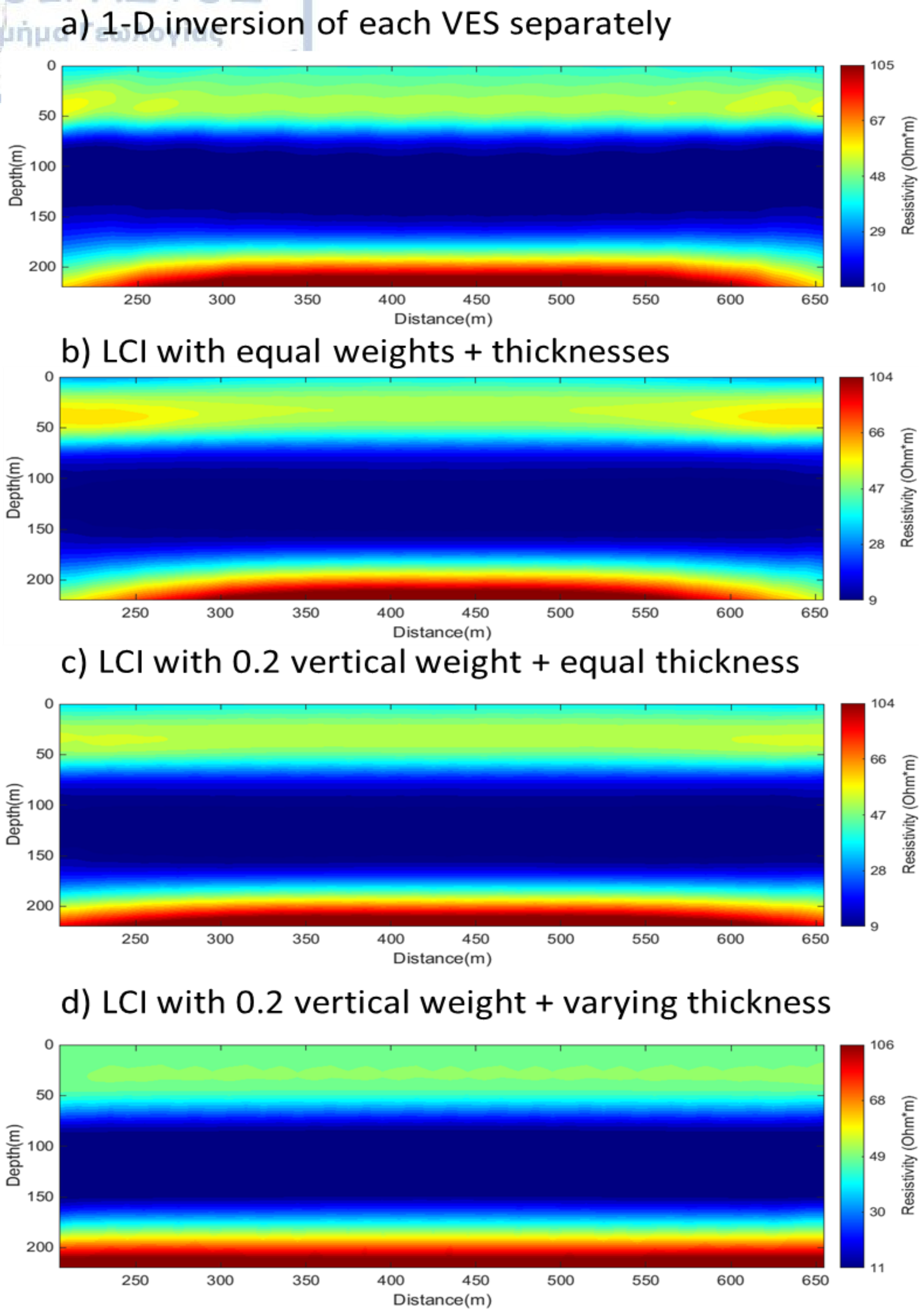

Figure 4.6: Example used to justify the modification of the smoothness matrix using synthetic data for model in figure (4.2a): a) 1-D inversion of each VES separately. b) LCI with equal weights on vertical and lateral constraints and fixed smoothness matrix. c) LCI with 1:5 ratio of the vertical versus the lateral weight and fixed smoothness matrix. d) LCI with 1:5 ratio and varying smoothness matrix.

matrix based on thickness changes, as described earlier, the inversion results in a very accurate solution as illustrated in case (d).

The example presented above is used to show the improvement of the solution using a modified smoothness matrix. Although this example represents a simple case of horizontal layers, the same applies for more complex models.

4.3 ACB Implementation

In previous work on the LCI method, a constant value was used as lagrange multiplier λ. In the present thesis, we implement the ACB method to assign lagrange values to each parameter of the full model. Using ACB resulted in more accurate solutions in most cases, while in some cases there were minor differences between inversion using ACB and when using a constant lagrange value and therefore a constant λ was sufficient in the latter.

A case where ACB improved the inversion results is demonstrated in figure (4.7). The model used to produce the synthetic data is shown in figure a), while b) and c) display the outputs of the LCI using a constant lagrange value of 0.01 and LCI using ACB, resepctively. It is clear that using ACB resolved more accurately the interfaces between the layers of the model compared to the solution using a constant lagrange, which failed to resolve the boundaries of the resistive half-space with ρ = 400 Ohm·m that exists at 20 m depth and at distance 35-120 m along the profile.

4.4 LCI Algorithm Description

LCI is a software that was developed through this thesis and performs laterally constrained inversion of electrical resistivity tomography data and includes the modifications described above. In this section, the algorithm behind the software will be described, whereas images of the program, instructions on how it can be used and parts of the code are included in the appendix.

In order for the program to function properly, the data must have been acquired using the Schlumberger or Wenner arrays during the survey due to their symmetry. For other arrays, like the dipole-dipole and multiple gradient, which are asymmetrical, a sensitivity analysis is required for this method of inversion. The sensitivity analysis was not part of this thesis.

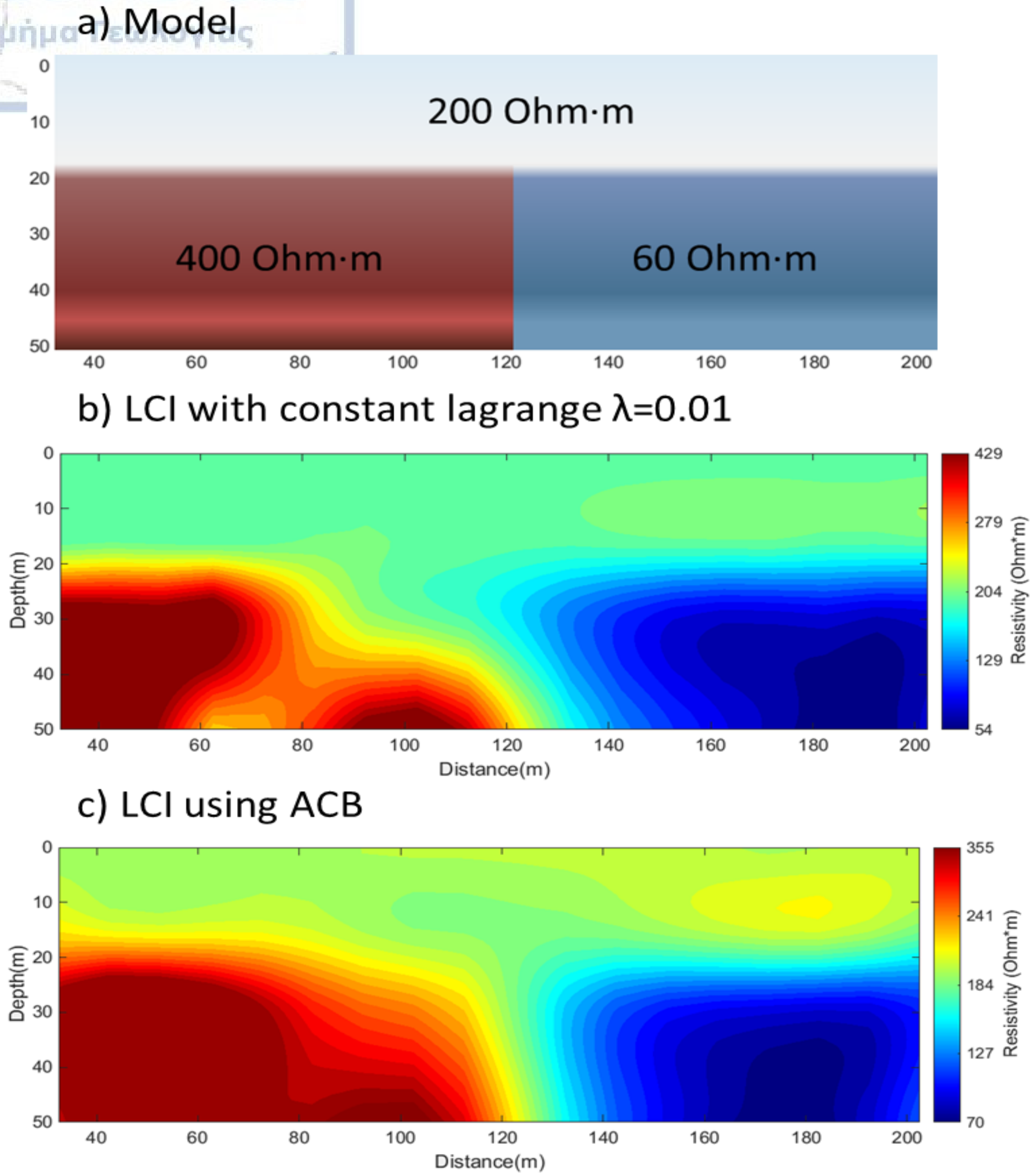

Figure 4.7: Improvement of inversion results using ACB: a) True model used. b) LCI using a constant lagrange value $\lambda = 0.01$. c) LCI using ACB.

After loading the ERT data file, the dataset is processed before inversion. At first these data are divided into soundings based on the center of each measurement. Then, the VES with small number of measurements are removed and the data are sorted by sounding order. Specifically, this algorithm is designed to keep only the soundings which have more than four data.

The next step is the calculation of the geometrical factors and the choice of the initial model. The program chooses by default an initial model, where both resistivities and thicknesses are varying, and inversion parameters, which can be altered by the user. The number of parameters of each 1-D model must be the same. The resistivities of all layers of each individual model are initialized to the median of each sounding. Based on the maximum separation distance of the current electrodes, the maximum penetration depth is calculated as the ¼ of this distance. Based on this depth and the number of layers, thicknesses are assigned to each layer. At this stage, all models are assumed to share equal thickness of each layer. For instance, the 1st layer of all models will have the same thickness t_1, the 2nd layer of all models will have t_2, etc. For each model, the thicknesses of the layers can be equal or increasing for deeper layers to account for the decreasing resolution with increasing depth. The latter is the default choice.

A default value of 0.01 for the lagrange multiplier is also assigned in case that the constant value option is enabled. The active constrained balancing, as mentioned above can also be enabled by providing two values that specify the lower and upper limits of values that lagrange can take. The default values used are 0.01 and 1 for lower and upper limits, respectively. Next, the smoothness matrix with the vertical constraints for the whole system is calculated. The default weight given to the vertical constraints is 0.2.

After defining the above, the iteration procedure begins. First, the forward model is solved separately for every 1-D model. Then, the RMS error between the observed data and the calculated data is computed. If one of the stopping criteria is satisfied the iterations stop, the model is saved and the results are presented in the screen. Otherwise, the inversion procedure continues with the calculation of the Jacobian matrix for each data-set. These matrices are merged in one matrix, which is the Jacobian for the whole system and has the separate matrices on its main diagonal. Due to the fact that this matrix has many zero elements, it is converted to a sparse matrix. The sparse matrix is a compressed matrix that keeps only the non-zero elements and their corresponding indeces in the initial matrix and this way the memory requirements by the software are reduced. Therefore, it is used in order to speed up the calculations. The Jacobian matrix is calculated using the perturbation technique, which was described in a previous chapter.

The process continues with the calculation of the modified smoothness matrix with the lateral constraints, which is calculated inside the loop because by default not only the resistivities but also the thicknesses of each layer change through the iterations and thus, the constraints between the parameters. After the calculation of C, if the ACB method is enabled, the spatially varying lagrange multipliers are calculated. Subsequently, the correction of the model is calculated and added to the previous model. The forward problem for the new model is calculated and this process continues as described in the previous chapter, until one of the stopping criteria is satisfied. Finally, the inversion results are displayed and a pseudo-2D plot is created.

Figure (4.8) demonstrates the initial steps that are followed before the iterative procedure starts in the form of a flow chart, whereas in figure (4.9) a flow chart describing the inversion procedure is presented.

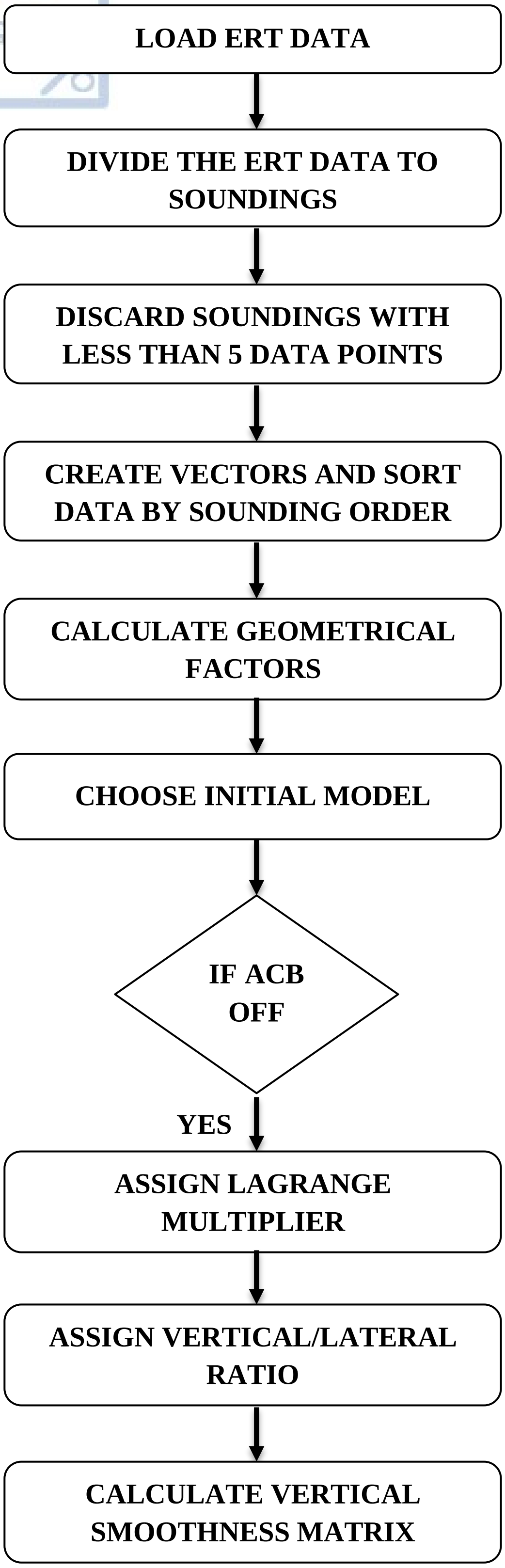

Figure 4.8: Flowchart of the initial steps which are followed to prepare the ERT data for the LCI inversion.

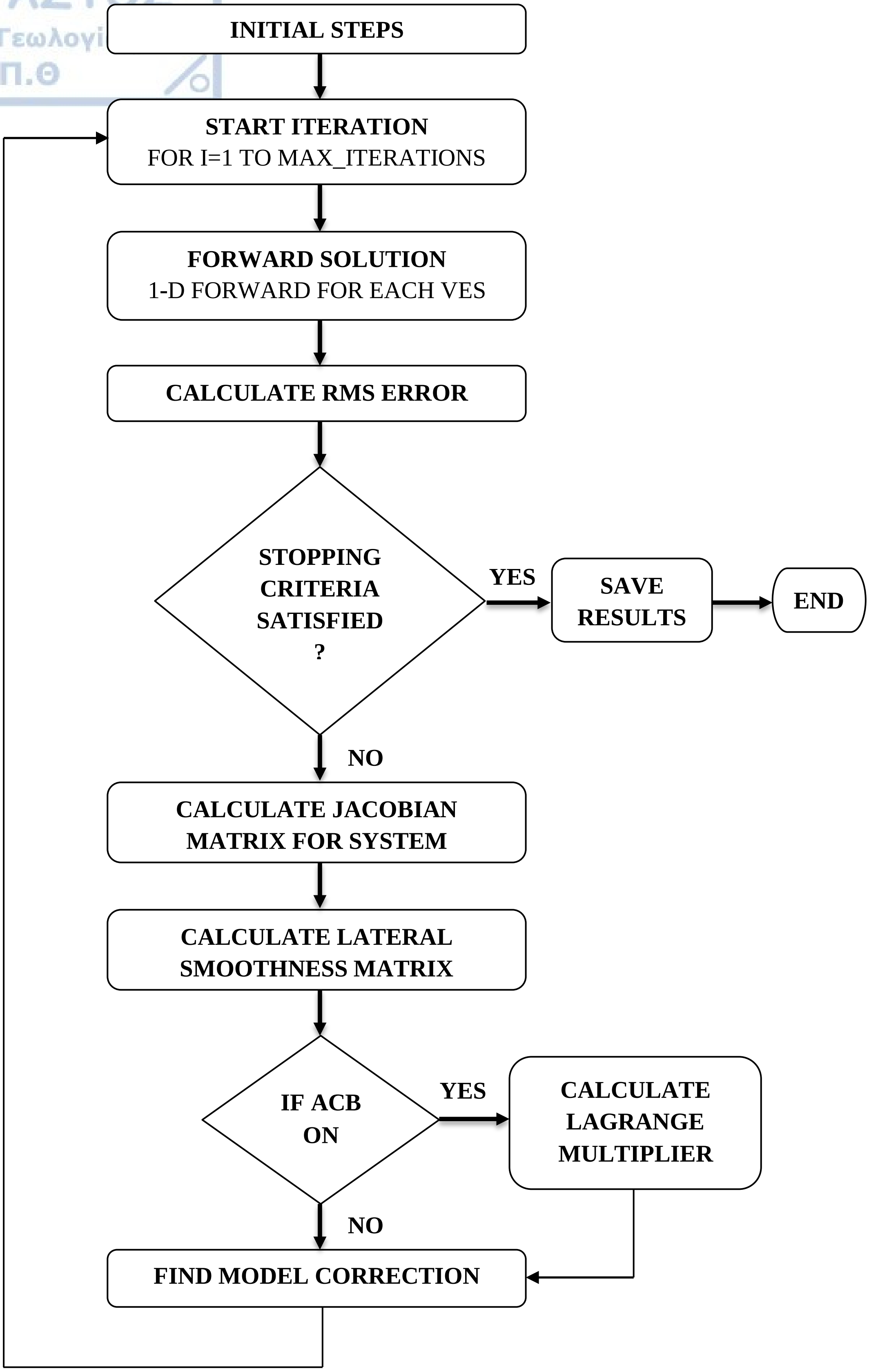

Figure 4.9: Flowchart of the inversion procedure.

4.5 Application to synthetic data

The algorithm, which was introduced above, was tested with a large number of synthetic data in order to evaluate its effectiveness with different geoelectrical models. The results were compared to a standard 2D smoothness inversion scheme using the software DC2DPRO (Kim, 2017). This software was also used to create the synthetic data. The same inversion parameters, such as the number of layers, the ACB method for calculating the lagrange multiplier and the maximun depth, were used in both programs. The number of layers was set to 7, while the maximum depth used is shown in each plot.

Although the running times are not directly comparable since LCI was coded in MATLAB, which is a slower programming environment than the C language, which was used for the development of DC2DPRO, in all cases the LCI proved to be faster due to the 1-D formulation of the forward problem. As an example, for a dataset of 408 points using 48 electrodes and 7 model layers, the running times of convergence, for 6 iterations, were 9.75s for the LCI and 29.43s for the DC2DPRO inversion on a Intel Core i7-7700 CPU, making the LCI 3 times faster in this case. For longer profiles, this difference will be more pronounced, and therefore LCI would be the preferable choice for long profiles with a layered structure.

Figure (4.10) shows a set of the models which were used to produce the synthetic data. Both simple and complex models were created and tested. These models are realistic and can be encountered in real-life problems. Different number of electrodes, spacings and as a result penetration depth was used. Furthermore, some noise was added to the data to make them more realistic. The synthetic data were inverted and the inversion results are presented as 2D plots in figure (4.11). For each model (a)-(h) the top side of the figure represents the inversion results using the LCI software, while the bottom shows the results using DC2DPRO. The color scale of the plots was chosen to be as similar as possible in both programs, in order for the results to be comparable. Attention should be given to the area covered by the LCI software, as it is smaller than the one used in DC2DPRO, for reasons that were stated earlier, and therefore, the boundaries are not the same. The boundaries of the domain that was used by LCI are shown with black lines in the graph for each dataset.

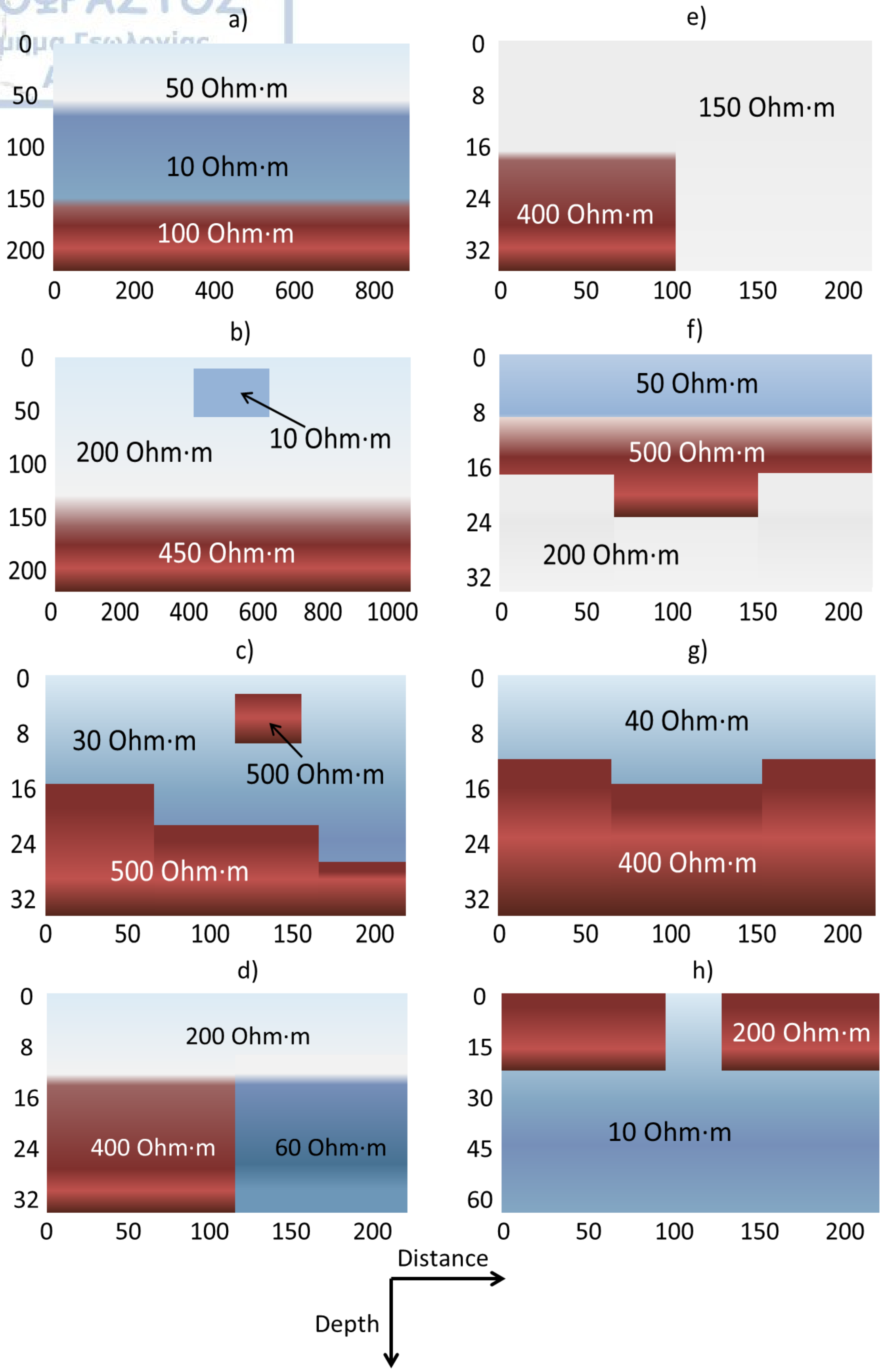

Figure 4.10: Models used to produce the synthetic data for evaluation.

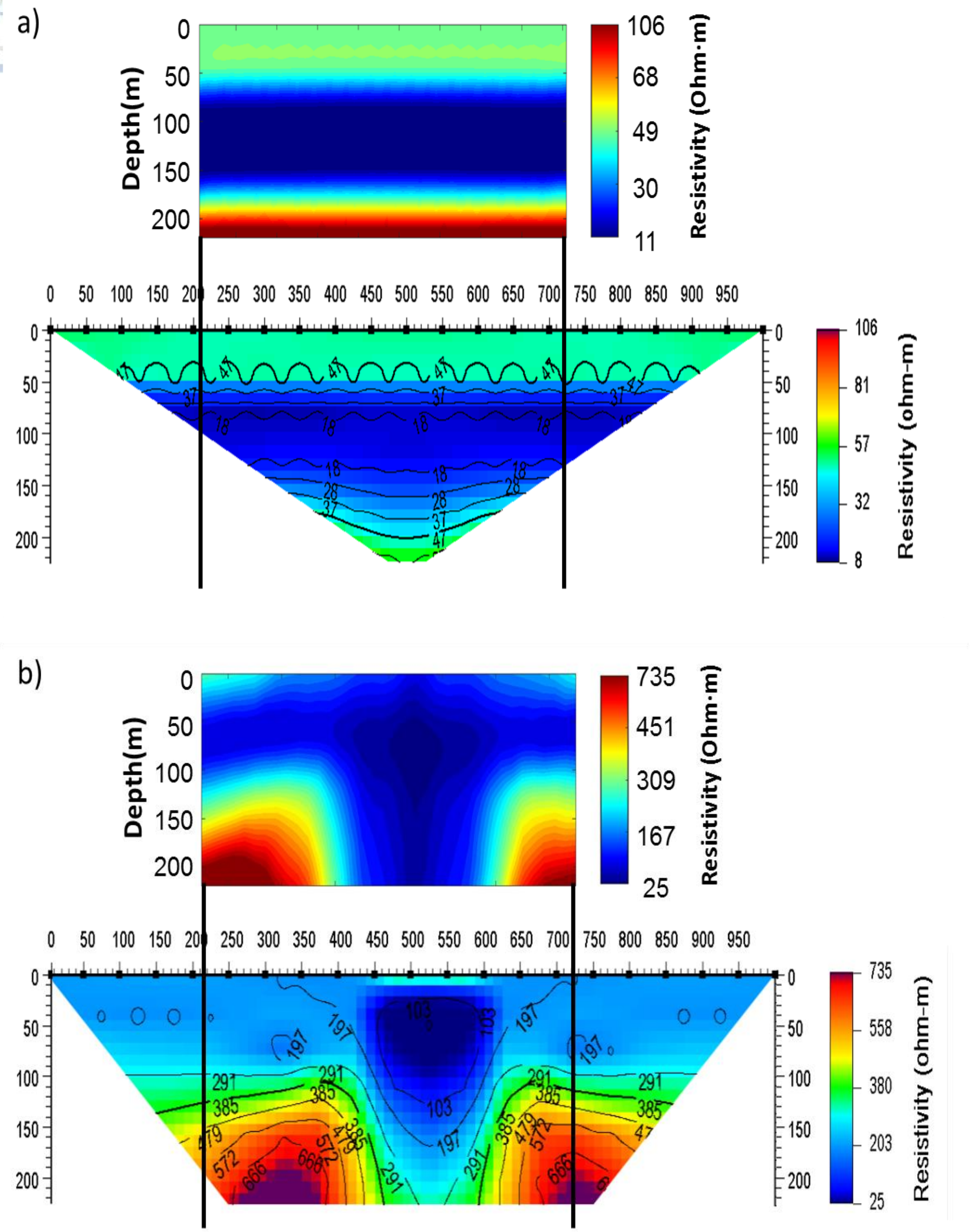
a)
Depth(m)
Resistivity (Ohm·m)
106
68
49
30
11
Resistivity (ohm-m)
106
81
57
32
8
b)
Depth(m)
Resistivity (Ohm·m)
735
451
309
167
25
Resistivity (ohm-m)
735
558
380
203
25

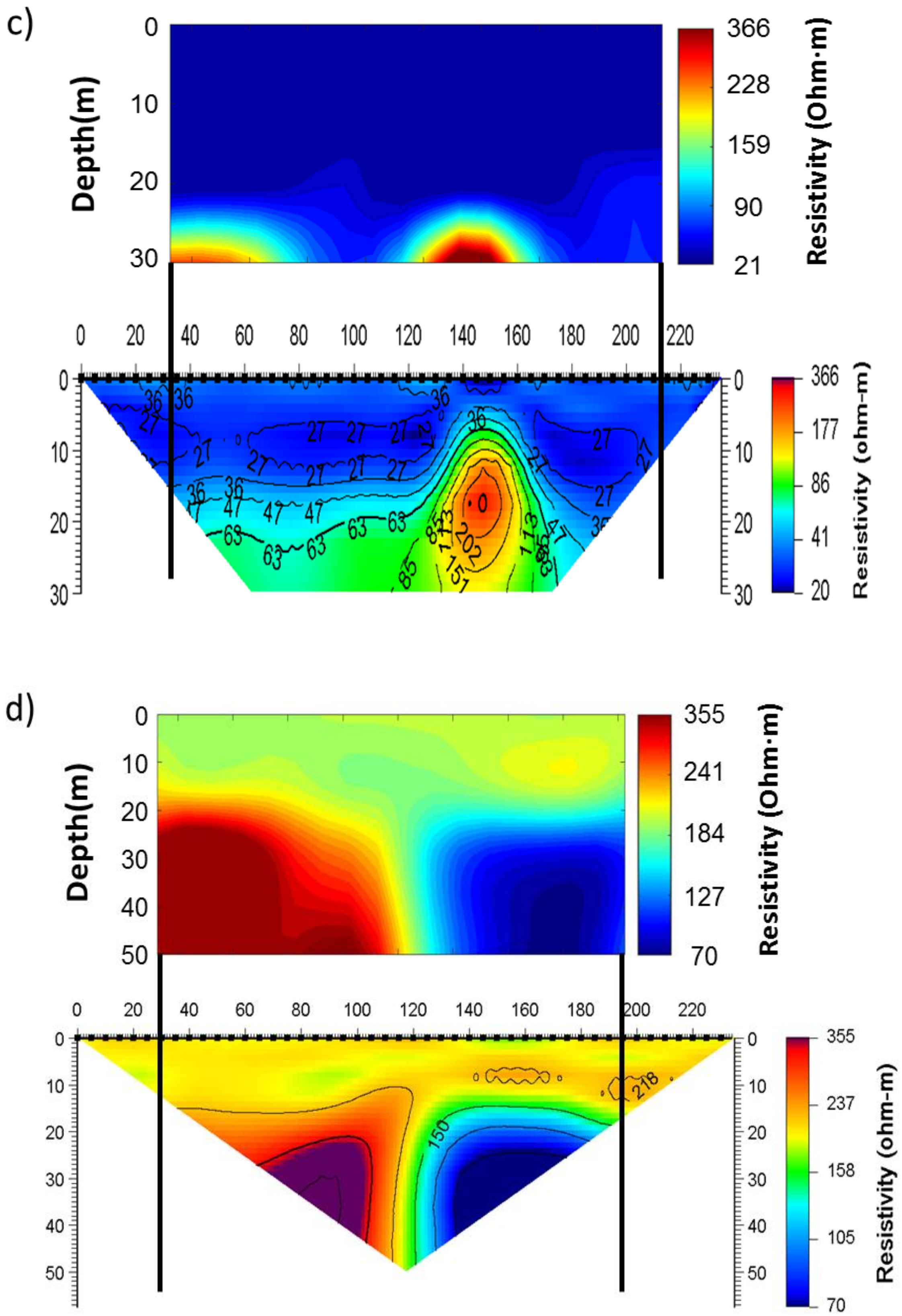
c)
Depth(m)
0
10
20
30
366
228
159
90
21
Resistivity (Ohm·m)
0 20 40 60 80 100 120 140 160 180 200 220
366
177
86
41
20
Resistivity (ohm-m)
d)
Depth(m)
0
10
20
30
40
50
355
241
184
127
70
Resistivity (Ohm·m)
0 20 40 60 80 100 120 140 160 180 200 220
355
237
158
105
70
Resistivity (ohm-m)
150
218

e)

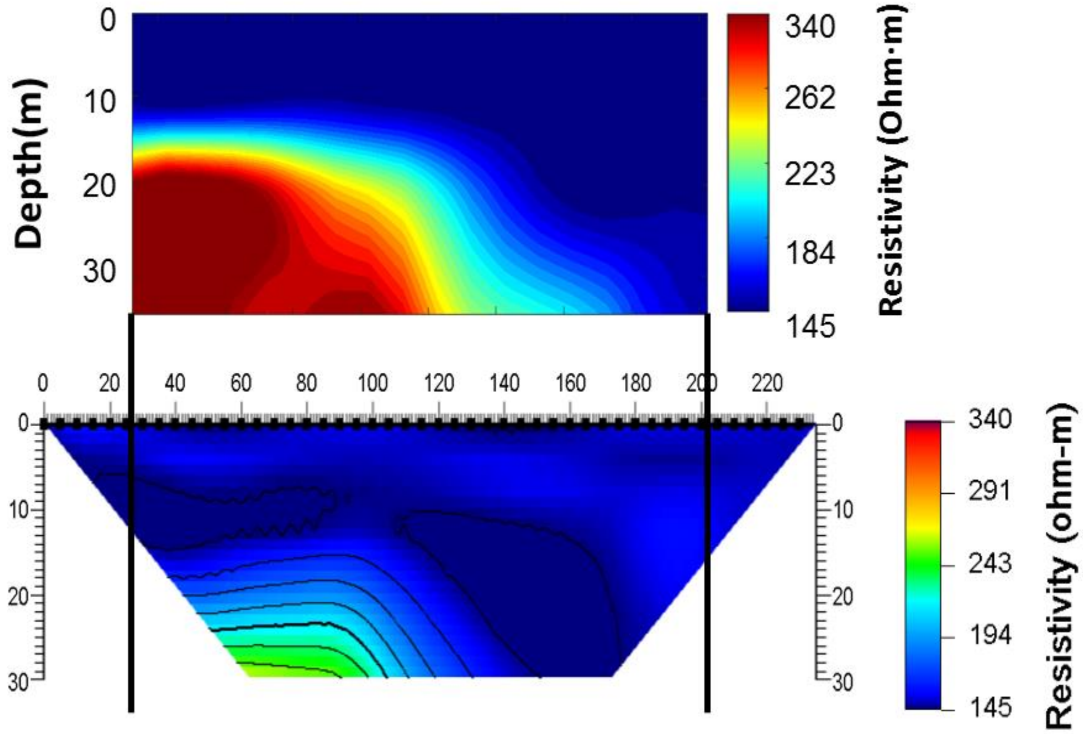
Depth(m)
0
10
20
30
340
262
223
184
145
Resistivity (Ohm·m)
0
20
40
60
80
100
120
140
160
180
200
220
291
243
194
Resistivity (ohm-m)

f)

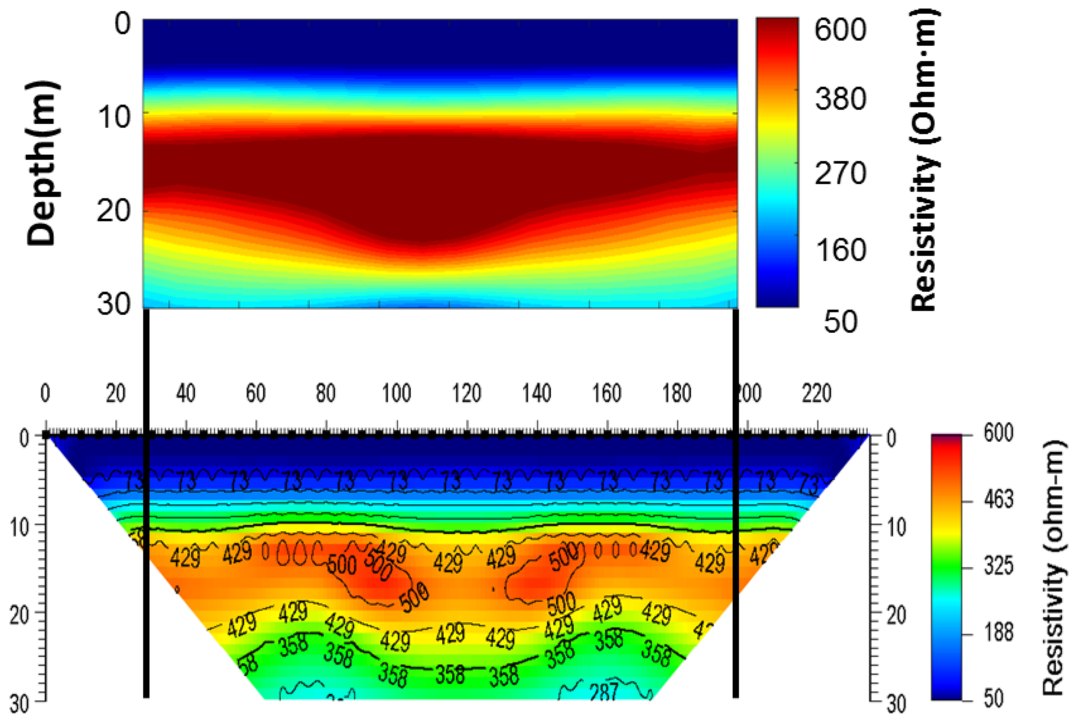
Depth(m)
0
10
20
30
600
380
270
160
50
Resistivity (Ohm·m)
0
20
40
60
80
100
120
140
160
180
200
220
463
325
188
Resistivity (ohm-m)
73
429
500
358
287

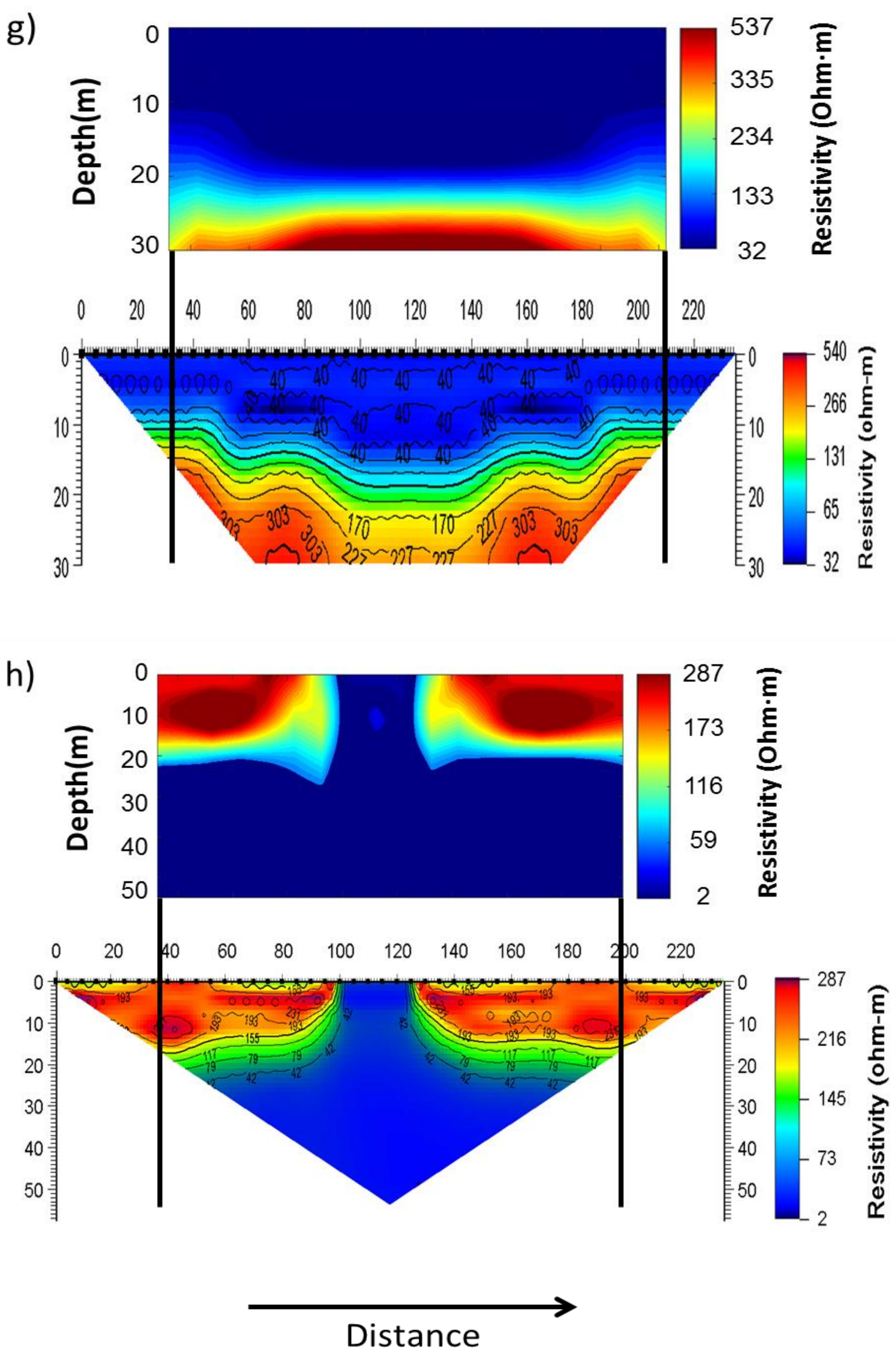

Figure 4.11: Inversion results of the synthetic data using the LCI program (top) and the DC2DPRO software (bottom).

All in all, the two different inversion schemes produced similar results, as illustrated in the figure (4.11). The results were compared with the true models used and proved to be accurate, as both simple and complex models were able to be reconstructed effectively with the LCI algorithm. Regarding the models with a layered structure and sharp interfaces (cases a and d-h), the layer interfaces and the depths of the layers in most of the models were resolved better using the LCI scheme, as this is the main feature of this method. Also, the resultant resistivities from LCI are realistic and a good approximation of the true resistivity distribution of each model.

Layered models with 2-D structures inside a layer were used to assess the response of the 1-D formulation with 2-D structures in cases b) and c). The results showed that the LCI scheme was not able to detect the presence of these targets and also that the 2-D structure greatly affected its surrounding area and distorted the final model. These results were expected as the inability of any 1-D scheme to locate 2-D or 3-D variations is known.

The RMS error using the LCI method was low (<5%) and the data converged after a few iterations (< 12). Moreover, the apparent resistivity curves of each VES of the data used for the inversion and the calculated data were used as another means to test the effectiveness of the algorithm. The curves were very similar for all models and thus, showed that the results were reliable.

4.6 Application to real data

The results from the laterally constrained inversion using synthetic data showed that the algorithm is accurate and effective. However, it is necessary to test this scheme with real data. In this section, the results using the LCI algorithm with real data, which were collected in the field, are presented. The software DC2DPRO software was used not only to compare the inversion results, but also to exterminate bad data points due to high noise level.

The real data were acquired as part of various geophysical projects using the Schlumberger and Wenner arrays. The surveys were conducted in different environments and conditions using different number of electrodes and spacings in each case. The inversion results are presented in figure (4.15). For each model the top section corresponds to the LCI solution, while the bottom to the DC2DPRO solution.

In cases (a)-(c), the existence of 2-D resistivive structures is clear, whereas the last two cases have a more layered appearance.

The data in the first three cases were collected during a survey for the detection of Bauxite residues in galleries (Tsourlos et al, 2005). The measurements took place in Anw Varianh, that belongs to the Parnassus–Ghiona geotectonic zone in central Greece. The measurements were collected inside the gallery using 24 electrodes with a spacing of 4m. The location of the tomographies is illustrated in figure (4.12). Tomographies T1 and T2 were conducted on the floor of the gallery, while T3 was conducted on the wall. The inversion results are demonstrated in figures (4.15a, b, c) for T1, T2 and T3 respectively. T4 represents a GPR survey line and not an ERT. Based on the DC2DPRO results, case (a) shows resistive areas close to the surface along the tomography and in the region 4-14 m distance and depth up to 12m, which are attributed to the bauxite residues. In the T2 inverted image, two highly resistive bodies exist between 10-30m and 40-60m along the profile and extend from 3 to 10m depth. These can be also attributed to the bauxite lenses. Similarly for T3, where a large resistive area is visible between 20-64m distance and 6-24m depth.

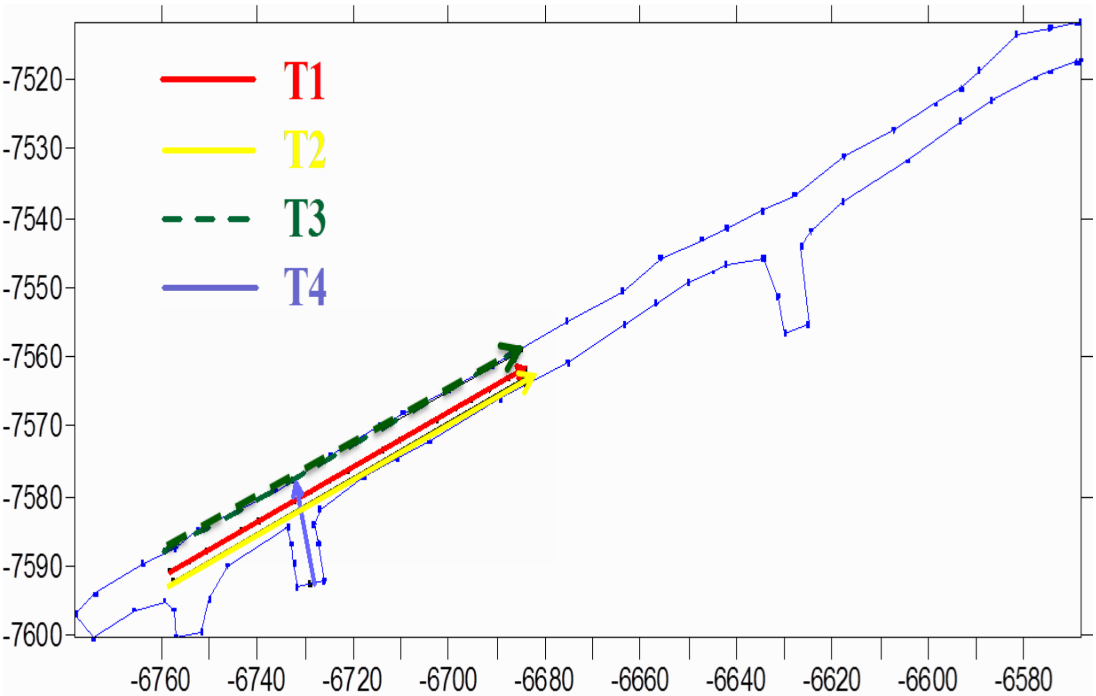

Figure 4.12: Location of ERT survey lines in Parnassus. The blue lines represent the gallery’s outline. T1 (red line) and T2 (yellow line) were conducted on the floor of the gallery, while T3 (green dashed line) was conducted on the wall. T4 (purple line) represents a GPR survey line.

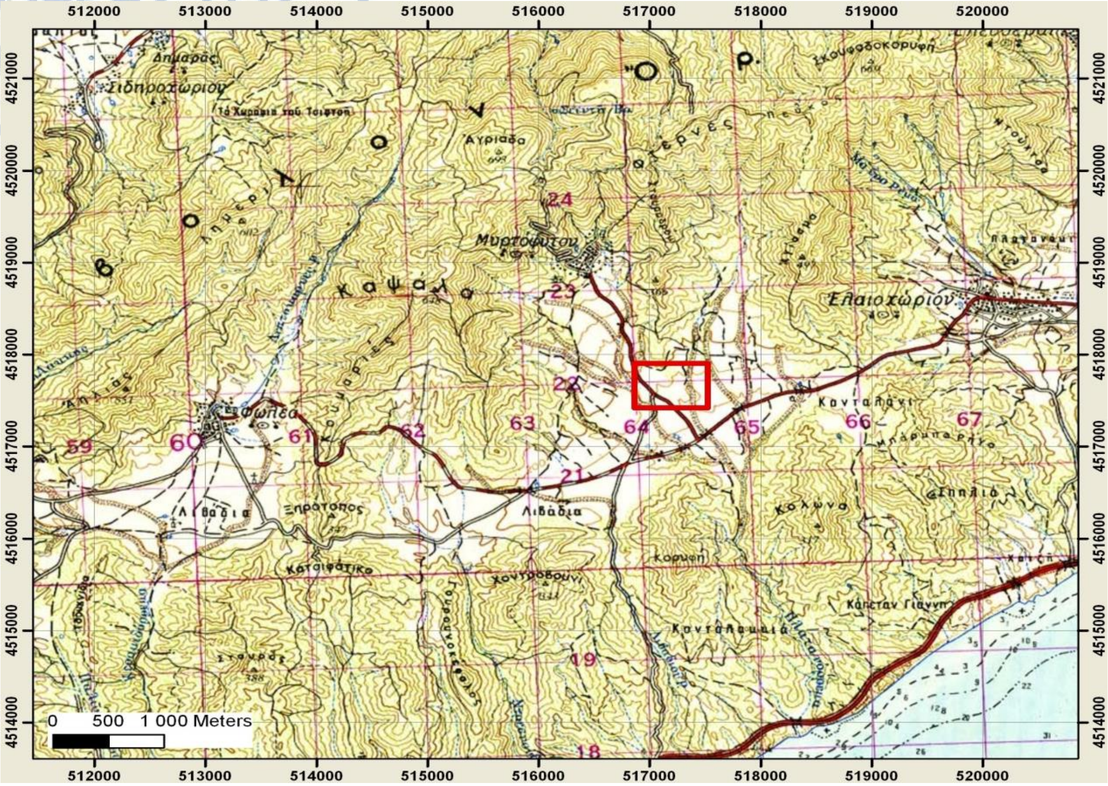

Figure 4.13: Mirtofito survey area. The red square shows the location where the measurements were collected.

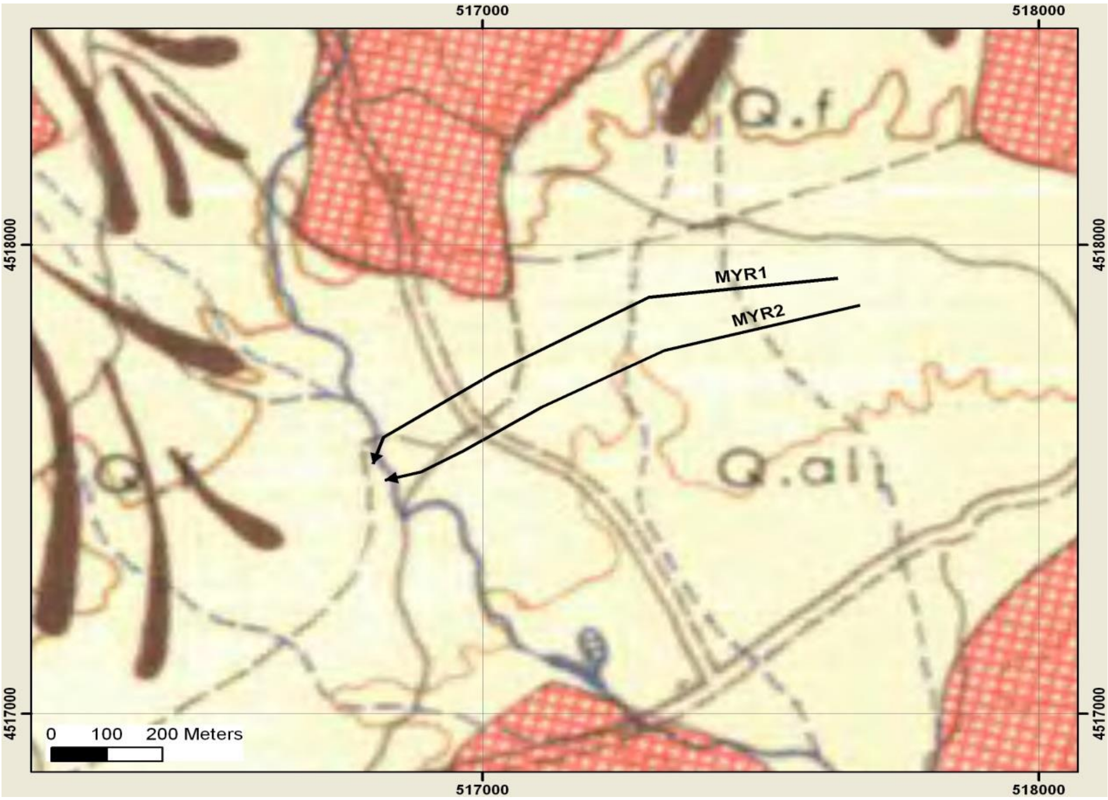

Figure 4.14: Survey lines in Mirtofito area.

The comparison of these results with the LCI solution showed that the LCI scheme was not able to provide an accurate solution for T1 and T2 due to the 2-D nature of the bauxite lenses, while the resistivity distribution is more similar between the two outputs for T3, probably due to the larger dimensions of the resistive structure.

The fourth case shows the inverted data of a survey located in Mirtofito. The area of the survey is shown in figure (4.13). It is consisted of boulders, conglomerates, pebbles, red clay and other fine-grained material. The bedrock is expected to be made of granite.

During the survey, 21 electrodes were used with 50m spacing. Two electrical tomographies, with a length of 1000m each and maximum penetration depth of ~200m, were conducted. The survey lines are shown in figure (4.14), but only the inversion of line MYR1 is shown in figure (4.15), as the inversion results for the two lines were very similar. The low resistivity values (<50 Ohm·m) at shallow depths represent the sedimentary deposits, whereas resistivities in the range of 50-160 Ohm·m are attributed to the weathering mantle of the granite. Below the depth of 50 m and from 150 to 650m of the survey line, the granite is expected to be found, with high resistivity values. After the 650th metre there is a transition zone to lower resistivity values, which was attributed to the existence of a vertical fault at the 650th metre. The LCI scheme was able to resolve both the granite and the fault accurately. The lower resistivity values at the left section of the LCI pseudo-2D between 250-400m can be justified by the lack of information at greater depths that affects the solution.

The last case is from Mygdonia basin, which is situated between the two lakes Volvi and Lagada around 45 km northeast of Thessaloniki, with significant seismic activity. Mygdonia basin consists of thick (~200-500m) sediments lying on a gneiss-schist basement. During the survey, 48 electrodes were used with a spacing of 5m. In figure (4.15e), two distinct regions are noticed extending along the profile, a resistive area at depth 0-12m and a conductive at 12-60m depth. The resistive layer can be interpreted as coarse deposits, such as gravel, while the conductive layer as finer deposits having silty sand, sand or clay. The outputs of the two different schemes proved to be similar. In this case, the LCI software did provide accurate results due to the fact that the subsurface had a layered structure, in contrast with previous examples that demonstrated the inability of the laterally constrained inversion to resolve 2D targets, which are better resolved with the 2-D smooth structure scheme.

The data fit rms error between the observed and the calculated dataset was at an acceptable level with values of ~3-6% and ~4-10% for the DC2DPRO and the LCI software, respectively.

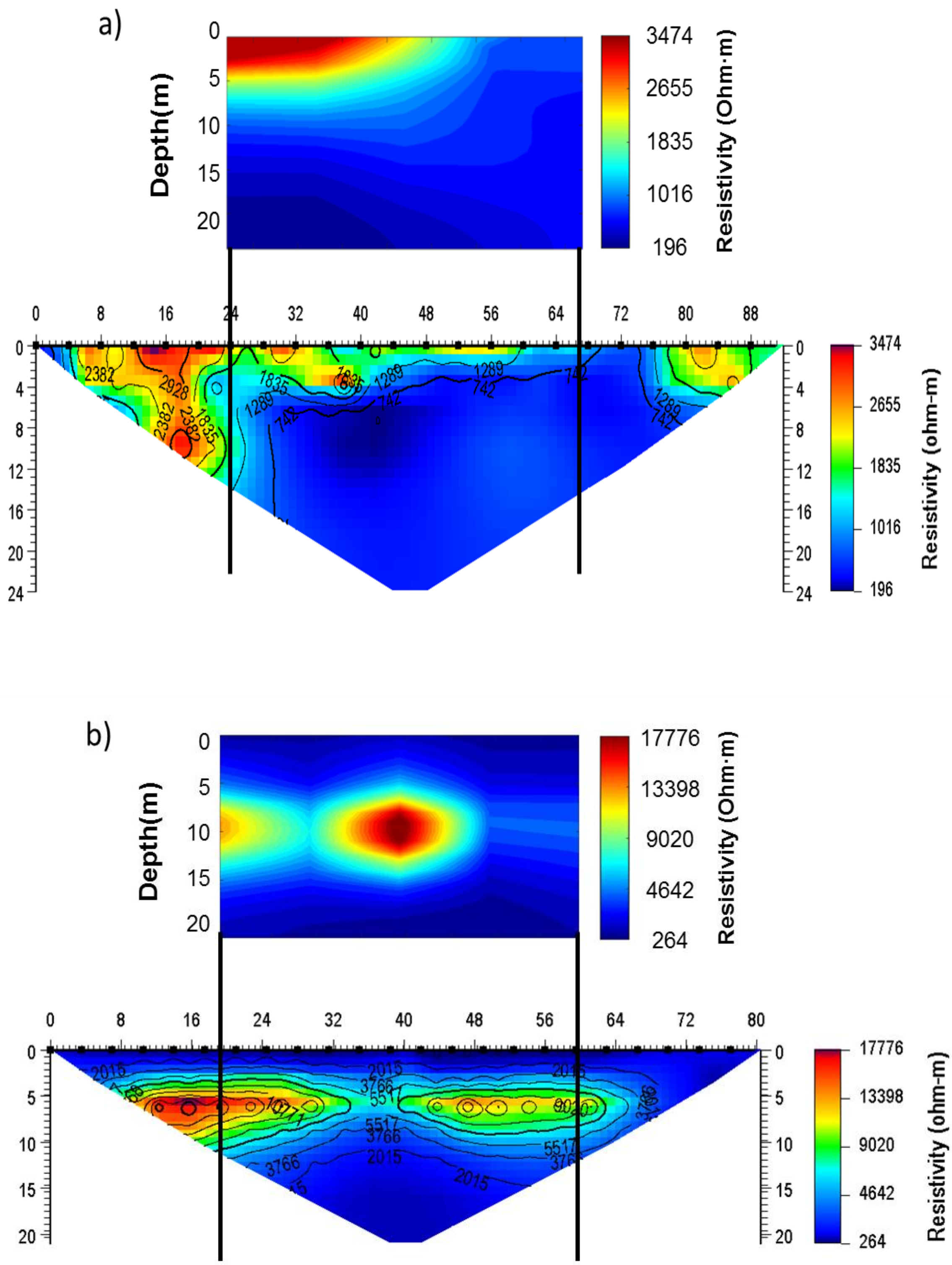

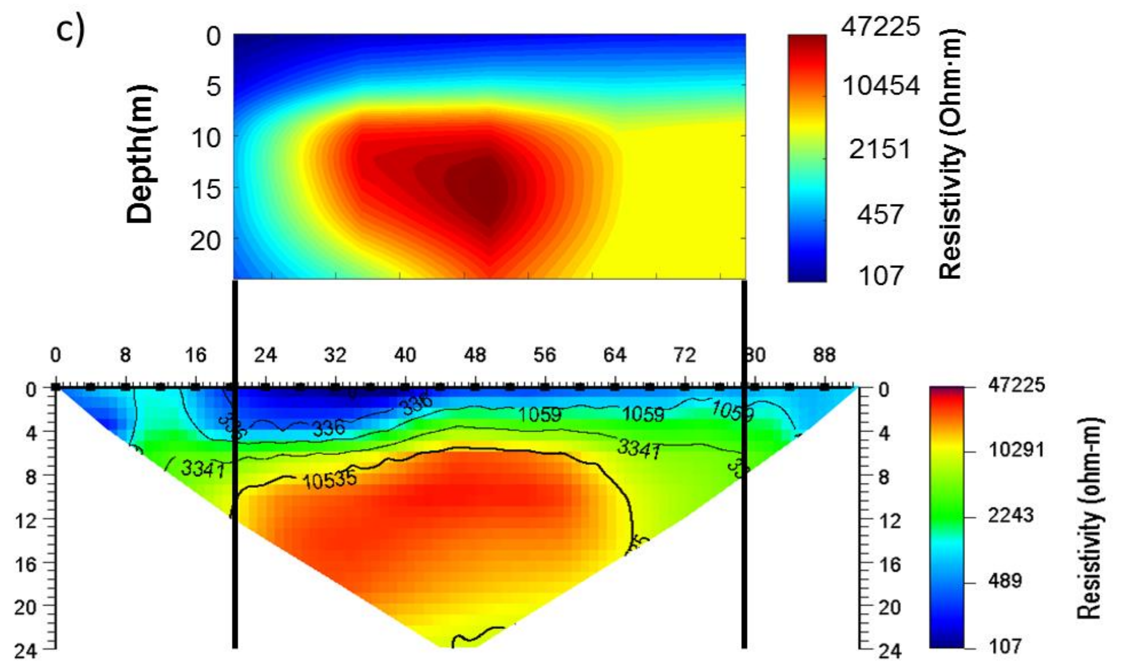
c)
Depth(m)
Resistivity (Ohm·m)
47225
10454
2151
457
107
Resistivity (ohm-m)
10291
2243
489

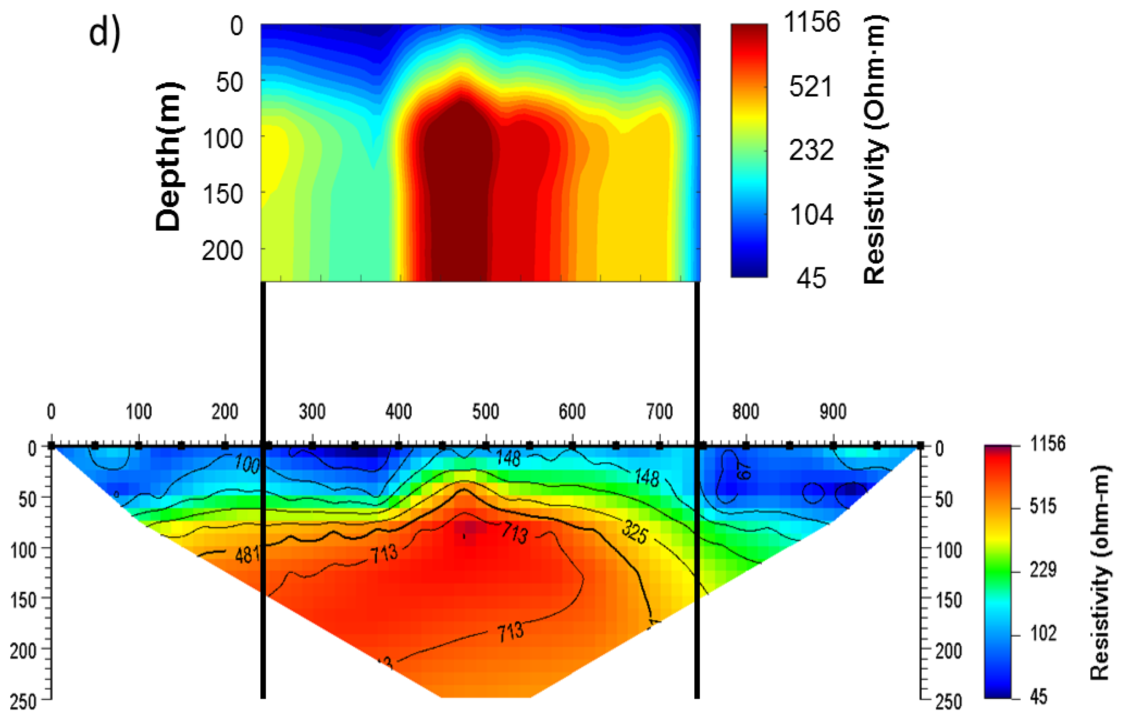
d)
Depth(m)
Resistivity (Ohm·m)
1156
521
232
104
45
Resistivity (ohm-m)
515
229
102

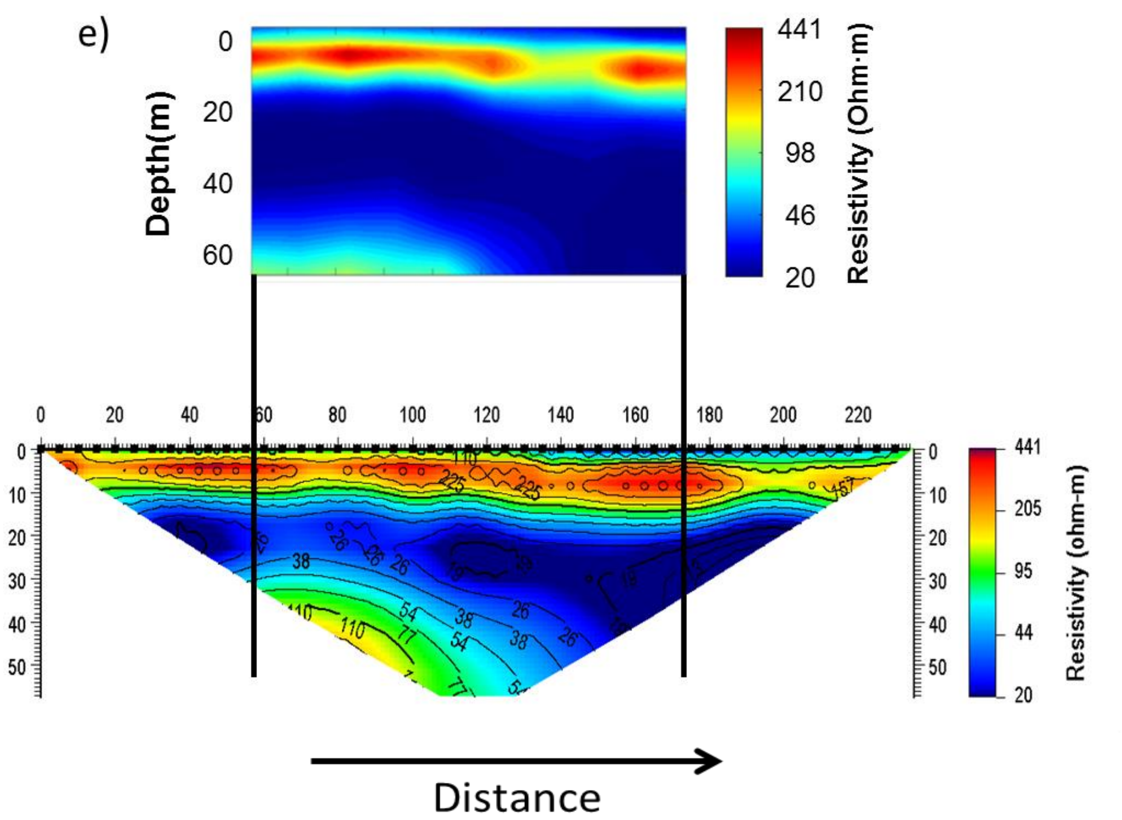

Figure 4.15: Inversion results of the real data using the LCI program (top) and the DC2DPRO software (bottom).

5. CONCLUSIONS AND RECOMMENDATIONS

5.1 Conclusions

The main aim of this thesis was to develop schemes for the laterally-constrained inversion of electrical resistivity tomography data and to evaluate the effectiveness of this method. The reason for developing LCI schemes was to provide a tool that can resolve sharp layer interfaces and thus, enhance the accuracy of the interpretation. The conclusions, which were drawn from this study, are presented below:

- The laterally constrained inversion scheme can locate sharp layer interfaces in contrast to the 2-D smooth-structure schemes. The two different techniques should be used in conjunction to improve the interpretation. Given a priori geological data, the joint interpretation of these methods can lead to a precise geological model.
- The LCI algorithm proved to be faster compared to a 2-D smooth-structure algorithm due to the 1-D formulation of the forward problem, as mentioned in paragraph 4.5 and from additional tests that were not presented in the thesis for the sake of brevity.
- Following section 4.1, removing the soundings with a small number of measurements at the boundaries resulted to more accurate models. Using all the soundings could lead to erroneous models due to lack of information at greater depths at the boundaries of the tomography (Figure 4.2).
- The modification of the smoothness matrix to change at each iteration depending on the thicknesses (see paragraph 4.2), which are allowed to vary throughout the inversion, proved to give more accurate results than using the same constraints in the smoothness matrix during the iterative procedure (Figure 4.6d). The thicknesses change and as a result the adjacent parameters and therefore, this change should be taken into account in order to provide the appropriate constraints.
- The choice of the vertical to horizontal smoothness ratio plays an important role in the LCI inversion. This ratio should be small with minor weight given

to the vertical constraints between parameters in order to achieve the optimum results (see section 4.2 and Figures 4.6b and c).

- The synthetic data showed that the LCI scheme was able to locate effectively the formation boundaries in cases of layered subsurface and even more accurately than the 2-D smoothness scheme, which produced a smoother image of the interfaces. A large number of different models were used and the LCI resulted to a very good approximation of the true model at each case (Figure 4.11).
- The synthetic data also showed that it is not possible to resolve models with significant 2-D structures with the laterally-constrained inversion due to the inability of any 1-D scheme to resolve 2-D or 3-D variations. In this case a 2-D formulation of the forward problem should be used or a smooth-structure technique.
- The application of the LCI scheme in real data proved that the algorithm cannot resolve accurately 2-D structures but can provide accurate results when the subsurface is almost layered (Figure 4.15).

5.2 Recommendations

The present thesis studied inversion schemes of ERT data, which are able to detect sharp layer boundaries. Useful conclusions were drawn by this study, but further research is required.

Acquisition of real data and modelling with more complex layered structures is necessary in order to evaluate the proposed laterally-constrained inversion scheme. The scheme should be tested with dipping structures within the layers to find the ability of the algorithm to detect them and the maximum slope that the 1-D code can resolve.

Regarding the configurations, a numerical integration of the 2-D sensitivity distributions should be implemented in this scheme, in order for the algorithm to be able to run with different and more common ERT arrays. This way the lateral focus point of each measurement can be found and thus, the algorithm will overcome the limitation of the asymmetrical arrays. In addition, the forward model should be modified to include different arrays, as this filter method applies to Schlumberger data only.

Regarding the laterally-constrained scheme, improvements should be made to make it capable of handling both sharp layer interfaces and 2-D structures more accurately.

Applications of the LCI scheme on large datasets should be examined in order to test the speed of the algorithm compared to a 2-D smooth inversion. LCI can significantly speed the inversion running times when dealing with large number of electrodes and data points. One such application would be the inversion of marine ERT survey data.

5.2 Recommendations

APPENDIX A

LCI SOFTWARE DESCRIPTION

LCI is a software that performs laterally-constrained inversion of electrical resistivity tomography (ERT) data. The program was created as a graphical user interface (GUI) and the code was written using the MATLAB environment. The 2015a MATLAB version was used. The only requirement to execute the program is the installation of the MATLAB platform. The LCI software was tested in every operating system supported by MATLAB (Windows, Linux, Mac, Solaris).

The main functions included in the LCI program and their functionality are listed in table (A.1). All functions contain MATLAB code and have .m extension. The code was organized to separate functions to improve its readability and maintenance and also to enable the portability of the functions. The LCI.m file along with its figure (LCI.fig) is the main program.

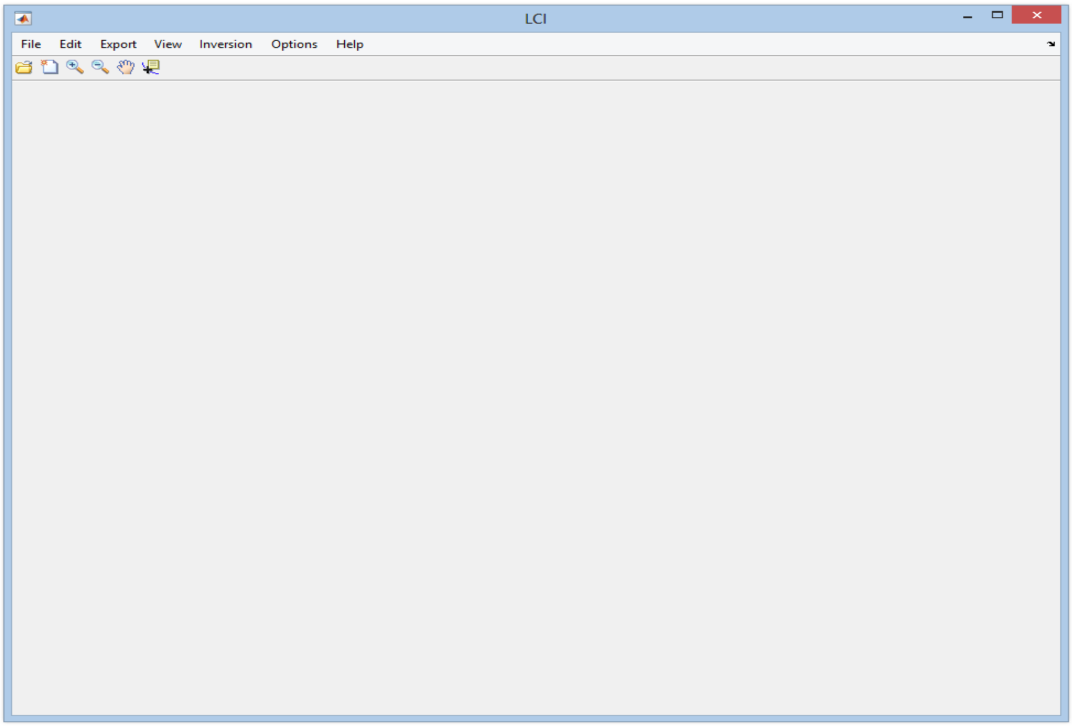

Figure A.1: The main window of the LCI program.

In figures (A.1) and (A.2) the main window of the program and the menu are illustrated. From the File option in the menu, the ERT data are selected. The data file formats used for DC2DPRO and Res2dinv software are supported by the program and the original binary files can be used as input as well. The default data file format is shown in figure (A.3). The 5 columns correspond to the positions of electrodes A, B, M and N and the apparent resistivity, respectively.

Function	Description
app_res	Calculates the apparent resistivity.
calc_ini_model	Sets initial resistivity model.
calc_jac	Calculates the Jacobian matrix using the perturbation technique.
calc_rms	Calculates the RMS error.
calculate_dx	Calculates the model correction using the smoothness-constrained method.
calculate_geom	Calculates the geometrical factor.
colorbar	Auxiliary function that generates a colorbar similar to the one used in DC2DPRO.
forward_fun	Solves the forward problem using the filter method.
LCI	Main program (GUI).
resolution_matrix	Calculates the resolution matrix.
smooth_matrix	Constructs the smoothness matrix.
spead	Calculates the Backus-Gilbert spread function.

Table A.1: List of the main functions included in the LCI software.

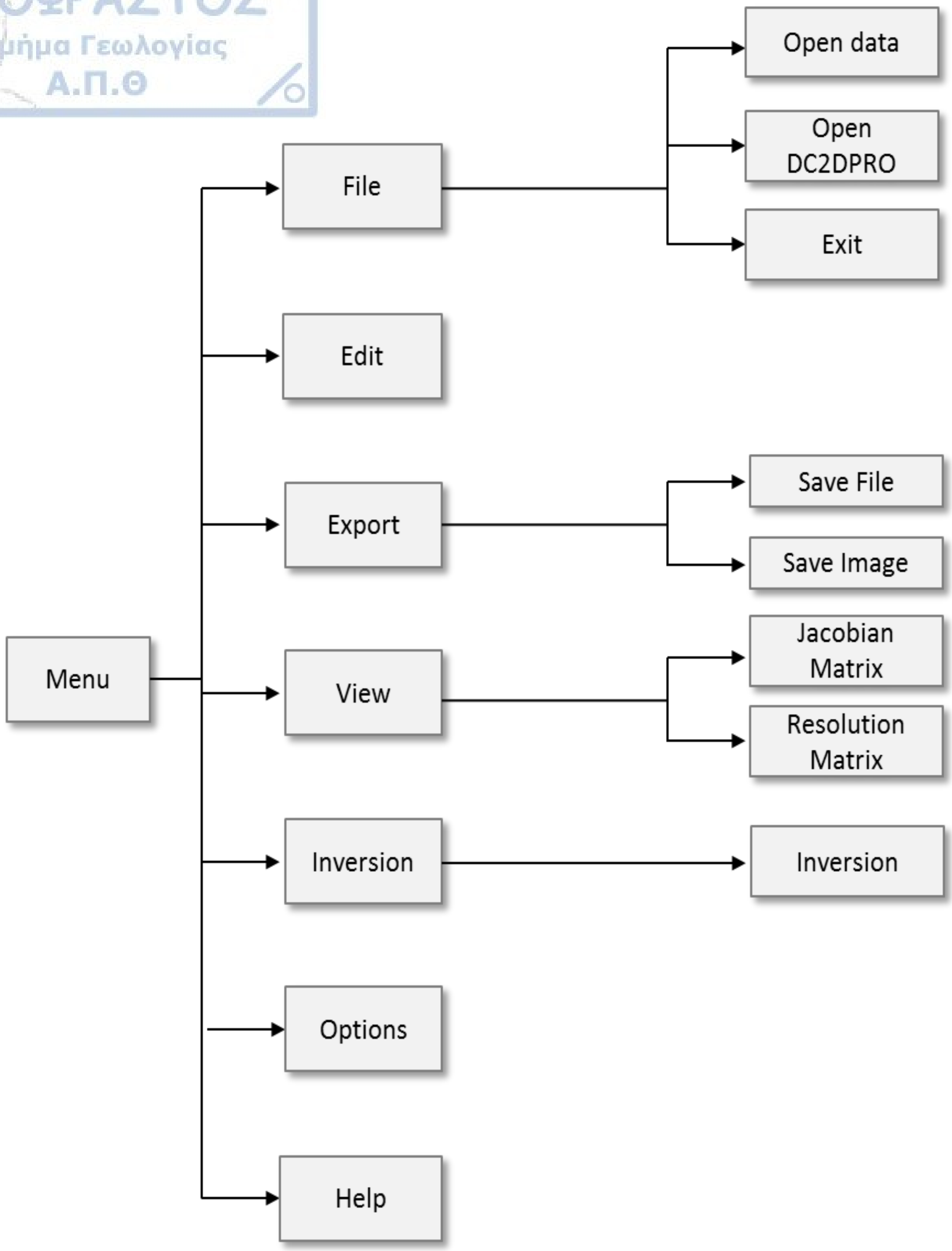

Figure A.2: Menu of the LCI software.

In addition, a typical DC2DPRO file with .A2D extension, is shown in figure (A.4), as the data files used in this work had this format. The first line shows the version of the software, the second is the filename and the third is the number of boreholes. The fourth line shows the number of electrodes used and is followed by a series of lines with the number and the x, y, z position of each electrode. The next line includes the number of topography data and is followed by the number of measurements and the data format, i.e. if the file contains apparent resistivity, potential or both values. Afterwards, each line corresponds to a specific measurement showing which electrodes were used and the value of the measurement.

```
475.00 525.00 495.00 505.00 27.799
470.00 530.00 495.00 505.00 30.700
460.00 540.00 495.00 505.00 31.700
450.00 550.00 495.00 505.00 32.400
450.00 550.00 490.00 510.00 32.700
435.00 565.00 495.00 505.00 31.799
435.00 565.00 490.00 510.00 32.700
420.00 580.00 490.00 510.00 35.900
400.00 600.00 490.00 510.00 40.400
```

Figure A.3: Sample of the default data file format that is supported by the program.

```
1000
File1.bin
0
10
    1       0.00       0.00          0
    2      50.00       0.00          0
    3     100.00       0.00          0
    4     150.00       0.00          0
    5     200.00       0.00          0
    6     250.00       0.00          0
    7     300.00       0.00          0
    8     350.00       0.00          0
    9     400.00       0.00          0
   10     450.00       0.00          0
0
       170         0
     1    9    4    6        170.233
     1    7    3    5        164.398
     1    5    2    4        155.417
     1   10    5    6        168.751
     1    8    4    5        170.060
     1    6    3    4        161.245
     1    4    2    3        153.370
     2   10    5    7        161.793
     2    8    4    6        162.353
     2    6    3    5        155.058
     2    9    5    6        165.535
     2    7    4    5        160.228
     2    5    3    4        153.206
                        ...
```

Figure A.4: Example of DC2DPRO data file format.

The inversion results can be saved to a text file with the format shown in figure (A.5).

```
----------------------------------------------------
   Laterally Constrained Inversion of ERT data
----------------------------------------------------

Data File: Model1.A2D
Path: C:\Users\User\Desktop\models\
Array: Schlumberger
Number of electrodes: 21
Occam Inversion: Smoothness on model changes
2D smoothness: Vertical-to-Horizontal: 0.5
Lagrange multiplier: From ACB
Number of soundings: 13
Number of data: 250
Number of layers: 7
Max Depth: 230 m
----------------------------------------------------

RMS error: 1.450 %
Number of iterations: 12
----------------------------------------------------

VES 1 - Center: 275.00 m
Res(Ohm*m)     Thick(m)
129.430000     6.890000
143.390000     14.230000
164.400000     21.740000
161.040000     28.890000
142.330000     35.240000
148.720000     40.830000
176.190000     999.000000

VES 2 - Center: 300.00 m
Res(Ohm*m)     Thick(m)
129.080000     6.850000
148.580000     14.250000
164.980000     21.800000
147.950000     28.930000
129.470000     35.240000
143.890000     40.600000
191.560000     999.000000


                            ...
```

Figure A.5: Example of an output file with the inversion results.

The first section of the output file, after the title, presents information about the input file and the inversion options. The sequence of elements included in each line is given above:

1. Name of input data file.
2. Path of the data file.
3. The type of array.
4. The number of electrodes.
5. The inversion option:
   -Smoothness on model changes
   -Smoothness on model
6. The type of smoothness:
   -1D smoothness
   -2D smoothness: If 2D is selected, the vertical-to-horizontal smoothness ratio is also given.
7. The lagrange multiplier:
   -Constant value
   -Active Constrained Balancing
8. The number of soundings
9. The number of data
10. The number of layers used for each VES
11. The maximum depth used.

The next section shows the RMS error of the inversion and the number of iterations required for the solution to converge. The following lines represent the resultant model of each VES. The section starts with the number of the first VES, which is given along with the position of its center. This is followed by the resistivity and thickness of each layer. Then, the model of the second VES is given and so on.

After opening the input file, two panels appear on the screen, as shown in figure (A.6). The first panel (“Options”) includes a number of inversion options. These options can be adjusted depending on user’s choice. In the second panel (“Block parameters”), a sketch of the initial model is presented, showing the position of each VES, the number of parameters, the number of layers and their thicknesses. Changing one of the inversion parameters will update the initial model dynamically.

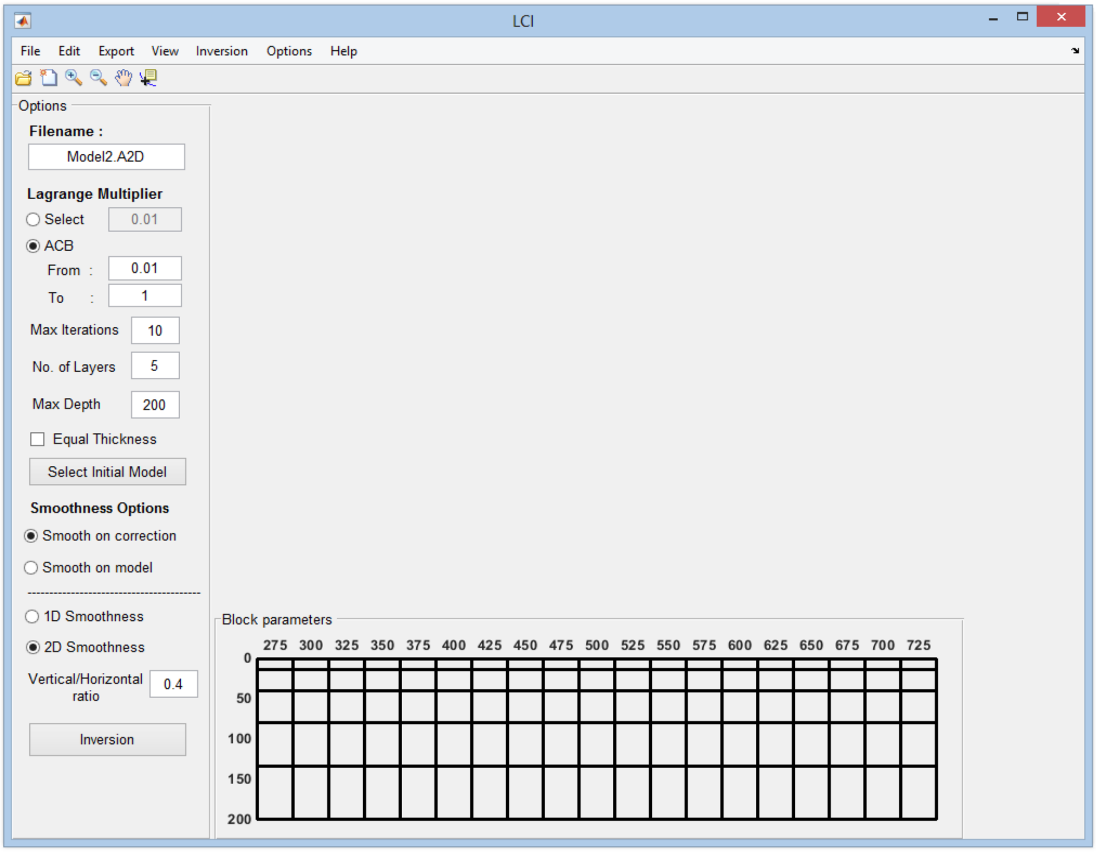

Figure A.6: The inversion parameters that can be modified and a graphical representation of the initial model.

From the options panel, user can define if the lagrange will have a single value or it will be calculated through ACB (Figure A.7a). Choosing ACB will enable the “from” and “to” text boxes, in order to choose the upper and lower limit of the lagrange multiplier. Also, the maximum number of iterations can be selected; otherwise the default value of 10 iterations will be used. In addition, there are options regarding the initial model, as displayed in figure (A.7b). These options are the number of layers, the max depth of investigation and a choice to determine if the layers will have equal thickness or their thickness will be increased gradually from top to bottom. Initial values for the model parameters can also be assigned.

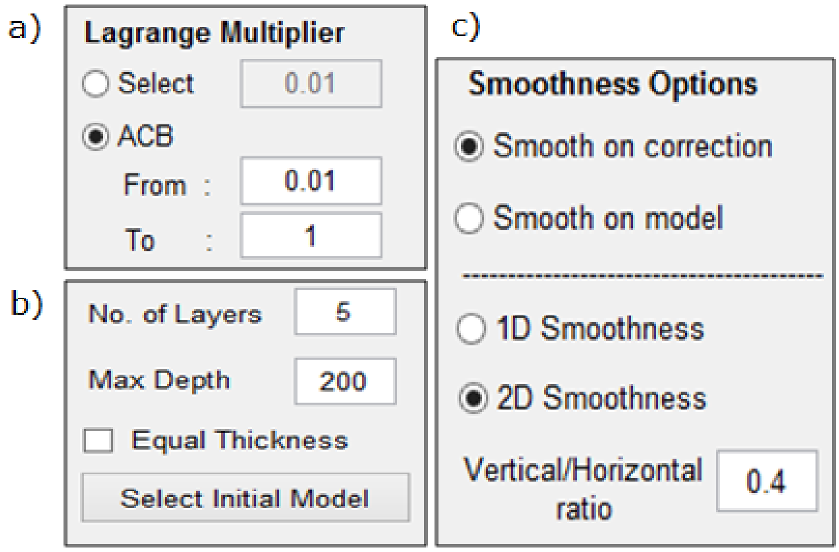

Figure A.7: Inversion options regarding: a) The lagrange multiplier, b) The initial model, c) The smoothness.

There are different smoothness options (Figure A.7c). The smoothness can be applied only to the model changes or it can include an extra term which also applies smoothness to the model. The first option is considered as the standard option, whereas the second is safer to use it only in cases of very noisy data. Apart from the 2-D smoothness, 1-D smoothness can be applied, which will produce the same results as if the soundings where inverted separately. In addition, the ratio of vertical to horizontal smoothness can be assigned. The smoothness can be applied only vertically or horizontally by creating two different smoothness matrices. If both are chosen, these two matrices are merged into one and the weight of each one is specified by their ratio. For instance, if 1 is chosen as the ratio, then both will contribute equally to the total smoothness in the inversion, whereas if 0.2 is chosen, then the horizontal smoothness will contribute five times the contribution of the vertical smoothness. For the laterally constrained method it is recommended that the weight of the horizontal smoothness is at least twice the weight of the vertical or even only lateral smoothness to be applied.

After all the inversion parameters have been chosen, the inversion can be executed from the Inversion menu → Inversion. An example with the results of running inversion is shown in figure (A.8). At the center of the window the pseudo-2D plot appears and a table containing the final model for each sounding. The values for the parameters are denoted as Res_1 and Thick_1 for resistivities and thicknesses of the first sounding, Res_2 and Thick_2 for the second sounding and so on. The units for resistivity and thickness are Ohm·m and meters, respectively. Next to this table a panel appears contained information about the inversion. It shows the RMS error, the value of the lagrange multiplier if it is a constant or the string 'ACB' if the active constrained balancing is on, the number of iterations required to converge, the number of data used and the number of soundings.

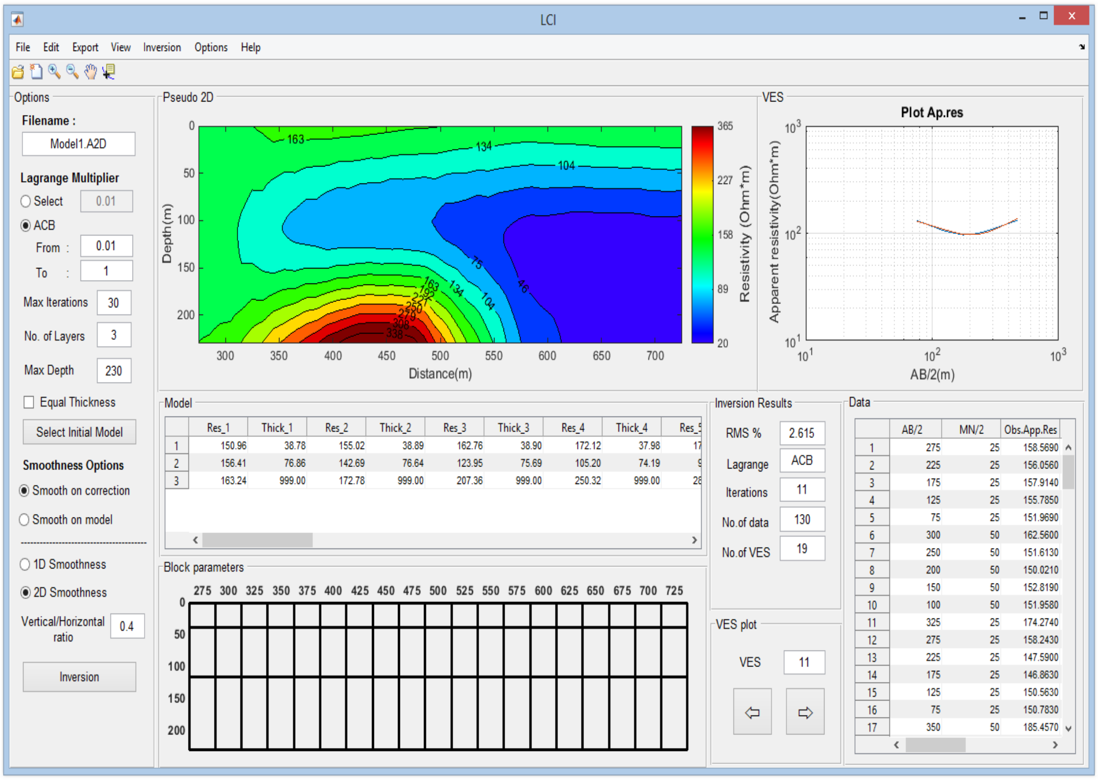

Figure A.8: An example of the window with the results after running the inversion with the LCI software.

On the right side of the window there is a plot showing the apparent resistivity curve of the real data, compared with the one from the calculated data for a certain sounding. The soundings can be switched using the two arrows on the bottom right of the screen, but only one sounding can be displayed at a time. Moreover a table with 6 columns, representing the AB/2 spacing, the MN/2 spacing, the geometrical factors, the observed and calculated apparent resistivities and the difference and the relative difference between the observed and calculated data, is given on the right side of the screen.

A better view of the inversion results and the way the VES are switched in the second plot is illustrated in the example in figure (A.9), whereas in figures (A.10) and (A.11) the final models and the full table containing with the 6 columns stated above, respectively, are shown.

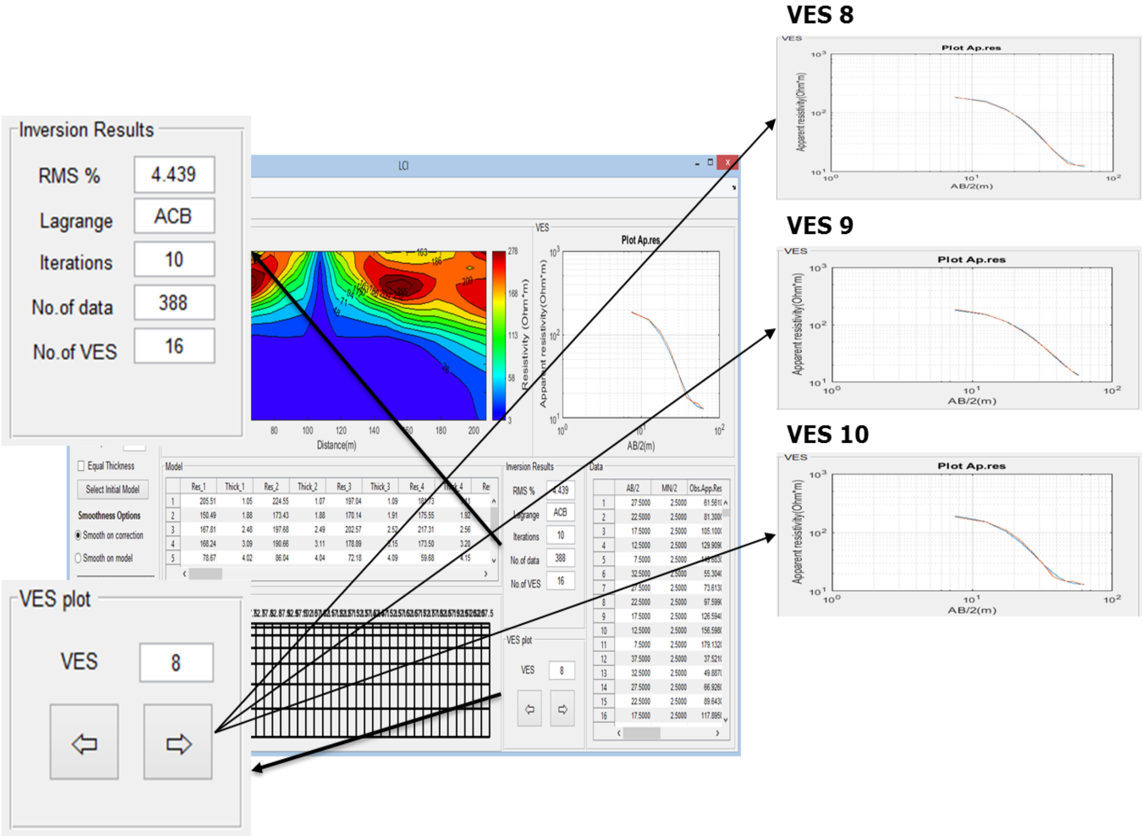

Figure A.9: Displaying apparent resistivity curves for different soundings using the left and right arrows.

The inversion results can be saved to an output file, with the format specified above and the pseudo-2D plot as an image. This is done by selecting from the Export menu → Save File and → Save image, respectively. The resolution matrix can also be displayed from the View menu → Resolution Matrix and thus, the accuracy of the parameters can be checked. Also, the Jacobian Matrix can be displayed from the same menu by choosing → Jacobian Matrix. An example of a resolution and a jacobian matrix is illustrated in figure (A.12).

Model

	Res_1	Thick_1	Res_2	Thick_2	Res_3	Thick_3	Res_4	Thick_4
1	205.51	1.05	224.55	1.07	197.04	1.09	181.73	1.11
2	150.49	1.88	173.43	1.88	170.14	1.91	175.55	1.92
3	167.81	2.48	197.68	2.49	202.57	2.52	217.31	2.56
4	168.24	3.09	190.66	3.11	178.89	3.15	173.50	3.20
5	78.67	4.02	86.04	4.04	72.18	4.09	59.68	4.15
6	31.10	5.62	33.28	5.65	26.28	5.76	20.40	5.89
7	22.58	999.00	23.78	999.00	17.96	999.00	13.69	999.00

Figure A.10: Final model for each sounding.

Data

	AB/2	MN/2	Obs.App.Res	Calc.App.Res	Δρ	Δρ%	Geom
1	27.5000	2.5000	61.5610	65.5012	-3.9402	6.4004	471.2389
2	22.5000	2.5000	81.3000	83.8954	-2.5954	3.1924	314.1593
3	17.5000	2.5000	105.1000	107.5935	-2.4935	2.3725	188.4956
4	12.5000	2.5000	129.9090	133.7413	-3.8323	2.9500	94.2478
5	7.5000	2.5000	149.6830	155.2522	-5.5692	3.7207	31.4159
6	32.5000	2.5000	55.3040	57.5367	-2.2327	4.0371	659.7345
7	27.5000	2.5000	73.6130	72.9304	0.6826	0.9273	471.2389
8	22.5000	2.5000	97.5990	94.5217	3.0773	3.1530	314.1593
9	17.5000	2.5000	126.5940	122.5179	4.0761	3.2198	188.4956
10	12.5000	2.5000	156.5980	153.5551	3.0429	1.9431	94.2478
11	7.5000	2.5000	179.1320	178.4934	0.6386	0.3565	31.4159
12	37.5000	2.5000	37.5210	39.1452	-1.6242	4.3289	879.6459
13	32.5000	2.5000	49.8870	49.5001	0.3869	0.7755	659.7345
14	27.5000	2.5000	66.9260	64.9266	1.9994	2.9874	471.2389
15	22.5000	2.5000	89.6430	86.9483	2.6947	3.0060	314.1593
16	17.5000	2.5000	117.8950	115.9623	1.9327	1.6393	188.4956
17	12.5000	2.5000	148.7050	148.4804	0.2246	0.1511	94.2478
18	7.5000	2.5000	174.2750	173.3985	0.8765	0.5029	31.4159
19	42.5000	2.5000	24.9680	26.4392	-1.4712	5.8922	1.1310e+03
20	37.5000	2.5000	33.3030	33.0586	0.2444	0.7337	879.6459
21	32.5000	2.5000	44.8400	43.4275	1.4125	3.1501	659.7345
22	27.5000	2.5000	60.7970	59.2958	1.5012	2.4692	471.2389
23	22.5000	2.5000	82.6220	82.5276	0.0944	0.1143	314.1593
24	17.5000	2.5000	111.0860	113.8486	-2.7626	2.4869	188.4956
25	12.5000	2.5000	144.1220	149.5591	-5.4371	3.7726	94.2478

Figure A.11: The results include a table with 6 columns, representing the AB/2, MN/2, the geometrical factors, the observed and calculated apparent resistivities and the difference and the relative difference between the observed and calculated data.

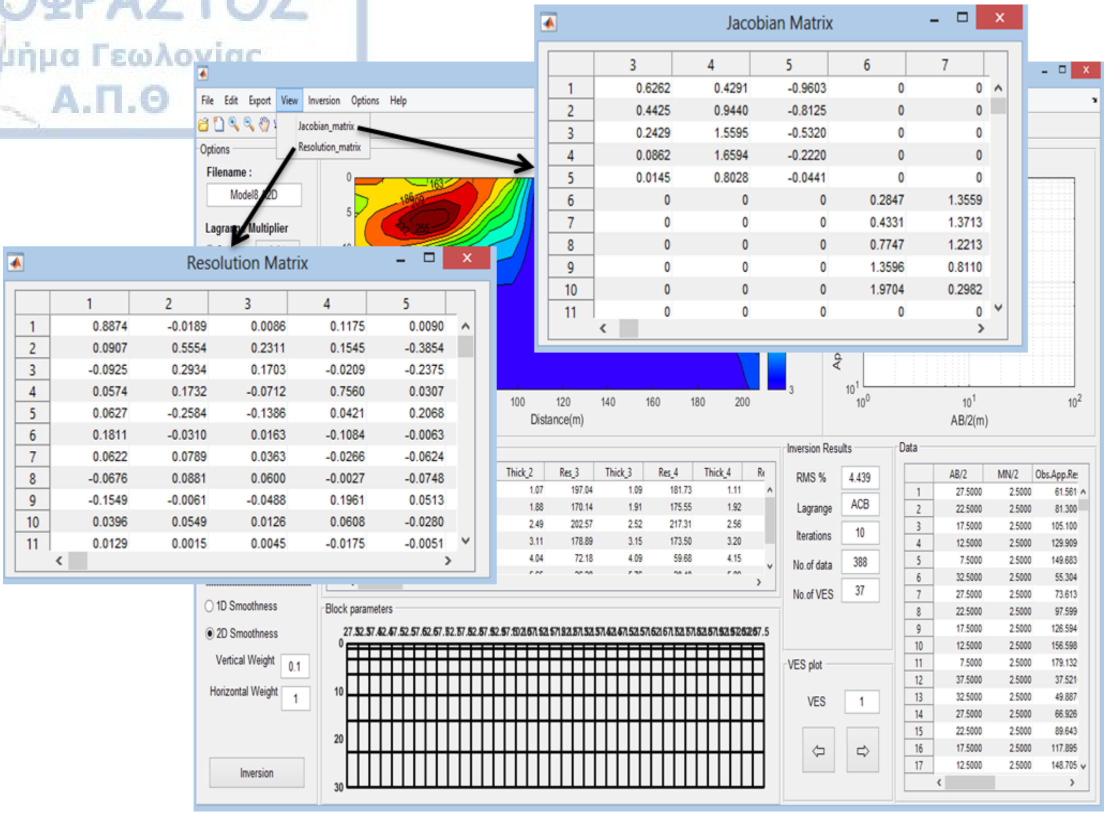

Figure A.12: An example showing the resolution and the jacobian matrix.

APPENDIX B

CODE OF THE SOFTWARE

In this section, the code of a number of functions, which were developed for the LCI inversion, is introduced. The parameters that were used are explained above:

- centres : center of each VES
- num_meas : number of measurements
- num_layers : number of layers
- ab2 : spacing between current electrodes
- mn2 : spacing between potential electrodes
- oldapres : observed apparent resistivity
- apres: calculated apparent resistivity
- max_spacing : max distance between current probes
- depthmax : penetration depth
- oldrt : model from previous iteration
- m : initial model
- num_param: number of total system parameters
- geom : geometrical factor
- lagrange : lagrange multiplier
- SP : spread function
- rms : RMS error
- R : resolution matrix
- jac : jacobian matrix
- c : smoothness matrix
- dx : model correction
- param : new model

```
%------------------------------Load data and separate to VES-------------------------

[name,path]=uigetfile('*.*'); %open data file
y=load(fullfile(path,name));
oldr_param=[];
thick_param=[];
xa=y(:,1); %a electrode positions
xb=y(:,2); %b electrode positions
xm=y(:,3); %m electrode positions
xn=y(:,4); %n electrode positions
old_apres=y(:,5); %measured apparent resistivities
centres=unique((xm+xn)/2); %find centres of each VES
for w=1:length(centres)
  s=1;
   for j=1:length(xn)
       if ((xm(j)+xn(j))/2)==centres(w)
           ab2(s,w)=abs(xb(j)-xa(j))/2;
           mn2(s,w)=abs(xn(j)-xm(j))/2;
           oldapres(s,w)=old_apres(j);
           s=s+1;
       end
       len_ves(w)=s-1;
   end
   max_spacing(w,1)=max(ab2(:,w));
   data.(strcat('ab2_',num2str(w)))=nonzeros(ab2(:,w));
   data.(strcat('mn2_',num2str(w)))=nonzeros(mn2(:,w));
   data.(strcat('oldapres_',num2str(w)))=nonzeros(oldapres(:,w));
   [data.(strcat('geom_',num2str(w))),data.(strcat('r_',num2str(w)))]...
    =calculate_geom(nonzeros(ab2(:,w)),nonzeros(mn2(:,w)));
end
```

Figure B.1: Code that loads the data file and divides the data-set into soundings.

```
%---------------------------Calculate Geometrical Factor------------------------------

function [geom,r]=calculate_geom(ab2,mn2)
z=1;
num_meas=length(ab2);
    for i=1:num_meas
        r(z,1)=ab2(i)-mn2(i);
        r(z+1,1)=ab2(i)+mn2(i);
        geom(i,1)=3.14159265359*(((ab2(i)^2)-(mn2(i)^2))/(2*mn2(i)));
        z=z+2;
 end
```

Figure B.2: Function that calculates the geometrical factor.

```
%--------------------------Calculate thickness of each layer----------------------------

% First checks if equal thickness for all layers is on
if get(handles.eq_thick_check, 'Value')==1;
     a=depthmax/num_layers;
     for l=1:num_layers
     thick(l,1)=a;
     end
else
 num_a=1;
 for i=2:num_layers
    num_a=num_a+2*i-i;
 end
    a=depthmax/num_a;
    b=0;
    for l=1:num_layers
    thick(l,1)=l*a; %matrix with initial thickness for 1 VES
    end
end
```

```
%-------------------------------------------------------------------------------------------------
%------------------------------------Set initial model------------------------------------

 for j=1:ves_num
    m(1:num_layers,j)=median(data.(strcat('oldapres_',num2str(j))));
    m(num_layers+1:2*num_layers-1,j)=thick(1:num_layers-1);
end
```

Figure B.3: Initial model chosen by default.

```
%----------------------------Active Constrained Balancing----------------------------

if iter == 1
  lagrange = 0.005;
else
  %Take lagrange min and max values
  lmin = str2num(get(handles.from_acb,'String'));
  lmax = str2num(get(handles.to_acb,'String'));
  %Calculate resolution matrix
  R = resolution_matrix(jac, cTc, lagrange);
  %Calculate spread function
  SP = spead(R, Cnew, X,depth, max_spacing);
  %Calculate lagrange values
  for i=1:length(SP)
        log_lag(i) = log10(lmin)+((log10(lmax)-log10(lmin))…
         /(log10(max(SP))-log10(min(SP))))*(log10(SP(i))-log10(min(SP)));
         lag(i) = 10^log_lag(i);
  end
  %Diagonal matrix with lagrange values
  lagrange = diag(lag);
end
```

Figure B.4: Active constrained balancing code.

The algorithms are written in MATLAB and can be executed directly providing the appropriate data file. The codes for the calculation of the forward solution and the jacobian matrix are not presented as they can be solved with any known forward problem algorithm with different sets of filters that have been proposed and perturbation schemes.

```
%------------------- CALCULATE SPREAD FUNCTION -------------------------

 for i=1:size_smooth(1)
     sum=0;
     for j=1:size_smooth(1)
         %Calculate weights
         w(i,j)=((XX(i)-XX(j))^2) +(YY(i)-YY(j))^2;
         %Calculate S matrix based on smoothness matrix
         if Cnew(i,j)~=0
             S(i,j)=1;
         else
             S(i,j)=0;
         end
         %Sum for SP value
         sum=sum+(w(i,j)*(1-S(i,j))*R(i,j))^2;
     end
     %Calculate SP
     SP(i)=sum;
 end
```

Figure B.5: Backus-Gilbert Spread function.

```
%---------------------Code to calculate to calculate RMS error--------------------

function rms=calc_rms(apres,oldapres)
sum=0;
num_meas=length(apres);
```

```
for i=1:num_meas
    sum=sum+((oldapres(i,1)-apres(i,1))/(oldapres(i,1)))^2;
end
rms=(sqrt(sum/num_meas))*100;
```

Figure B.6: Function that calculates the RMS error.

```
%-----------------------------------Model Correction----------------------------------

function param=calculate_dx(jac,iter_num,apres,oldrt,oldapres,cTc,lagrange,
num_layers,ves_num,handles)

if length(lagrange)==1
  if iter_num>1 && iter_num<4
          lagrange=lagrange/2;
  end
end
 oldrt=reshape(oldrt,[],1);
 num_param=length(oldrt);
 num_meas=length(apres);

 %Calculate difference between observed and calculated data

 for i=1:num_meas
     dy(i,1)=log10(oldapres(i,1))-log10(apres(i));
 end
 ss=lagrange*cTc;

 %Calculate model correction

 if get(handles.smooth_corr,'Value')~=0
 dx=inv(jac'*jac+ss)*jac'*dy;
 else
```

```
dx=inv(jac'*jac+ss)*jac'*dy-(ss*log10(oldrt));
end

%New model parameters

for i=1:num_param
   param_all(i,1)=10^(log10(oldrt(i))+dx(i,1));
end
w=1;
for i=1:ves_num
   param(:,i)= param_all(w:w+2*num_layers-2,1);
   w=w+2*num_layers-1;
end
```

Figure B.7: Function that calculates the correction of the model.

REFERENCES

Auken, E., Foged, N., and Sørensen, K. I. (2002). Model recognition by 1-D laterally constrained inversion of resistivity data: 9th Meeting, Environmental and Engineering Geophysical Society—European Section, Proceedings, 241–244.

Auken, E., and Christiansen, AV. (2004). Layered and laterally constrained 2D inversion of resistivity data. Geophysics, 69, 752-761.

Auken E., Christiansen A.V., Jacobsen B.H., Foged N. and Sørensen K.I. (2005). Piecewise 1D laterally constrained inversion of resistivity data. Geophysical Prospecting 53, 497–506.

Auken, E., Christiansen, A., Jacobsen, L., Sørensen, K. (2008). A resolution study of buried valleys using laterally constrained inversion of TEM data. Journal of Applied Geophysics.

Constable, S.C., Parker, R.L. and Constable, C.G. (1987). Occam's inversion : A practical algorithm for generating smooth models from electromagnetic sounding data. Geophysics, 52, 289-300.

Christiansen, A. V., and Auken, E. (2003) Optimizing the 2D laterally constrained inversion (2D-LCI) using a quasi-Newton method and 1D derivatives. 9th Meeting, Enviornmental and Engineering Geophysical Society, European Section, Proceedings, O-030.

Christiansen, A., Auken, E., Foged, N., Sørensen, K. (2007). Mutually and laterally constrained inversion of CVES and TEM data: a case study. Near Surface Geophysics, Vol 5, No 2, pp. 115 - 123

Dahlin, T. and Zhou, B. (2006). Gradient array measurements for multi-channel 2D resistivity imaging, Near Surface Geophysics, 4, 113-123.

deGroot-Hedlin, C. and Constable, S. (1990). Occam's inversion to generate smooth, two-dimensional models from magnetotelluric data. Geophysics, 55, 1613-1624.

Ghosh, D.P. (1971a). The application of linear filter theory to the direct interpretation of geoelectrical resistivity sounding measurements. Geophysical Prospecting 19, 176–180.

Ghosh, D.P. (1971b). Inverse filter coefficients for the computation of apparent resistivity standard curves for a horizontally stratified earth. Geophysical Prospecting 19, 769–775.

Guptasarma, D. (1982). Optimization of short digital linear filters for increased accuracy: Geophys. Prosp., 30.501-514.

Kearey, P., Brooks, M., & Hill, I. (2002). An introduction to geophysical exploration. Malden, MA: Blackwell Science.

Kim J.H. (2010). DC2DPro – User's Manual, KIGAM, KOREA

Koefoed, O. (1970). A fast method for determining the layer distribution from the raised kernel function: Geophys. Prosp., 18, 564 570.

Koefoed, O. (1979). Geosounding Principles 1: Resistivity sounding measurements. Elsevier Science Publishing Company, Amsterdam.

Kreyszing, E. (1992). Advanced engineering mathematics. John Wiley and Sons.

Lanczos C. (1960). Linear differential operators. D. Van Nostrad Company Ltd.

Lawson C. and Hanson R. (1974). Solving least squares problems. Pentice-Hall.

Levenberg, K. (1944). A Method for the Solution of Certain Non-Linear Problems in Least Squares. The Quarterly of Applied Mathematics, 2. 164-168.

Lines L.R. and Treitel S. (1984). Tutorial : A review of least-squares inversion and its application to geophysical problems. Geophysical Prospecting, 32, 159-186.

Loke, M. H. (2001). Tutorial : 2-D and 3-D electrical imaging surveys.

Marquardt D. (1963). An Algorithm for Least-Squares Estimation of Nonlinear Parameters. SIAM Journal on Applied Mathematics, 11, 431–441.

McGillivray, P.R. and Oldenburg, D.W. (1990). Methods for calculating Frechet derivatives and sensitivities for the non-linear inverse problem : A comparative study. Geophysical Prospecting, 38, 499-524.

McGillivray P.R. (1992). Forward modeling and inversion of DC resistivity and MMR data. PhD thesis, The University of British Columbia, Vancouver, Canada.

Meju M.A. (1994). Geophysical data analysis: Understanding inverse problem, theory and practice. Course notes series, Vol. 6, Domenico, S.N., Editor.

Menke, W. (1984). Geophysical data analysis : Discrete inverse theory. Academic Press Inc.

Milsom, J. (2003). Field geophysics. 3rd ed. Chichester: Wiley

Oldenburg, D.W., Li, Y., 1999. Estimating depth of investigation in DC resistivity and IP surveys. Geophysics 64, 403–416.

Parasnis, D. (1986). Principles of applied geophysics. Chapman and Hall.

Tarantola, A. (1987). Inverse problem theory. Elsevier, Amsterdam.

Telford, W., Geldart, L., Sheriff, R., and Keys, D. (1991). Applied geophysics. Cambridge University Press.

Tikhonov A.N. (1963). Solution of incorrectly formulated problems and the regularization method. Soviet Mathematics, 4, 1035-1038.

Tikhonov A.N. and Glasko V.B. (1965). Application of a regularization method to nonlinear problems. J.Comp. Math. and Math. Physics, 5, no. 3.

Tikhonov, A. N., and Arsenin, V. Y.. 1977, Solutions of ill-posed problems: John Wiley and Sons, Inc.

Tsourlos P.I. (1995). Modeling, Interpretation and Inversion of Multielectrode Resistivity Survey Data. Ph.D. Thesis, Department of Electronics, University of York.

Tsourlos P., Szymanski J., Tsokas G. (1998). A smoothness constrained algorithm for the fast 2-D inversion of DC resistivity and induced polarization data. Journal of the Balkan geophysical society, Vol. 1, No 1

Tsourlos P., Tsokas G. and Yiamas A. (2005). Detecting bauxitic lenses in galleries using geophysical techniques. Proceedings of the 2nd Conference of the Committee of Economic Geology, Mineralogy and Geochemistry of the Greek Geological Society.

Vedanti, N., Srivastava, R., Sagode, J., Dimri, V.P. (2005). An efficient 1D Occam's inversion algorithm using analytically computed first- and second-order derivatives for DC resistivity soundings. Computers & Geosciences 31, 319–328

Ward, S. (1990). 6. Resistivity and Induced Polarization Methods. Geotechnical and Environmental Geophysics: pp. 147-190.

Yi M.J., Kim J.H., Chung S.H. (2003): Enhancing the resolving power of least-squares inversion with active constraint balancing. Geophysics, 68, No.3: 931-941.

Zhody, A. (1989). A new method for the interpretation of Schlumberger and Wenner sounding curves. Geophysics, 54, 245-253.

Zienkiewicz, O.C., and Taylor, R.L. (1989). The finite element method. 4th ed., Vol. 1, Basic formulation and linear problems. McGraw-Hill.